12-2022

Photoproducts and Transformations of Organic Pollutants in Aquatic Environments

Elizabeth Whisenhant
eawhisen@uno.edu

Photoproducts and Transformations of Organic Pollutants in Aquatic Environments

A Thesis

Submitted to the Graduate Faculty of the
University of New Orleans
in partial fulfillment of the
requirements for the degree of

Master of Science
in
Chemistry

By

Elizabeth A. Whisenhant

B.S. Chemistry University of Alaska Anchorage, 2019

December, 2022

Table of Contents

List of Figures

List of Tables

Nomenclature and Abbreviations

AI_{mod}	Modified Aromaticity Index
ANS	Alaska North Slope
ATR-FTIR	Attenuated Total Reflectance Fourier Transform Infrared Spectroscopy
BA	Benzoic Acid
BTEX	Benzene-Toluene-Ethylbenzene-Xylene
CA	Condensed Aromatics
CPE	Cloud Point Extraction
DOC	Dissolved Organic Carbon
DOM	Dissolved Organic Matter
DOM_{HC}	Hydrocarbon-derived Dissolved Organic Matter
EEM	Excitation-Emission Matrix
ESI	Electrospray Isonization
FFA	Furfuryl Alcohol
F_{OH}	Formation Rate for Hydroxyl Radical
FT-ICR MS	Fourier Transform Ion Cyclotron Resonance Mass Spectrometry
FTIR	Fourier Transform Infrared Spectroscopy
h	Planck's Constant
HIX	Humification Index
IR	Infrared
k_P	Rate Constant
k's	Pseudo first order rate constant
MGR	Merry-Go-Round
NOM	Natural Organic Matter
NOSC	Nominal Oxidation States of Carbon
$^1O_2$	Singlet Oxygen
·OH	Hydroxyl Radical
PAH	Polycyclic Aromatic Hydrocarbons
PARAFAC	Parallel Factor Analysis

PCA	Principle Component Analysis
PE	Polyethylene
PET	Polyethylene Terephthalate
***p*-HBA**	*para*-Hydroxybenzoic Acid
PP	Polypropylene
PS	Polystyrene
PU	Polyurethane
PVC	Polyvinylchloride
$\mathbf{R_P}$	Rate of the probe
$\mathbf{R_S}$	Rate of the natural scavenger
ROS	Reactive Oxygen Species
SPE	Solid Phase Extraction
ss	Steady State
TPH	Total Petroleum Hydrocarbons
UHO	Unsatured High Oxygen
ULO	Unsaturated Low Oxygen
v	Frequency
6-hp-one	6-hydroxy-2H-pyran-3(6H)-one

Abstract

The degradation of petroleum-derived organic pollutants in aquatic systems occurs through lengthened exposure to UV and visible light. In this thesis, organic pollutants include crude oil, refined fuels, and plastic particles or films. The photo-oxidation of these pollutants are monitored over natural waters. To characterize the molecular signatures of photo-oxidized petroleum, bench-scale spills of refined fuels and crude oil were irradiated over Alaskan waters. A 4-component fluorescence PARAFAC model revealed a unique feature associated with photo-oxidized refined fuel unlike traditional “microbial”- or “terrestrial-like” components. In contrast, crude oil photolytically decomposed into humic-like components and oxidized aliphatics. FT-ICR MS data corroborated the optical data. Overall, refined fuels produce a significantly higher mass of photoproducts than crude oil and carry a unique chemical signature.

To characterize degradation pathways of plastic particles mediated by reactive oxygen species (ROS), chemical probes were added to solutions of plastic in water to react with reactive transients produced from plastic irradiation. ROS examined were hydroxyl radical and singlet oxygen. A higher ROS production rate was observed in nanosized particles versus microsized particles, and higher in plastics with backbones containing ester bonds than that of backbones made of carbon-carbon bonds. Cloud point extraction was successfully used to separate plastic particles from water, and surface chemistry changes on shopping bags show early signs of degradation from UV light. Results in this thesis give encouraging precedent to future methods of studying photodegradation of environmentally relevant organic pollutants.

Keywords: photo-oxidation; dissolved organic matter; petroleum; PARAFAC fluorescence; reactive oxygen species; nanoplastics

Chapter 1: Introduction

The widespread use, and subsequent rise in pollution, of petroleum-derived products is of current environmental concern. The introduction of foreign materials in the environment has been studied due to the increase of oil drilling and spills, as well as the rise in manufacturing, use, and pollution of single-use, petroleum-derived products. Introduction of pollutants is an unnatural disturbance to existing energy and matter levels in the environment, which may lead to the modification and degradation of a natural system.[1] Photochemical transformations of crude oils, refined fuels, and petroleum-derived products such as plastics, have been studied in multiple fashions in attempts to identify their fate in the environment. However, despite prior studies, little has been done to understand photochemical impacts of fuel spills in high latitude conditions where drilling is present, the climate is unique, and spills are remote and difficult to remediate. In a similar fashion, the short-term mechanisms of photooxidative patterns in plastics are poorly understood.

This thesis addresses three topics:

1. Monitoring of photoproducts in Arctic conditions using optical techniques
2. Role of ROS in photo-oxidation of plastic polymers
3. Surface chemistry changes of plastic polymer films after light exposure

Photochemistry

Chemical reactions initiated by light only occur when a compound absorbs light. Compounds with the ability to absorb light are known as chromophores. Absorption of light allows for compounds to move from a ground state energy level to an excited state energy level, which is equal to the energy, *E*, of incident quantum light:

$E=h\nu$

Where h is Planck's constant and ν is the frequency of light absorbed.

Electronic excitation leads to the promotion of an electron from a bonding to an antibonding or nonbonding orbital.[2] The electronic transition responsible for the majority of organic photochemical reactions are $\pi - \pi^*$ transitions.[2] In environmental photochemistry, the effect of light energy on organic compounds comes from the solar spectrum which is highest between 300 – 750 nm. Molecular bonds absorb at different wavelengths of light according to the structure of the molecule. Several organic compounds have maximum absorption sensitivity within the UV-visible wavelengths of the solar spectrum. Plastic polymers absorb at 290-400 nm, which is entirely in the UV region of the solar spectrum.[3] Oil is made of a mixture of aromatics, naphthenes, paraffins, and olefins in which aromatics absorb in both the UV and visible region.[4]

After a molecule absorbs a photon and transitions from ground state (S_0) to an excited state, the excited state of the molecule can exist in two arrangements: an excited singlet state (S_1) where electrons are paired and an excited triplet state (T_1) where the electron spins are unpaired (***Figure 1.1***). A series of relaxation stages in aromatic or conjugated molecules may convert electrons from S_1 to T_1 through intersystem crossing.[2] Relaxation eventually returns the molecule to its ground state energy level by losing energy through a variety of transitions.

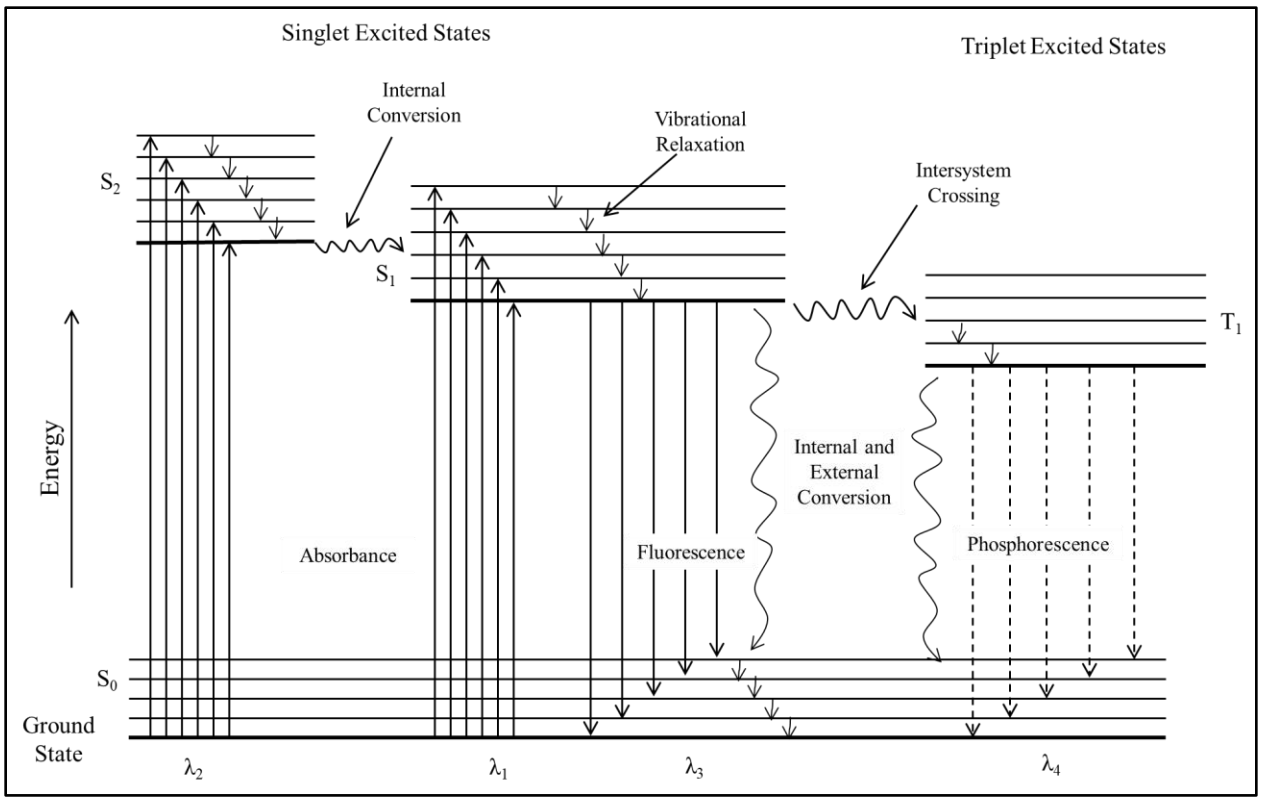

Figure 1.1. Jablonski diagram

Photochemical reactions occur through direct or indirect photolysis mechanisms. Direct photolysis occurs when chromophoric material directly absorbs light, leading to changes to chemical structure such as bond cleavage, chain scission or fragmentation.[5] Indirect photolysis occurs when a reaction is initiated as a result of light absorption by some other chromophore separate from the substrate of interest.[6] Reactive intermediates are produced through these processes, which can initiate chemical change to the substrate of interest by a series of reactions.[5, 6] These reactions are the focus of all processes taking place in this thesis.

Environmental Phototransformations:

Naturally occurring dissolved hydrocarbons in environmental waters have been studied to show that light interacts with organic material in water to produce chemically altered products.[7]

These hydrocarbons, with accompanying oxygen and nitrogen substances, are also known as dissolved organic matter (DOM), a heterogeneous mixture of humic substances, hydrocarbons, carbohydrates, and proteins derived from decomposed plant material and other organisms.[7, 8] DOM in natural waters contains chromophores that allow for light absorption and subsequent generation of photochemical products, in which the nature of production varies according to its source and precursor materials. Photo-oxidation can occur through the presence of oxygen and light radiation. It has also been found that hydrophobic organic substances, such as crude oil and fuels, are able to transform into hydrophilic substances due to photo-oxidative processes.[9] A significant chromophoric component of crude oil consists of polycyclic aromatic hydrocarbons (PAH); these moieties are susceptible to photo absorption and are able to undergo photooxidation and phototransformation. The chromophoric composition in DOM allows fingerprinting methods to trace DOM back to its source, which has been used to monitor the dissolvable photoproducts from oil spills in the environment.[10-19]

Through exposure to sunlight, DOM and crude oil can produce reactive oxygen species (ROS) such as hydroxyl radical (·OH), singlet oxygen ($^1O_2$), organic radicals and superoxide.[5, 20-26] The role of ROS has been established as being a vital species involved in the photo-oxidation of DOM and oil films.[2, 5, 6, 8, 20-26] Using methods and research established for monitoring ROS produced from DOM and oil spills, the production of ROS from nano- and micro-sized plastics is another focus of this thesis. Plastic polymers have vastly different structures than DOM or crude oil, but some plastic structures have chromophores that allow them to absorb UV radiation and photo-degrade. Even if polymers do not have naturally occurring chromophores, it is likely that there will be impurities and additives in the polymer structure which absorbs light and promote

photo-oxidative chemical reactions.[27-29] By using chemical probes to monitor for the presence of ·OH and $^1O_2$, the photo-oxidative mechanism of plastic degradation can be established.

The ground state of molecular oxygen is a triplet; the indirect degradation of plastic polymers involving oxygen occurs with the use of radical species.[27] This occurs when a polymer absorbs photons of light and excited electrons are transferred to a molecular oxygen forming into a superoxide anion. The formation of superoxide anion can lead to the production of other ROS such as hydroxyl radical. These ROS species are reactants for indirect photolysis of polymer materials.

Hydroxyl Radical:

Hydroxyl radical is the most reactive ROS involved in photo-oxidative pathways due to its strong oxidation potential, high electrophilicity, and ability to react with multiple species.[25, 30] Because of its high reactivity, ·OH has a low steady state concentration and is difficult to monitor directly using common methods of analysis (electron spin resonance).[25] Therefore, methods performed by Zhou and Mopper were used to indirectly monitor total ·OH trapped and the ·OH steady state concentration of UV-exposed micro- and nano-sized plastic particles.[25]

Pathways for the production of hydroxyl radical from plastic polymers have been proposed,[27, 29, 31, 32] where hydroxyl radical is formed from superoxide. After initial reduction of O_2 to form superoxide, subsequent dismutation reactions with superoxide yields hydrogen peroxide. Hydroxyl radicals are then finally produced from the reduction of hydrogen peroxide.[2, 5, 27, 29-32] The presence of free radicals in aquatic systems leads to further reactions; the hydroxyl radical is a reactive species that can aid in the photo-oxidation of a hydrocarbon polymer and by doing so, can result in fragmentation, chain-breaking, and cross-linking of polymer chains.[31]

Singlet Oxygen:

Singlet oxygen is an ROS that has been found to be another vital species to photo-oxidative pathways.[5] Singlet oxygen is produced through reactive pathways with molecular oxygen. When an organic compound absorbs light and is promoted to an excited state, a change of electron spin may occur transitioning the compound to an excited triplet state. Singlet oxygen is produced when the triplet state molecule transfers energy to the ground state molecular oxygen, thereby quenching the excited triplet state of the sensitizer compound.[5, 29] Like hydroxyl radicals, singlet oxygen can be indirectly monitored through the use of a chemical probe.[20]

Chapter 2: Instrumentation

Solar Simulation and Merry Go Round Photoreactor

For simulated oil spills, an Atlas XLS+ solar simulator was used to irradiate oil over the entire spectrum of solar radiation at an intensity of 250 W/m^2, which is equivalent to the daily summer maximum in Southcentral Alaska.[33] For plastics studies, a merry-go-round (MGR) photoreactor equipped with 350-nm lamps was employed. These lamps were chosen due to absorbance capabilities of plastic (290 – 400 nm)[3] and the chemical probes.[20, 25]

Fluorescence Spectroscopy

By absorbing photons of light at specific wavelengths, a molecule will be excited from its ground electronic state to an excited electronic and vibrational state. After excitation, a molecule can relax back to its ground electronic state through multiple mechanisms. Fluorescence occurs when a molecule relaxes from its singlet excited state (S_1) back to its ground state (S_0), emitting light energy in the process (see Jablonski Diagram, ***Figure 1***). Fluorescence spectroscopy measures the wavelength of light that successfully excites a given sample as well as the wavelength that is emitted from the sample through relaxation. In this way, both fluorescence excitation and emission will exhibit relative maximum values based on the fact that aromatic bonds accept photons with wavelengths of light, and in turn, emit wavelengths of energy through relaxation. The fluorescence intensity of both the excitation and emission wavelengths will be unique to a chromophore within a sample and can be used to display a unique, three-dimensional excitation-emission matrix.

Substances possessing aromatic molecules capable of absorbing light are naturally fluorescent allowing easy measurement of characteristic fluorescence behaviors that may be present in a sample. In the following studies, fluorescence spectroscopy was used to observe dissolved organic matter in natural waters. Fluorescence measurements were taken using a Horiba Aqualog Fluorometer (Horiba Scientific, Kyoto, Japan). Excitation, emission, and fluorescence intensity data were exported for identification of chromophores in a complex aquatic sample.

Parallel Factor Analysis

Parallel Factor Analysis (PARAFAC) is a statistical technique that can be used to deconvolute an excitation-emission matrix from fluorescence spectroscopy into multiple components statistically different from one another. PARAFAC assumes that: no two chemical components have identical fluorescence spectra, the same three factors underlie every dataset, and the total signal is due to linearity of a fixed number of components.[34] PARAFAC decomposes a given fluorescence signal into trilinear variables with an allowed residual:

PARAFAC model:

$$x_{ijk} = \sum_{f=1}^{F} a_{if} b_{jf} c_{kf} + e_{ijk}$$

Variables in the PARAFAC algorithm are achieved where *i, j,* and *k* are consistent with the sample, emission and excitation, respectively. Each variable *f* represents a spectral component where each component has *i* number of *a*-values (scores) for each sample, *j* number of *b*-values

for each emission wavelength, and *k* number of *c*-values for each excitation wavelength. e_{ijk} is the sum of squares of the residuals and *F* represents the number of total samples measured.[34, 35] For this research, data collected from the Aqualog was imported into MATLAB and modeled using the drEEM toolbox, where outliers were removed and the scatter regions were smoothed.[34] A multidirectional analysis by PARAFAC was generated.

Fourier Transform Ion Cyclotron Resonance Mass Spectrometry

Mass spectrometry is a method used to examine multiple analytes in a sample based on their different mass to charge (m/z) ratios. Analytes are ionized and desolvated by an ion source then directed through electric and/or magnetic field for mass separation and analysis. Ions will travel through the applied electric or magnetic fields respective and characteristic to their m/z. In this way, mass and structural information of the analytes may be determined based on fragmentation behavior. Mass spectrometers utilize different types of ion sources and mass analyzers. A mass analyzer used for ultrahigh resolution capabilities is the Fourier transform ion cyclotron resonance mass spectrometer (FTICR-MS). This mass analyzer utilizes a hybrid linear ion trap mass spectrometer equipped with a 21 tesla superconducting solenoid magnet. This technique is able to confine ions and measure the ion cyclotron motion using the ion's frequency of travel amongst an applied magnetic field.[36, 37]

High-Performance Liquid Chromatography

Reverse-phase high performance liquid chromatography (HPLC) is an analytical technique that is used to separate nonvolatile and thermally fragile species in a complex mixture.[38] This method utilizes a mobile and stationary phase to separate molecules based on

their polarity and affinity to a nonpolar stationary phase and a polar mobile phase. Molecules that are more nonpolar have a higher affinity for the nonpolar mobile phase, while more polar molecules have a higher affinity for the polar mobile phase. After separation, analytes can be detected by absorption spectroscopy. In this way, analytes in a complex mixture are separated, detected, and measured for respective concentration levels using an Agilent 1200 series high-performance liquid chromatograph (HPLC) (Agilent Technologies, California, USA).

Fourier Transform Infrared Spectroscopy

Since each type of chemical bond within a molecule can populate specific vibrational and rotational energies, each bond absorbs specific frequencies of infrared (IR) radiation. IR radiation is not energetic enough to produce electronic transitions; instead, small energy differences exist between vibrational and rotational states of a chemical bond.[38] As a result of vibrational and rotational change, a molecule undergoes change in its dipole moment brought about by atomic electron densities. The frequency of radiation must exactly match the vibrational modes within a molecule for a transfer of energy of molecular vibration to occur.[38, 39] Polar molecules with naturally occurring dipole moments are easily measured by Fourier transform infrared spectroscopy (FTIR) where the vibrational and rotational energy transitions in a molecule reveal a net change in dipole moment indicative of a specific molecular bond or group of bonds. The absorption of infrared radiation at various frequencies are collected and each chemical compound possess a unique FTIR absorbance spectrum.

In comparison to traditional FTIR transmittance methods, attenuated total reflectance (ATR) is an accessory used with FTIR spectrometers allowing for non-transparent materials to be measured. This technique works by pressing a sample with a refraction index larger than air

toward an ATR crystal. Incident IR radiation permeates the sample at an incident angle (45°) and is absorbed partly by the sample. The IR radiation not absorbed by the sample will be reflected from the crystal interface. This signal is compared to total reflectance of the incident IR radiation when no sample is pressed toward the ATR crystal. Absorbance is measured as the difference between IR radiation reflected back from the crystal with and without a sample present.[39]

These techniques are useful for classifying unknown substances by functional group identification, inspecting qualitative changes among a known sample, and measuring quantitative information of increase or decrease of infrared absorption.[38] This thesis describes the use of these methods to observe aging and changes to surface functional groups in polymer particles and films.

Chapter 3: Unique Molecular Features of Water-Soluble Photo-oxidation Products among Refined Fuels, Crude Oil, and Herded Burn Residue under High Latitude Conditions

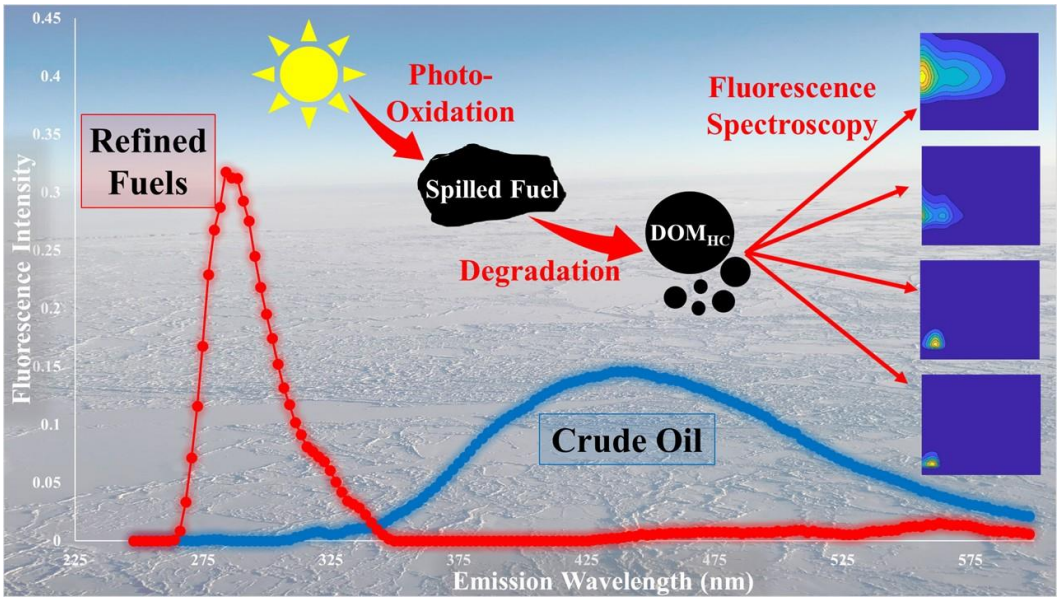

Abstract:

Photo-oxidized petroleum hydrocarbons are a unique class of water soluble bioavailable compounds that have gained emerging recognition within toxic regulatory management bodies as an urgent and priority research need in high latitudes. In order to characterize the molecular signatures of photo-oxidized petroleum, bench-scale spills were irradiated over Alaskan seawater and freshwater at 5.5 °C. “Refined fuels” included heating oil, diesel, Jet-A, kerosene, and gasoline, with ANS crude reference. An additional experiment assessed the photolytic aging of ANS crude “remediated” using a recently-popularized strategy of *in-situ* burning with and without herder application. A 4-component fluorescence PARAFAC model revealed a unique short-wavelength feature associated with photo-oxidized refined fuel that is not associated with traditional “microbial”- or “terrestrial-like” components. In contrast, crude oil photolytically

Reprinted with permission from Whisenhant, E. A.; Zito, P.; Podgorski, D. C.; McKenna, A. M.; Redman, Z. C.; Tomco, P. L., Unique Molecular Features of Water-Soluble Photo-Oxidation Products among Refined Fuels, Crude Oil, and Herded Burnt Residue under High Latitude Conditions. *ACS ES&T Water* **2022,** *2* (6), 994-1002. http://pubs.acs.org/articles onrequest/AOR-UC64BU2C52339BATE57N.

decomposes into long wavelength humic-like components (high humification index) and oxidized aliphatics. FT-ICR MS data corroborated the optical data. Overall, on a per-volume basis, the refined fuels diesel, heating oil, kerosene, and Jet-A produce a significantly higher mass of photoproducts than crude oil and carry a unique chemical signature. This warrants new considerations regarding marine biota toxicity. This study also highlights new potential for tracking photo-modified water-soluble fractions of crude and refined fuels in high latitudes with fluorescence spectroscopy.

Introduction:

As the Subarctic and Arctic continue to be a hub for oil exploration and production, methods of drilling, transportation, and product storage form a combination of efforts that enhance the risk of oil and fuel residuals entering the environment by large-scale spills and mechanical failures. Since tracking began in 1970, there have been over 57,000 spill incidents in Alaska reported by the Alaska Department of Environmental Conservation with 12,000 of these reported incidents resulting from a structural or mechanical leak, line failure, or tank failure.[40] Spill incidents pose an increased risk in Alaska as spill detection is logistically difficult and expensive to access in remote regions. Additionally, the fate and transport of spilled chemicals in high-latitude regions are uniquely different from temperate environments due to sub-zero surface temperatures, short annual thaw season, and for terrestrial systems, restricted flow regimes from permafrost.[41] The ability to detect and fingerprint spilled fuel products, and to develop spill response strategies in remote areas is imperative to locations susceptible to oil drilling and exploration, as well as in areas that store aging fuel oil containers.

Petroleum introduced into the environment is subject to abiotic and biotic degradation processes. Photodegradation can oxidize petroleum to produce photoproducts by reacting with aromatic compounds that absorb light in the solar spectrum.[19, 21-24] Microorganisms also produce oxygenated products through aerobic and anaerobic biodegradation processes.[42-45] Both photodegradation and biodegradation pathways can enhance water solubility of petroleum products, resulting in the production of hydrocarbon-derived dissolved organic matter (DOM_{HC}), which encompasses the entire continuum of parent and partially-degraded compounds.[9, 14, 19, 46] Once mobilized as a result of dissolution, DOM_{HC} can spread throughout the water column, potentially traveling undetected vast distances ahead of any signs of a visible oil front, increasing bioavailability, and impacting aquatic ecosystems both marine and freshwater. Photo-oxidized DOM_{HC} has received significant recent attention and has been identified as an urgent research priority to support oil spill response models.[47, 48]

Several recent methods of petroleum fingerprinting have been described that characterize DOM_{HC} in aquatic systems.[12, 49-52] DOM_{HC} contains chromophores that allow measurement and visualization through optical tools such as three-dimensional excitation-emission matrix spectroscopy (EEMs).[34] These approaches have been shown to be an effective method of detecting dispersed oil and chemically dispersed oil in open oceans, fingerprinting oil based on EEMs, determining concentrations of benzene-toluene-ethylbenzene-xylene (BTEX), as well as total petroleum hydrocarbons (TPH) and polycyclic aromatic hydrocarbons (PAH).[53-58] Fluorescence spectroscopy has also been applied to dissolved organic matter in arctic systems, largely in the context of labile and refractory pools.[10, 56, 59] DOM_{HC} is also commonly analyzed

using modern Fourier Transform Ion Cyclotron Resonance Mass Spectrometry (FT-ICR MS).[19, 21, 50, 60, 61] These tools are complementary as parallel factor (PARAFAC) analysis can be used to deconvolute EEM spectra into individual components in an effort to identify chromophores present in DOM_{HC}[13, 16], while FT-ICR MS can deconvolute complex petroleum spectra into molecular components aliphatic, aromatic, condensed aromatic, and unsaturated high/low oxygenated species in van Krevelen space.[62, 63] DOM_{HC}, treated as a unique complex mixture, has received recent attention in cold climates.[61] However, the photolytic decomposition of DOM_{HC} has not been classified in this regard, and to-date, no information to our knowledge exists that assess water-soluble photo-oxidized molecular features across a spectrum of fuel types and a gradient of irradiation times using these advanced techniques.

This study investigates the molecular properties of DOM_{HC} produced from films of crude oil and refined fuels (heating oil, diesel, Jet A, kerosene, and gasoline) that were subjected to simulated spill conditions of high-latitudes. Additionally, this study assesses photo-modified dissolution of a popular crude oil spill remediation strategy, *in-situ* burning following chemical herder application, which has gained recent popularity as a strategy for oil removal in cold regions.[64-67] This study aims to discover two main areas that are of urgent concern to stakeholders in the Arctic: 1) the extent of photo-modified solubility potential of each of these fuel types, and 2) patterns in DOM_{HC} that can be used for early detection of spills in remote Arctic regions. We hypothesize that there is a positive relationship between DOC concentration and irradiation period, and that photo-oxidation will produce unique molecular signatures as evidence of added petroleum-derived DOM_{HC} to aquatic ecosystems. The ability to identify

distinct optical signatures of the DOM_{HC} formed from each treatment may facilitate new methods to rapidly screen for leaked DOM_{HC} in remote areas of the Arctic that are susceptible to spills and are unable to be reached in a timely manner.

Materials and Methods:

Materials and Sample collection:

Refined fuels were commercially obtained throughout Southcentral Alaska in January 2020. Heating oil and diesel fuel were obtained in Anchorage, Alaska by Shoreside Petroleum, Jet A-50 fuel was provided by International Aviation Services, and both kerosene and unleaded gasoline were sourced locally in Anchorage. Alaska North Slope (ANS) crude oil was obtained from the Valdez Marine Terminal in March 2018. Freshwater was collected from Otter Lake on Joint Base Elmendorf-Richardson, Alaska, and seawater was obtained from Resurrection Bay in Seward, Alaska at the Alaska Sealife Center. Water was filtered through pre-combusted (500 °C, >5 h) 0.27 µm glass microfiber filters (Advantec) prior to experiments. Glassware was acid-washed and combusted at 500 °C for 5 hours.

Simulated exposures

In the first experiment, films of fuel/crude oil were created at an oil load of 1.15 mL per 90 mL water in thermostatically controlled 100 mL jacketed beakers (Chemglass USA). Fuel types included heating oil, Jet A-50 fuel, unleaded gasoline, diesel fuel, kerosene, ANS crude oil, and burnt ANS crude oil. Each fuel treatment was applied over either freshwater or seawater (replicates of 3, total of 384 samples) and placed inside a solar simulator 12 samples at a time

(Atlas Suntest XLS+, Atlas Material Testing Technology LLC). Solar irradiance was programmed at 250 W/m^2, equivalent to the daily summer maximum in Southcentral Alaska.[33] Each jacketed beaker was thermostatically controlled at 5.5 °C and represents a single time period from 0 to 240 h (0 to 10 days). Beakers were covered with quartz lids to allow for light transmittance and secured to reduce evaporation. After incubation, samples were transferred to separatory funnels in order to isolate undissolved fuel from water. Water layers were filtered with 0.27 µm glass fiber filters. Samples were stored at 4°C in the dark until analysis within 24 hours or kept frozen until analyzed.

In the second experiment, crude oil (50 mL) was added to 4.5 L seawater in 5 L HDPE jars secured with acrylic UV-transmitting covers. Two treatment types were tested: (1) in-situ burned crude oil and (2) in-situ burned crude oil after addition of a chemical herder (Siltech OP-40). In the first treatment group, crude oil was set aflame immediately after a thin film of oil covered the water. In the second treatment, Siltech OP-40 chemical herder was added to the perimeter of the spilled oil film, then burned. After burning, treatment groups underwent light regiments of UV exposure or complete darkness for 0 to 240 h (0 to 10 days). Each exposure chamber was controlled at 15 °C, the lowest achievable temperature for the given light intensity and experiment duration using the SunCool air conditioner. The remaining exposure and post-processing parameters followed procedures outlined in the first microcosm experiment.

Dissolved Organic Carbon and Excitation-Emission Matrix Measurements:

Dissolved organic carbon measurements occurred on a Shimadzu TOC-L (Kyoto, Japan). Samples were acidified to pH 2 using 12M HCl and sparged for 5 minutes with ultrapure air to

eliminate volatiles and inorganic carbon. Excitation-emission matrix (EEM) spectra were collected using a Horiba Aqualog Fluorometer (Horiba Scientific, Kyoto, Japan). Further details of spectral acquisition, processing, and model validation are provided in Supplemental Information.

Ultrahigh resolution mass spectrometry:

DOM_{HC} was isolated by a solid-phase extraction (SPE) method and prepared for Fourier transform ion cyclotron resonance mass spectrometry (FT-ICR MS) analysis. Aqueous samples were first acidified to pH 2 and passed through a Bond Elut PPL (Agilent Technologies) cartridge.[68] Acidified water (pH 2, Milli-Q water) was then passed through the cartridge to rinse any salts from the sample. DOM_{HC} selectively adsorbed onto the solid stationary phase, which was then dried by N_2 gas and eluted with 100% MeOH to a final concentration of 50 ugC mL^{-1}. DOM_{HC} extracts were infused by microelectrospray ionization at 500 nL min^{-1}, then analyzed by a hybrid linear ion trap FT-ICR mass spectrometer equipped with a 21 tesla superconducting solenoid magnet.[36, 37] ESI(-) is a common ionization source for determining oxidized petroleum products due to its ability to ionize acidic and polar compounds. Molecular formulas were assigned to signals with a magnitude greater than 6σ from RMS baseline noise at *m/z* 500 using PetroOrg(c) software developed at the National High Magnetic Field Laboratory.[69] The reproducibility of FT-MS spectra for DOM analysis is reported in detail by Hawkes *et al.* 2020.[70] The molecular formulae were classified based on stoichiometry: condensed aromatic (CA) (modified aromaticity index ($AI_{mod} \geq 0.67$), aromatic ($0.67 > AI_{mod} > 0.5$), unsaturated, low

oxygen (ULO) (AI_{mod} < 0.5, H/C < 1.5, O/C < 0.5), unsaturated, high oxygen (UHO) (AI_{mod} < 0.5, H/C < 1.5, O/C ≥ 0.5), aliphatic (H/C ≥ 1.5).[62, 63, 71]

Results and Discussion:

Dissolved Organic Carbon:

Non-purgeable dissolved organic carbon (DOC) concentrations in treatments exposed to sunlight increased with exposure time (Figure 3.1), while minimal change was observed in the treatments without light. DOC among all samples without light ranged from 0.79 ± 0.08 mg/L to 3.34 ± 2.95 mg/L at Day 0 and ranged from 2.72 ± 0.30 mg/L to 10.58 ± 11.12 mg/L at Day 10 (Table S3a-d). DOC among all samples after light treatment ranged from 0.80 ± 0.08mg/L to 2.50 ± 0.95 mg/L at Day 0, and 1.65 ± 0.56 mg/L to 323.67 ± 29.27 mg/L at Day 10 (Table S3a-d). Concentrations of DOC at Day 10 varied significantly by fuel type after light treatment but did not show a positive correlation between the boiling point of fuel and concentration of DOC present (Figure 3.1). Increases in DOC for refined fuels (kerosene, jet fuel, diesel, heating oil) were greater compared to crude oil, consistent with what is known about the heavy components of crude oil requiring more extensive oxygenation before becoming water soluble.[72] Gasoline did not exhibit an increase in DOC concentrations as the samples were sparged prior to analysis. DOC concentrations, along with other molecular features (discussed below) did not differ between freshwater and seawater conditions; for Figure 3.1, data were pooled for both water types (N=6).

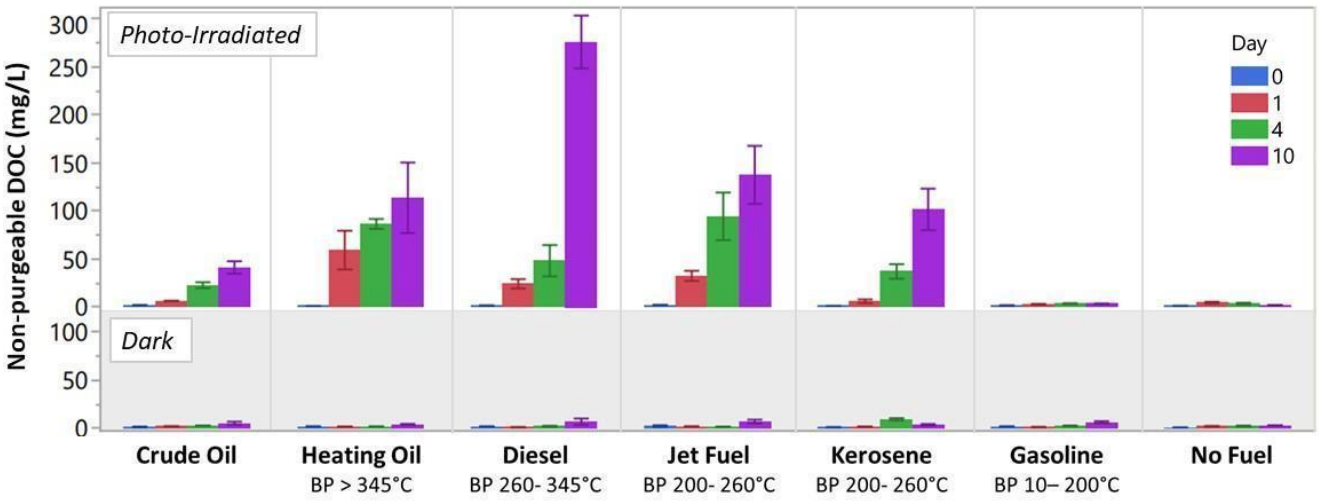

Figure 3.1. Temporal trends in non-purgeable dissolved organic carbon (DOC) accumulation in water-soluble fraction following solar irradiation (top) and dark-incubated (bottom) among crude and refined fuels, with no-fuel control (natural water) (N=6, +/- 1 SE). Petroleum types are listed in order of decreasing boiling point.[73]

Parallel Factor (PARAFAC) analysis:

PARAFAC highlights several changes in the DOM_{HC} composition over time. Figure 3.2 presents the four-component model validated for the DOM_{HC} samples. Component 1 (C1) exhibited excitation and emission (Ex/Em) maxima of 245/440 nm associated with signatures similar to terrestrial fulvic and humic-like substances (98% OpenFluor similarity score), suggesting that as petroleum is photodegraded, DOM_{HC} products resemble, among others, terrestrial materials (i.e., high MW, oxidized, alicyclic/aromatic compounds).[10, 74, 75] The remaining components identify with common fluorophores with a 95% OpenFluor similarity score. Component 2 (C2, Ex/Em: 240/350 nm) resembles a tryptophan-like peak and is

comparable to sources of seawater and freshwater streams.[13, 18] Component 3 (C3, Ex/Em: 275/300 nm) represents a tyrosine-like peak comparable to terrestrial DOM offshore studies.[17, 74] Component 4 (C4, Ex/Em: 260/284 nm) exhibited Ex/Em similar to one other component in the OpenFluor database, which matches the amino acid phenylalanine.[76] However, no phenylalanine was present in the samples when further examined (data not shown, see supporting information). C4 is a new signature that is not indicative of a microbial-like (C2, C3) or terrestrial-like (C1) component, suggesting that there is a unique component revealing a petroleum fingerprint.

Humification index (HIX) values are determined by a ratio of long:short wavelength fluorescence. Typically, large HIX values are consistent with "humified", water soluble, oxidized compounds.[77] An increase in HIX is an indication of a relative increase in long wavelength DOM and/or depletion of short wavelength DOM. HIX changes were noted across the incubation period for light-exposed treatments versus dark controls (Table S3a-d). Among irradiated samples, there is a consistent HIX increase for crude oil (Table S3d). For heating oil and jet fuel, HIX increased from 0 to 4 days, while no increase was noted for gasoline, diesel, or kerosene. This trend is consistent with the compounds that are expected to be present within the reported boiling points of each fuel type. Among the fuels we tested (N=6 and 4 for EEMs and FT-ICR MS, respectively), DOM_{HC} produced from crude oil exhibited the most consistent increase in humification. This result is due to the broad range of molecular structures that are present in a whole crude, including those with high boiling points.[19] Conversely, gasoline revealed no increase in humification because it consists of a narrow range of carbon numbers from C4-C12. However, among DOC measurements (Figure 3.1), we observed greater extent of

photo-modified DOC production from fuel types that are lighter than crude oil. This result indicates that the compounds that comprise these relatively (to whole crude oil) narrow carbon number range distillation cuts are susceptible to photo-oxidation. This point can be visualized by double-bond equivalent versus carbon number plots (Figure S3) and nominal oxidation states of carbon (NOSC, Figure S4). Moreover, the concentration of DOC produced from the refined fuels was an indication of the higher per-volume proportion of compounds in a distillate cut that can partition into the aqueous phase after a given period of photo-oxidation. This process provides a plausible explanation for the high DOC concentrations produced after 10 days of exposure from the diesel relative to the heating oil. It is expected that an increase in exposure period would result in an increase in DOC production from the fuel oil which would eventually exceed that of the diesel fuel. This result would be consistent with a DOC production continuum model that was previously reported on two crude oils with different chemical compositions.[7] Nevertheless, the compounds in the refined fuels are photolabile and more susceptible to photolysis, yet the product of degradation (DOM_{HC}) does not appear to be humic-like. Further study is needed to test optical variances among products of different refining techniques to understand how these processes react photochemically.

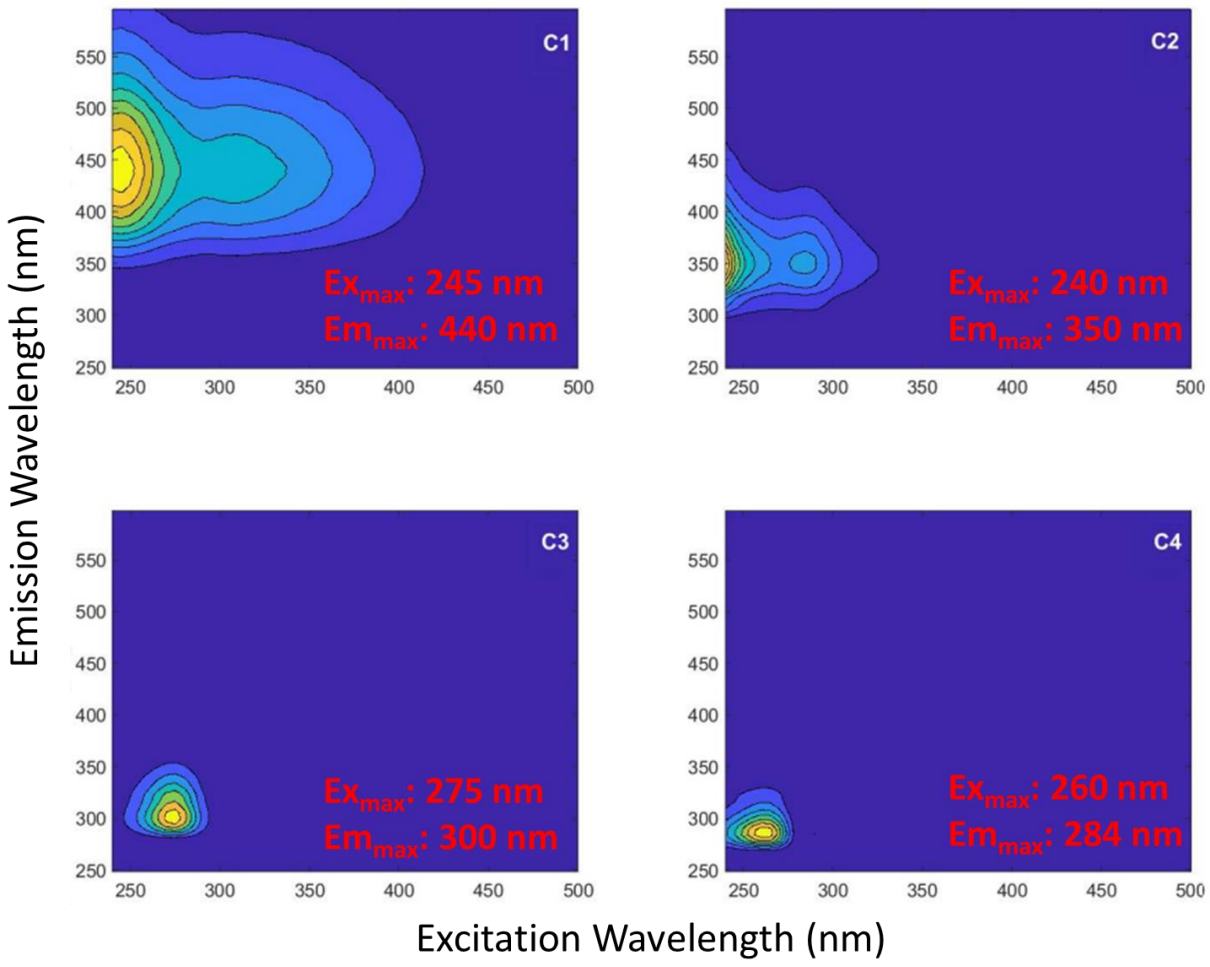

Figure 3.2. Two-dimensional contour plot of 4-component model validated by PARAFAC.

Temporal Molecular Characteristics of DOM_{HC} following irradiation:

Ultrahigh resolution mass enables closer examination of the chemical composition of the polar DOM_{HC} products derived from each fuel type at the molecular level.[78] The percent relative abundance of the formulae classifications for each treatment are reported in Table S6a-b. In

summary, the results obtained by mass spectrometry indicate that the chemical composition of photosolubilized DOM_{HC} is dependent on the composition of the initial distillate. This result corroborates previous reports showing that the composition of DOM_{HC} from whole crude oils is dependent on the initial composition of the crude.[19] To emphasize oxidation trends among the entire range of distillate cuts, Figure 3.3 highlights compositional differences in the aliphatic and unsaturated, low oxygen classes DOM_{HC} produced from kerosene, crude oil, and heating oil after 10-days of light exposure and a dark control.

Crude oil produced the highest relative abundance of aliphatic DOM_{HC} (43.0 ± 4.0%). The DOM_{HC} produced from the heating oil, which has the highest boiling point of the distillates that we analyzed, has the second most abundant class of aliphatics (17.1 ± 3.8%). The abundance of aliphatics in the DOM_{HC} from kerosene, the second lowest boiling distillate cut, was the least (6.8 ± 0.3%) relative to the crude oil and heating oil. On the other hand, trends in unsaturated low oxygenated relative abundances were inversely correlated to aliphatics for these fuels (Figure 3.3), with crude oil, heating oil, and kerosene at 41.0 ± 1.9, 46.9 ± 2.3, and 55.8 ± 2.5 %, respectively. These data indicate a relationship exists between the distillate fraction boiling point and abundance of water-soluble photoproducts. van Krevelen subtraction plots for endmember timepoints T0, T10, and T10-0 further illustrate the compositional patterns for each fuel type in seawater and freshwater (Figure S5-S6).

When compared to dark controls, aliphatic-like DOM_{HC} was produced by photo-irradiating crude oil, heating oil and kerosene. This is consistent with previous studies that investigated other photo-oxidized crude oils and weathered tarballs, where similarly, water-

soluble aliphatic production was noted following exposure to simulated sunlight.[19, 21, 72, 79] Unsaturated low oxygen (ULO) relative abundances increased only for kerosene (Figure 3.3). This suggests that distillate cuts at lower boiling points will form photoproducts with higher relative abundances of ULO and lower relative abundances of aliphatics. Nominal oxidation state of carbon (NOSC) was, in general, lower for irradiated samples versus dark controls (Figure S4). Interestingly however, the NOSC data indicates temporal variations among fuel types. Jet fuel and heating oil exhibited minimum NOSC with 1 day irradiation, while NOSC decreased with irradiation time throughout 10 days. These trends note the unique temporal and fuel type dependency on photoproduct formation.

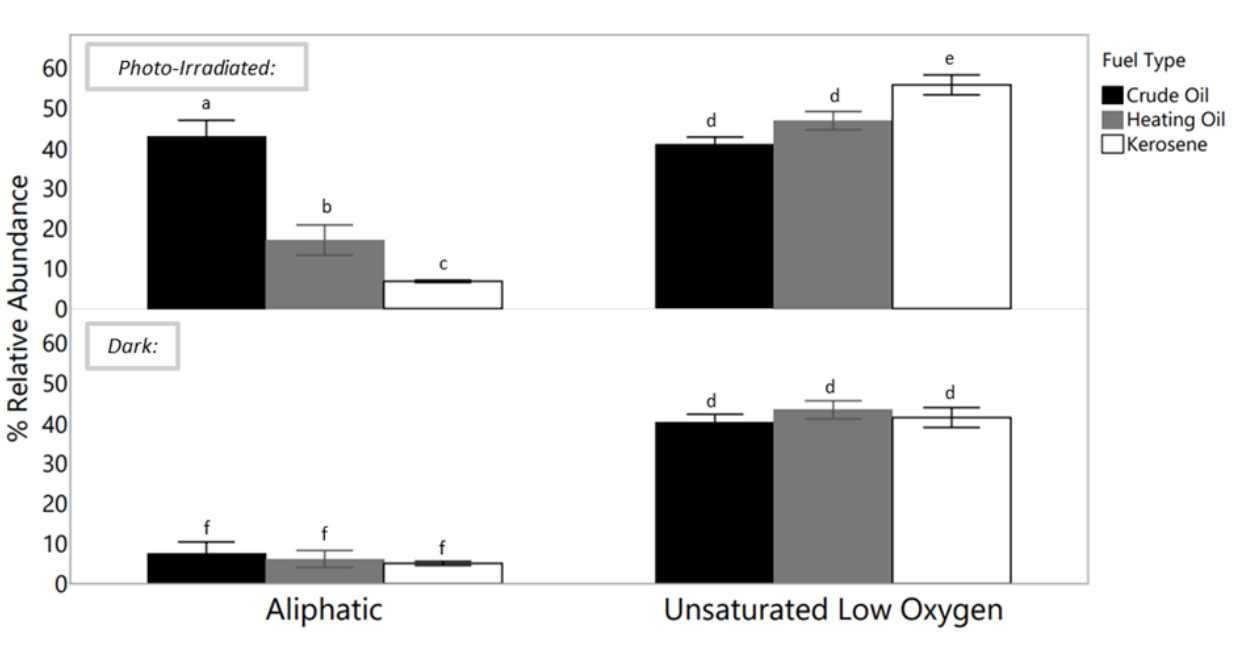

Figure 3.3. Aliphatic and unsaturated low oxygen molecular characteristics of DOM_{HC} at 10 day irradiation time for crude oil, heating oil, and kerosene. Data are expressed as % relative abundance, N=4 ± SE. Connecting letters for aliphatic (a,b,c,f) and ULO (d,e) are student's t-test pairwise comparisons at 95% confidence.

Principal component analysis (PCA) further supports the uniqueness of component C4; as refined fuel samples experienced photo-irradiation, fuel-derived DOM_{HC} fluorophores were formed with an increased relative abundance of molecular signatures representative of C4 (Figure 3.4A). This trend is consistent for most refined fuels (Figure 3.4B), as PCA of all fuel types at 10-day exposure demonstrates that DOM_{HC} produced from diesel, kerosene, Jet-A, and heating oil clustered with loadings for C4, which itself clustered with the loadings for unsaturated low oxygen, aromatic, and condensed aromatic. It is important to note that these groupings represent ESI(-) ionizable compounds, which are polar in nature and the operational definition of CA, aromatics, and aliphatics are not bracketed by O/C; therefore the features observed represent polar, oxidized forms. Crude oil is unique from these other fuel types, closely resembling C2 and aliphatic (oxidized aliphatic) over time. The temporal trends toward C4 did not differ between freshwater and seawater (Figure S1, S2). We found C4 to be a unique fluorescent component accompanying the photo-production of DOM_{HC} from diesel and kerosene, and to a lesser extent, jet fuel and heating oil.

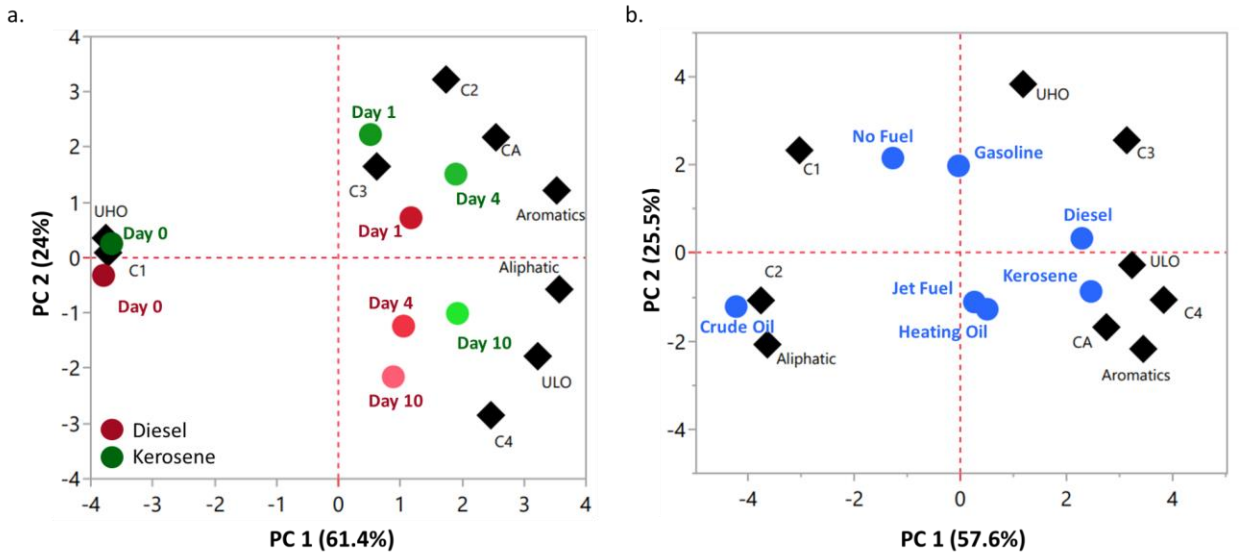

Figure 3.4. Principal Components Analysis (PCA) biplots; loadings represent molecular features (Fluorescence Components C1-C4 and FT-ICR MS van Krevelen Space). (a) Compositional trends illustrated across time (irradiation period) from 0 to 10 days for two representative refined fuels, diesel and kerosene. These fuels exhibited similar trends compared to most other distillate cuts. (b) Molecular features present at irradiation period = 10 days, the end irradiation time and where maximum photo-product formation had occurred.

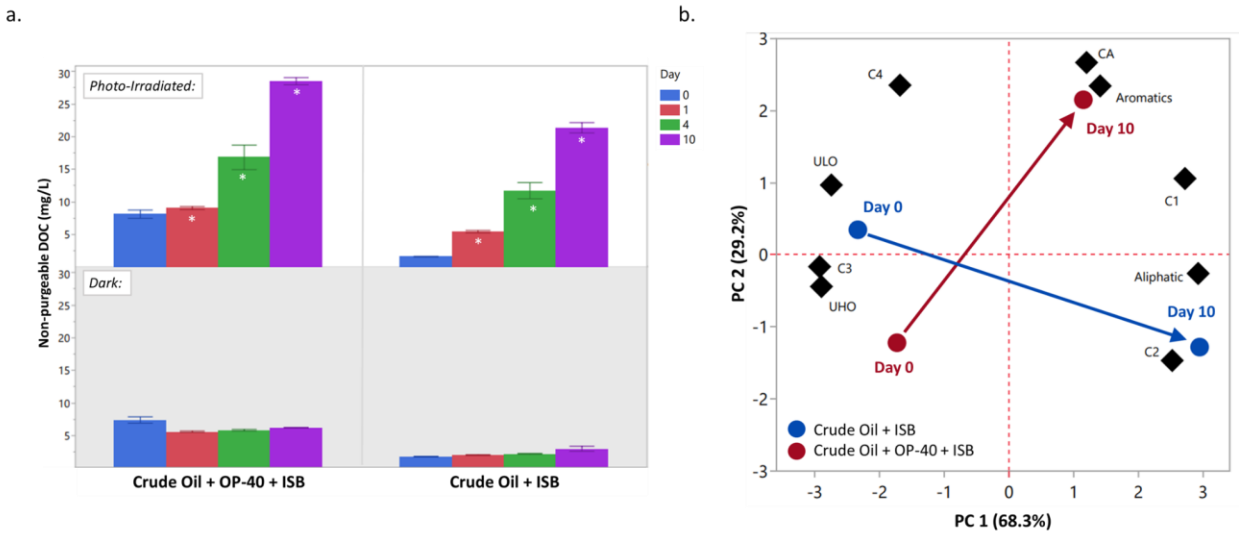

Figure 3.5. DOC and PCA plots of in-situ burned crude oil treatments. (a) Non-purgeable dissolved organic carbon under light and dark conditions (N=3, +/- 1 SE). Significance (*) between light and dark conditions for the same time point are denoted by pairwise comparisons (student's t-test, 95% confidence). (b) Principal Components Analysis of photo-irradiated ISB and OP40+ISB samples over time, day 0 and 10.

Photo-modified solubility of burned vs. herded burned crude oil

Following exposure to simulated sunlight, DOC concentrations for both *in-situ* burned (ISB) and OP40 (herder)+ISB increased relative to samples under total darkness (Figure 3.5A). Samples that were irradiated for 10-days yielded DOC concentrations that were 13.3 and 3.5 times higher than Day 0 for Oil+ISB and Oil+OP40+ISB, respectively (Table S8). Absent of photo-irradiation, DOC concentrations for Oil+OP40+ISB and Oil+ISB at Day 10 were 1.2 times lower and 1.7 times higher, respectively, than at Day 0. Furthermore, the overall DOC concentrations in Oil+OP40+ISB were higher than that of Oil+ISB (Figure 3.5A). This result indicates strongly that herder addition increases DOC relative to non-herded burned oil, and that herded burnt residues are capable of producing more photo-products that have more oxidized aromatic and oxidized condensed aromatic character (Figure 3.5B). These results are consistent with known pathways of formation, dissolution, and reactivity of other classes of pyrogenic black carbon substrates in aquatic ecosystems.[80-83] PCA plots revealed that samples at day 0 are dominated by C3 (tyrosine-like), and over 10-day sunlight exposure, modulate towards C1 (humic-like) (Figure 3.5B). Still, DOM_{HC} produced from each crude oil treatment yields terrestrial-like chromophoric products under sunlight exposure and there is a consistent HIX

increase for both crude oil treatment groups among irradiated samples (Table S8). Future research is needed to better classify specific byproducts and their corresponding toxicity.[15, 84-90]

Conclusions

This study presents preliminary, but important data comparing the photo-modification effects of spilled petroleum on solubility, which is a significant factor that accompanies weathering. We describe the temporal trends in molecular features among several common fuel types, primarily indicating an increased production of oxidized aliphatics and aromatics. Increased DOC concentrations were observed in all spilled samples after light treatment relative to no fuel, with the exception of gasoline, which did not weather into a non-purgeable form of DOM_{HC}. Most notable is the uniqueness of photo-products between crude oil and refined fuels. PARAFAC and FT-ICR MS analysis highlighted the continuum where spilled fuels and crude oil were oxidized into DOM_{HC} and were discernible by specific fluorescence components and molecular features. All crude oil samples, including burnt and herded burnt residues, exhibited humic-like fluorescence wavelengths while refined fuels exhibited an undefined component discernable from crude oil-derived and protein-derived components. PCA and HIX demonstrated that DOM_{HC} from refined fractions may not weather into humic-like components but rather C4-like, oxidized aromatics, and oxidized condensed aromatics. This difference sets an encouraging precedent for fuel photo-oxidation studies and detection protocols of these compounds in cold climates.

Chapter 4: Mechanisms of Plastic Particles and Films Photodegradation: The Role of Reactive Oxygen Species and Surface Chemistry Change

Abstract:

Efforts to understand degradation processes of plastic polymers in the environment and the risks posed to organisms is essential for future mitigation solutions. Total hydroxyl radical (·OH) trapping and steady state concentration were monitored for the photodegradation of micro and nanoplastics using a benzoic acid chemical probe under UV radiation. Polystyrene micro and nano particles as well as polyethylene terephthalate microparticles produced ·OH as a result of UV exposure. Hydroxyl radical production rates were higher for nanoplastics than for microplastics, owing to higher surface area of nano-size plastics. Initial experimentation on polystyrene in natural waters showed that plastic in natural organic matter had a decreased ·OH production rate. Alternatively, singlet oxygen ($^1O_2$) production from plastics under UV radiation remained indecisive using chemical probes described in this study. Cloud point extraction (CPE) successfully separated plastic particles from aqueous systems giving encouraging precedent for further studies of pollutants in the environment where isolation is needed. Finally, surface chemistry changes on plastic shopping bags were monitored for functional group changes as a result of UV radiation exposure. This study introduced methods that will help understand the behavior of plastic photodegradation in natural waters.

Introduction:

Plastic manufacturing, and subsequent pollution, is a present and future global reality. Presently, pollution by plastics in the environment is an emerging and widespread issue with 19-23 metric tons of plastic waste reaching aquatic environments per year.[91] This number is expected to reach 80 metric tons by the year 2030.[91] Plastic pollution is an emerging concern

because as plastic manufacturing increases over time (334 - 422 metric tons from 2010 to 2016) [92], total plastic waste has also increased (reaching 242 metric tons in 2016).[93, 94] Renowned examples of the severity of aquatic plastic pollution lies with the existence of large gyres of plastic in the Pacific, Indian, and Atlantic Oceans.[95, 96]

Primary sources of plastic can be deposited in waterways by directly releasing plastic into the ocean from ships, carried to the ocean from land, or from losses in transport.[97, 98] Items deposited include domestic articles such as packaging, shopping bags, beverage bottles, personal care products, cigarettes and more.[1, 97, 98] These items mostly fit in the criteria of mega (>100 mm diameter) and macro (<20 mm diameter) sized plastics, however micro (1-5000 μm) and nano (< 100 nm) sized plastics exist through secondary sources: Fragments of larger plastic pieces.[99] Mega and macro sized plastics can fragment to produce micro and nano-sized particles through mechanical, chemical, and oxidative processes often leading to the dissolution of plastic polymers into the environment.[28, 31] The distribution of all sizes of plastic in natural ecosystems poses a risk to biological systems; various human health conditions have been associated with plastic pollution such as obesity, diabetes and reproductive harm as well as damage to gut health, DNA, and lungs.[1, 100]

The degradation of micro and nano sized plastic particles is of utmost concern due to its wide presence in the environment, its larger surface area, and physical and chemical ability to interact with biological organisms. One of the most important types of degradation in the environment is photo-oxidation.[101] Research on plastic photo-oxidative degradation mechanisms and pathways has been ongoing for the last 50 years, leading to our current understanding today.[29, 31, 102-112] During this process, chromophores of plastic polymers may absorb UV radiation and produce polymer radicals or be converted to an excited triplet state by intersystem

crossing.[2, 31, 113] The excited species can react with ground state molecular oxygen and produce reactive oxygen species (ROS) such as hydroxyl radical (·OH) and singlet oxygen ($^1O_2$). ROS induce chemical bond cleavage and formation of functional groups containing oxygen.[30, 114] However, the subsequent propagation by which a polymer photodegrades depends on the polymer backbone: Carbon-carbon backbone or backbones containing heteroatoms.[31] Common plastic polymers with a carbon-carbon backbone are polystyrene (PS), polyethylene (PE), polypropylene (PP) and polyvinyl chloride (PVC), while plastics with heteroatoms are polyethylene terephthalate (PET) and polyurethane (PU).[28, 31] Photo-oxidation of carbon-carbon backbones occurs through the production of polymeric radicals through hydrogen abstraction and integration of oxygen into the polymer structure, both of which ultimately leads to chain scission, cross linking, and autoxidation. This process generates low molecular weight species such as carboxylic acids, alcohols, aldehydes, and ketones. Photo-oxidation of backbones with heteroatoms often produces carboxylic acid and vinyl end groups via ester bond attack.[27, 31, 32]

Recent studies have demonstrated that ROS induced chemical bond cleavage and formation of functional groups containing oxygen largely attributes to photodegradation of plastic.[30, 114] Hydroxyl radical and singlet oxygen have been shown to be produced from plastic microparticles placed in water after irradiation, providing evidence for formation of ROS from plastic. [114] However, this study did not examine free radical formation of micro or nano size plastics irradiated in water. ROS generated from microplastics in water suspensions was analyzed by Duan *et al.* using electron spin resonance spectrometry and also found that microplastics undergo attack by both hydroxyl radical and singlet oxygen.[30] This study quantified ROS and proposed new photodegradation pathways but did not test true nanosized plastics (<100 nm) and did not examine plastics in relevant environmental media. Despite

research on common polymer degradation mechanisms, little to no research has been done on ROS production from nanoplastics, especially in natural waters. Due to the high reactivity of free radicals, there have been multiple studies done to indirectly monitor for free radicals using chemical probes.[20-25, 115, 116] Zhou and Mopper proposed a mechanism to determine the production of ·OH from irradiated organic matter utilizing a chemical probe that reacts directly with ·OH.[25] Similarly, Haag and Hoigne used chemical probes to monitor the production of $^1O_2$ in natural waters.[20, 117] These methods have proved to be effective in studying ROS production from natural organic matter and crude oils.[20-25, 115, 116] This study utilized these techniques to determine ROS production from micro- and nano-size plastics.

Furthermore, mechanisms of polymer degradation have largely been studied using methods such as FTIR to examine chemical structure and functional group changes.[112] As a result of photo-irradiation, carbonyl groups and ketones were observed in exposed PE, PS, PP and PET[27, 112, 118, 119], and changes to functional groups were identified as a variable of degradation in plastic shopping bags and packaging materials.[120] However, these studies did not research plastic films in aquatic systems. Lee *et al.* and Walsh *et al.* performed irradiations on plastic bags and films and found that photo-degraded plastic films and commercial shopping bags produce DOM and inorganic additive leachates in natural waters.[11, 121] While these studies showed that polymers photodegrade to produce dissolvable, petroleum-derived DOM in water, surface chemistry changes were not observed. Little research has been done to characterize aging and functional group changes to plastic films (e.g. plastic bags) in water using FTIR.

It is clear that research gaps exist concerning the degradation and transport of ROS mediated pathways of plastic photo-oxidation, including micro- and nanoplastics as well as plastic films. More work is needed to understand the behavior of plastic pollution under sunlight and in

aquatic systems. This study focused on two key areas: 1) the hydroxyl radical and singlet oxygen production and steady state concentrations from commonly used plastic particles in water: polystyrene (PS) and polyethylene terephthalate (PET); and 2) the surface chemistry changes of plastic films and shopping bags in water. Additionally, research was conducted that will help isolate plastics in environmental media for future purposes of chemical analysis. Knowledge of these concepts will help further understanding of the fate and behavior of photodegraded plastic in the environment.

a. Role of Reactive Oxygen Species

Methods and Materials:

Materials:

Nanopure water was acquired from a Milli-Q water purification system (Sigma Aldrich). Dissolved natural organic matter (NOM) fulvic acid from Suwannee River, Georgia was obtained from the International Humic Substances Society. Benzoic acid (99%) and furfuryl alcohol (98%) were purchased directly from VWR. Polystyrene nanoparticles (50 nm) were obtained from Bangs Laboratories, polystyrene microparticles (10 µm) were acquired from Sigma Aldrich, and polyethylene terephthalate was purchased as a rod from Curbell Plastics (New York, USA) and ground to micro-sized particles using a cryo mill then sieved down to 75 µm diameter particles using precleaned metal sieves. 20-mL quartz tubes purchased from the Southern New England Ultraviolet Company (Rayonet, Connecticut, USA). 100-mL jacketed beakers were obtained from Chemglass (New Jersey, USA). Three-inch quartz lids were purchased from VWR. Acetonitrile (ACN) and trifluoroacetic acid (TFA), both HPLC grade, were obtained from VWR.

Hydroxyl Radical Trapping:

10 mM of benzoic acid (BA), pH altered to benzoate (pH 8), was prepared with 0.1 mg/mL of a plastic particle and diluted to a total volume of 17 mL with nanopure water. Plastic particles tested were polystyrene nanoparticles (PSn), polystyrene microparticles (PSm), and polyethylene terephthalate microparticles (PETm). For a comparison of water types, the same amounts of BA and PSn were prepared and diluted with 5 ppm of Suwannee River fulvic acid natural organic matter water (NOM water) in place of nanopure water.

Each solution was transferred to a 20 mL quartz tube. Quartz tubes were capped with aluminum foil and placed in a merry-go-round (MGR) photoreactor (Southern New England Ultraviolet Company, Rayonet) equipped with 350 nm lamps. Samples were irradiated for 24 – 72 hours. After irradiation, samples were removed from the photoreactor, filtered with 45 µm polypropylene syringe filters, transferred to 2 mL vials and acidified to pH 2 for detection of p-HBA using an Agilent 1200 series high-performance liquid chromatograph (HPLC) (Agilent Technologies, California, USA). An Agilent Zorbax Eclipse Plus C18 column (4.6 x 250 mm, 5 µm particle size) was used for separations. The mobile phases were acetonitrile with 0.1 % TFA (A) and 0.1 % TFA in nanopure water pH 2.5 (B). The gradient used was 20 % A initially, increasing to 50 % A linearly over 5 minutes, then kept constant at 50 % A for 5 more minutes. A flow rate of 1.00 mL/min was used. Absorbance spectra of the eluents were collected, and quantitation was performed at 254 nm.

For samples tested under solar simulation, 10 mM of BA (pH 8) was prepared with 0.1 mg/mL PSn and diluted to 30 mL with nanopure water. Samples were transferred to 100 mL jacketed beakers, secured with quartz lids, and placed in a solar simulator (Atlas XLS+) for 10 days. Each beaker was thermostatically controlled at 20°C and solar simulation parameters were set at instrument maximum irradiance (765 W/m^2).

The number of moles of hydroxyl radical can be calculated indirectly from the number of moles of p-HBA produced in the reaction. Based on the research of Zhou and Mopper (1990), for every 1 mol of p-HBA produced, 5.9 mol of OH is trapped.[25] These calculations were then utilized to determine the production rate of hydroxyl radicals from every plastic and water type.

Steady State Concentration:

A mixture of benzoic acid, plastic, and pure water was added to quartz tubes to a total volume of 17 mL. Benzoic acid was added in varied concentrations (1 – 10 mM). All samples were irradiated for 48 hours. The steady state hydroxyl radical concentration ($[OH]_{ss}$) was determined following the work of Zhou and Mopper (1990).[25]

Singlet Oxygen Steady State:

Furfuryl alcohol (FFA) was used as a chemical probe to monitor $^1O_2$ produced from polystyrene nanoparticles in nanopure water. The major product from the reaction of FFA and $^1O_2$ is 6-hydroxy-2H-pyran-3(6H)-one, shortened as 6-hp-one, and is easily monitored through HPLC. The method established by Haag *et al.* to determine steady state concentration of singlet oxygen using FFA as a chemical probe was applied to this study.[117] Here, the concentration of 6-hp-one is determined, converted to loss of FFA, then used to determine pseudo first order rate constant for the reaction with $^1O_2$.

FFA was prepared with 0.1 mg/mL of polystyrene nanoparticles and diluted to a total volume of 17 mL with nanopure water in 20-mL quartz tubes. Samples were capped with foil

and placed in a MGR photoreactor equipped with 350-nm lamps. Samples were irradiated for five to 60 minutes. Since FFA absorbs at < 290 nm, 350-nm lamps were chosen for irradiations. Following irradiation, samples were filtered with 45 µm polypropylene syringe filters and transferred to 2 mL vials for analysis with HPLC. The HPLC mobile phases were prepared as follows: Acetonitrile (A) and nanopure water (B). The mobile phases were kept constant at 20 % A for eight minutes. A flow rate of 1.00 mL/min was used. Absorbance spectra of the eluents was collected, and quantitation was performed at 219 nm.

Results and Discussion:

This study exhibits the production of hydroxyl radical and singlet oxygen from the irradiation of micro- and nano-sized plastic particles. For hydroxyl radical determination, this was done in two ways: First by determining the total moles of hydroxyl radical produced by adding a large amount of a chemical probe which would react with all hydroxyl radicals produced and then increasing the time at which the plastic would be irradiated; and second, by adding a chemical probe in varying concentrations in order to determine the steady state concentration of hydroxyl radical. In addition to particle size, plastic and water type were altered to examine changes in different photochemical systems.

For singlet oxygen determination, research and subsequent results focus on the concentration of product formed from reaction of FFA and $^1O_2$ under a pseudo first order rate constant. FFA was added at low concentrations to react with singlet oxygen species. Irradiation times in which samples were exposed were increased. Using the known rate constant of furfuryl

alcohol, the initial concentration of FFA, and the concentration of product formed from the reaction and the subsequent concentration of singlet oxygen could be explored.

Total hydroxl radical trapping:

p-HBA and ·OH were produced in all plastic irradiations, while control samples without plastic or light produced no detectable *p*-HBA/·OH. ***Figure 4.1*** shows the production of ·OH from PSn, PSm, PETm, and PSn + NOM water versus control exposures of only BA in nanopure water. The lack of *p*-HBA formed in control experiments shows that ·OH trapped in all photo-exposures with plastic is indeed a result of ·OH production from plastic photo-oxidation. ***Table 4.1*** shows a comparison of production rates between different plastic types: PSn, PSm, and PETm in nanopure water, as well as different water and light types: PSn in NOM water, and PSn under solar simulation.

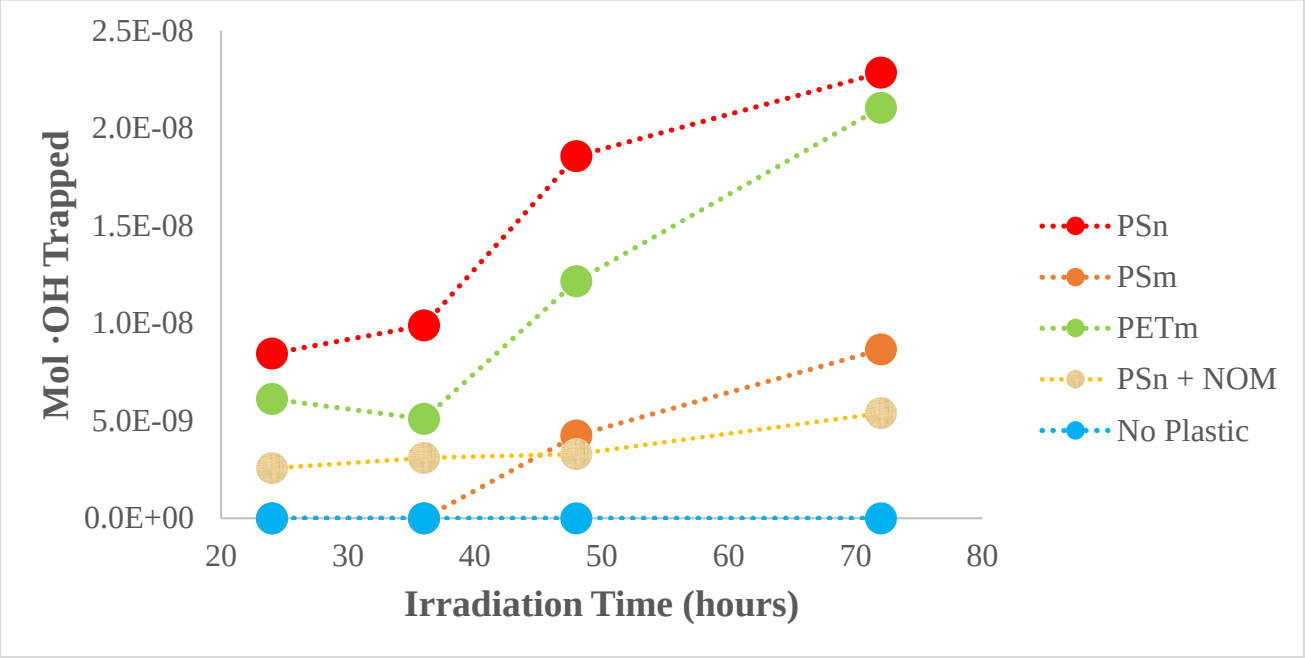

Figure 4.1. Moles of ·OH produced under UV irradiation from 24 to 72 hours for PSn, PSm, PETm, and control exposures in nanopure water; and PSn in NOM water.

Between PSn and PSm, PSn had higher production rates than PSm exhibiting that the rates of ·OH production is correlated to size. Nanosize particles had higher exposure surface areas than microsize particles, thereby resulting in faster production rates of reactive transients. Between microsize particles, PET had higher production rates than PS. This could be due to a multitude of reasons: 1) PS is manufactured into spheres while PET is milled into jagged fragments, jagged fragments increase surface area and thus increase areas susceptible to photo-oxidation; 2) milled polymer material contains a range of sizes from micro to nano particles which would also increase total exposure surface area; and 3) hydroxyl radical is produced according to different mechanisms in PET versus PS. It has been found that PET and PS degrade similarly due to the presence of aromatic rings in the plastic polymer; the addition of hydroxyl radical to aromatic rings leads to chain scission and the presence of carboxylic acid end groups.[30-32] However, it has also been discussed that the ester bond of the PET polymer breaks forming carboxylic acid and vinyl end groups.[27, 31, 32] Possible differences in hydroxyl radical production from plastic degradation and higher amounts produced from PET could be due to cleaving of ester bonds versus the complete lack of heteroatoms in the PS polymer backbone.

	Average Rate of ·OH Production (mol/s)				
	PSn ($\times 10^{-14}$)	***PSm*** ($\times 10^{-14}$)	***PETm*** ($\times 10^{-14}$)	***PSn + NOM water*** ($\times 10^{-14}$)	***PSn + Solar Simulation*** ($\times 10^{-11}$)
Average Rate =	9.2	2.7	6.5	2.2	1.4
Standard Deviation=	1.3	0.2	1.8	1.0	0.4

Table 4.1. Production rates of OH from plastic types: polystyrene nanoparticles (PSn), polystyrene microparticles (PSm), polyethylene terephthalate microparticles (PETm); and from different water sources: PSn in NOM water (N=12 ± s.d.). PSn under solar simulation represents production from triplicate samples (N=3 ± s.d.).

Hydroxyl radical had a lower observed production rate from polystyrene in NOM as opposed to that in nanopure water. NOM easily absorbs light and produces reactive transients

due to its aromaticity, meaning that NOM can either have the ability to promote photodegradation due to the production of reactive species, or to act as a light screening agent so that PSn is unable to absorb any photons.[32] NOM can also influence and even inhibit ROS degradation performance with plastic by acting not only as a sensitizer but a scavenger.[32] The lower production rate of polystyrene in NOM is likely due to competitive inhibition as NOM acts as a scavenger to hydroxyl radicals. These studies show initial change in ROS concentration due to scavenging in natural waters versus that in nanopure water but are largely indecisive as to the exact relationship and mechanism of plastic degradation in NOM water. Applying additional analytical methods, such as FTIR of surface chemistry changes or electron spin resonance spectrometry of reactive transients, would help understand plastic pollution degradation in natural waters.

Finally, PSn was also reacted in a solar simulator to allow for initial insight of experimentation parameters using this light source. At 10-days of irradiation under solar simulation, polystyrene produced ·OH at a production rate of $1.44 \pm 0.41 \times 10^{-11}$ mol/s which was orders of magnitude larger than the ·OH production rate of PSn in the MGR photoreactor (***Table 4.1***). Solar simulation exposure would allow plastic particles to be subject to excitation wavelengths and thus yield more photo-oxidative products. This value gives encouraging precedent for future exposure studies using solar simulation to determine total hydroxyl radical and steady state concentrations. Despite long irradiation times, solar simulation might serve as a source of more environmentally relevant data.

Steady state determination

Hydroxyl radical has a low steady state concentration in natural waters, which makes directly monitoring its production difficult.[25] Therefore, a chemical probe is used in various

concentrations to conduct competition kinetics experiments with scavengers. The hydroxyl radical reaction rate is measured in the presence of an added scavenger at different probe concentrations. This study examined the role of plastic polymers as a source of hydroxyl radicals. Hydroxyl radical reaches a steady state concentration when the formation rate (F_{OH}) is equal to the rate of reaction with scavengers (S) in the sample, including any added probe (P), R_S and R_P, respectively. This relationship is given by ***Equation 1***.

(1) $F_{OH} = R_S + R_P$

The steady state concentration of hydroxyl radicals $[OH]_{SS}$ produced under these conditions is measured through a pseudo first order reaction with a chemical probe with a known rate constant (k_P = 5.87 x 10^9 $M^{-1}s^{-1}$) using multiple concentrations of the probe across experiments.[122] The pseudo first order rate constant (k'_S) and $[OH]_{SS}$ are then calculated from ***Equations 2 and 3***.

(2) $\frac{1}{R_P} = \frac{1}{F_{OH}} + \frac{k'_S}{F_{OH} \times k_P} \times \frac{1}{[P]}$

(3) $[OH]_{SS} = \left[\frac{(k'_S + k'_P)}{(k'_S \times k'_P)}\right] \times R_P$

The plot of $1/R_P$ and 1/[P] gives a line where the slope can be used to find the pseudo first order rate constant (k'_S) and the y-intercept is equal to $1/F_{HO}$. $[OH]_{SS}$ can then be found from this information (***Equation 3***).

Figure 4.2 exhibits a plot of $1/R_P$ and 1/[P] where the slope and intercept of this line are used to determine k'_S and F_{OH}, respectively. The average $[OH]_{SS}$ produced in this system was 5.74 ± 1.81 x 10^{-17} M. Average values of $[OH]_{SS}$ from all triplicate samples of PSn in nanopure water, PSn in NOM water, and PETm in nanopure wate are included in ***Table 4.2*** and were calculated following equations included above. Compared to the value reported previously for

PSn in nanopure water, PSn in NOM water had a larger steady state concentration of 1.04 ± 0.52 x 10^{-16} M. The increase of steady state concentration in NOM waters is expected due to the fact that NOM is an added source of hydroxyl radicals. PSn and PETm in nanopure water did not show significant differences between one another. A possible reason is that the production and scavenging of ·OH in both PS and PET initially occurs through the aromatic rings of both polymers.[30-32] 48-hours of irradiation time may not be long enough to notice significant changes to ·OH steady state concentrations. Further research and controls should be experimented with to have a better understanding of how size and plastic type differ.

PSm steady state concentrations were not established due to the need to increase radiation time to obtain results. As established previously, there is lower production of hydroxyl radicals in microparticles than in nanoparticles.

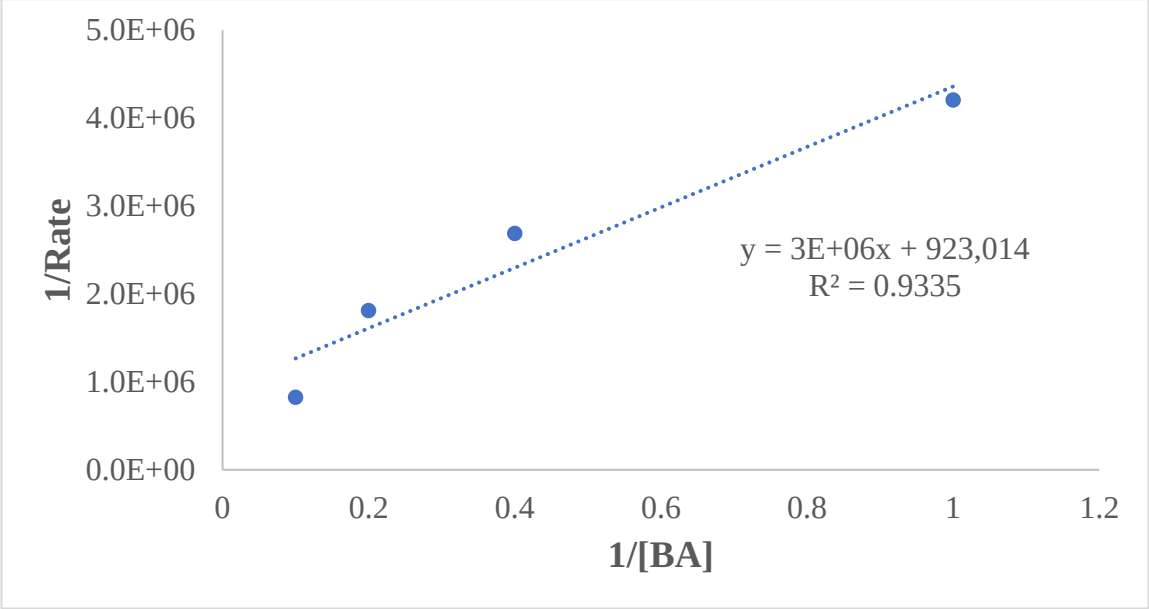

Figure 4.2. Plot of 1/[BA] vs. 1/Rate for the irradiation of 0.1 mg/mL PSn in 17 mL of 10 mM benzoic acid in nanopure water. The slope and intercept of this line are used to find F_{HO} and k'_S to determine $[OH]_{SS}$. This relationship was determined and employed for each plastic type.

	Average [OH]$_{ss}$ **(M x 10^{-17})**

	PSn	***PSn (in NOM water)***	***PETm***
Average [OH]$_{ss}$ =	5.7	10.4	4.2
Standard Deviation =	1.8	5.2	0.7

Table 4.2. Average $[OH]_{SS}$ of polystyrene nanoparticles (PSn) in nanopure water, PSn in NOM water, and polyethylene terephthalate microparticles (PETm). Samples are irradiated in triplicates.

Singlet Oxygen Steady State Determination

The production of singlet oxygen from polystyrene nanoparticles were determined. The formation of 6-hp-one from the reaction of FFA and $^1O_2$ was monitored using HPLC where the concentration of 6-hp-one was determined and converted to singlet oxygen steady state concentration ($[^1O_2]_{SS}$). Using a kinetic model approach by Haag *et al.*, pseudo first order kinetics was applied to the loss of the chemical probe and the production of 6-hp-one to determine $[^1O_2]_{SS}$.[117] It was understood that the concentration of singlet oxygen produced from an organic source can be monitored if FFA is added in a low enough concentration to allow for minimal alteration of the singlet oxygen concentration.[117] Under these conditions, ***Equations 4-7*** were employed:

(4) $R = k\,[^1O_2][FFA]$

(5) $R = k'\,[FFA]$

(6) $k' = k\,[^1O_2]_{SS}$

(7) $[^1O_2]_{SS} = \frac{k'}{k}$

These equations exist where R is the rate of reaction for FFA with $^1O_2$, k is the second order rate constant for FFA with $^1O_2$ ($k = 1.2 \times 10^8\ M^{-1}s^{-1}$)[123], and k' is the pseudo first order rate constant which can be obtained from the slope of ln[FFA] versus exposure time. ***Figure 4.3*** gives a plot of ln[FFA] vs. time from FFA+PSn and FFA only treatment groups where the slope

of each line was used to determine *k'* and subsequently $[^1O_2]_{SS}$ for each treatment group. The slope of FFA+PSn is -6.88 x 10^{-5}, while the slope of FFA-only is -6.55 x 10^{-5}, (p = 0.71). Statistical analysis shows that there is no significant difference between k' values of FFA+PSn and FFA only. ***Table 4.3*** shows $[^1O_2]_{SS}$ for PSn with FFA and FFA only. However, under the current exposure conditions, there is a degree of interference from FFA chemical probe, $[^1O_2]_{SS}$ from these results are not significantly different, and little mechanistic determinations can be established from the role of $^1O_2$ in plastic degradation. Possible changes to this experiment might yield effective results for plastic degradation, these changes include repeating this exposure under solar simulation and increasing degradation time for over 10-days.

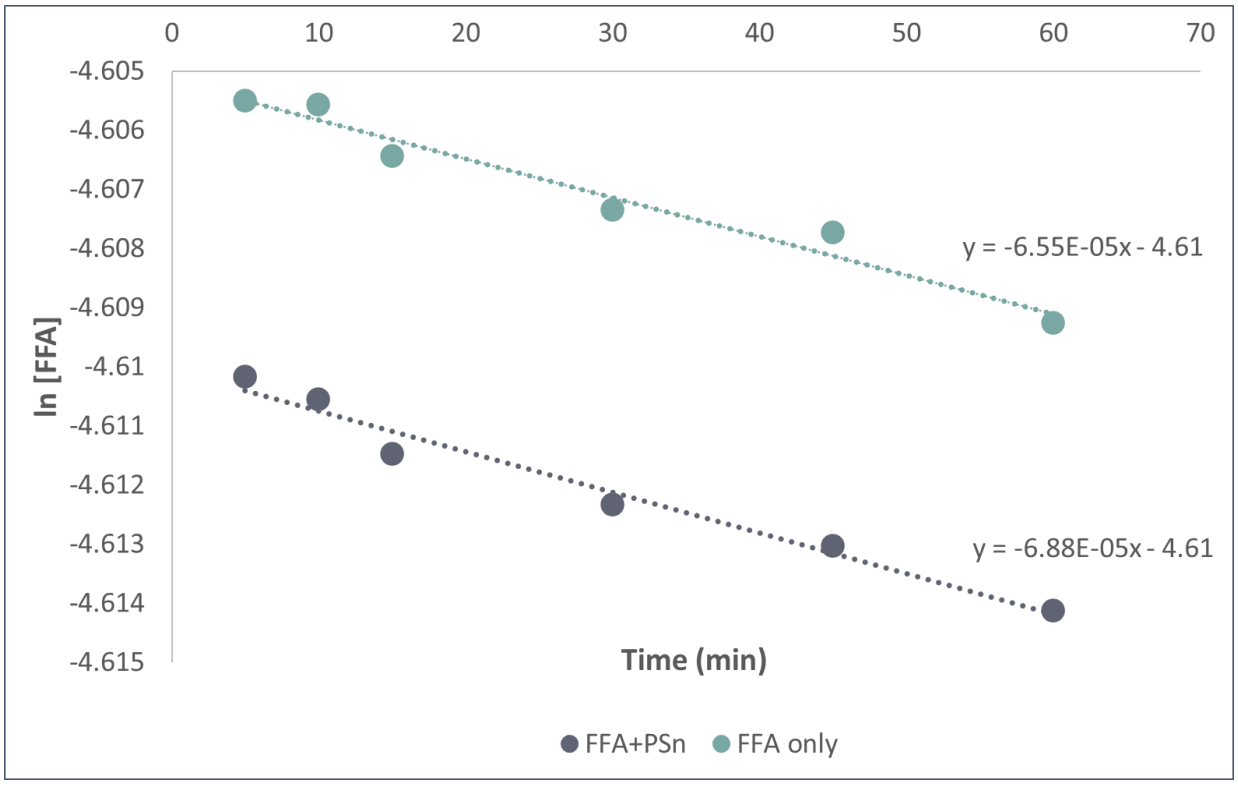

Figure 4.3 Plot of ln [FFA] versus exposure time for FFA+PSn and FFA only treatment groups. The slope of each line was used to find the pseudo first order rate constant (k') for respective groups. The slope of FFA+PSn is -6.88 x 10^{-5}, while the slope of FFA only is -6.55 x 10^{-5}, (p = 0.71).

$[^1O_2]_{SS}$ (M x 10^{-13})	
FFA + PSn	FFA only
5.74	5.46

Table 4.3 Steady state concentration for singlet oxygen ($[^1O_2]_{SS}$) produced from FFA+PSn and FFA only. $[^1O_2]_{SS}$ produced from PSn irradiated under UV light for up to 60 minutes of exposure (FFA + PSn). FFA was used as a chemical probe; control experiments are included (FFA only).

b. Isolating Plastic Particles in Aqueous Media: Cloud Point Extraction

To determine a method of plastic particle isolation from complex aqueous media, cloud point extraction procedures were tested. Plastic particles undergoing extraction from this method were examined by FTIR to confirm that no aging or functional group changes occurred from the procedure.

Methods and Materials:

Materials

Polystyrene microplastic with a diameter size of 10 µm was obtained from Sigma Aldrich. All reagents used, including magnesium sulfate and TX-45 surfactant, were purchased from VWR and were used without additional purification. Nanopure water obtained from a MilliQ purification systems was used throughout the extractions.

Cloud Point Extraction (CPE)

The cloud point extraction technique closely follows the research of Zhou *et al*. and is described in detail here.[124, 125] First, 10 mL of 1.0 mg/mL suspension of polystyrene microplastic in nanopure water was added to a 15 mL centrifuge tube. 30 µL of 10% (m/v) TX-45 aqueous

solution was added next, followed by the addition of 100 µL of 1 M MgSO4 solution. The solution was mixed, and the centrifuge tube was placed in water bath set at 45°C for 15 minutes. The tube was then centrifuged at 3000 rpm for 10 minutes at 4°C. At this stage, the TX-45-rich phase with plastic particles separated from the salt-rich phase. The surfactant rich phase was removed from the tube and transferred to a 2-mL glass amber vial, then placed in a muffle furnace for 3 hours controlled at 190°C to remove the TX-45 surfactant from the plastics.

Fourier Transform Infrared Spectroscopy (FTIR):

After CPE, samples were tested with FTIR to ensure that the isolation technique yielded pure plastic product. Attenuated total reflection Fourier transform infrared spectroscopy (ATR-FTIR) was used to monitor possible aging and changes to the material's functional groups. Spectra was obtained using an Agilent Cary 630 FTIR with a diamond crystal and recorded in the range of 650-4000 cm^{-1}, with a resolution of 4 cm^{-1} and scan number of 100. The samples were in contact with the diamond crystal for spectra collection. The common polymer functional groups were normalized and compared to common polymer spectra of an internal library. In this way, a qualitative and quantitative analysis of the polymer sample is obtained.

Results and Discussion:

Separation of plastic particles from aqueous media was evident using CPE following the technique outlined by Zhou *et al*.[125] ***Figure 4.4*** shows a visualization of CPE before and after thermal treatment and centrifugation. While there is no separation of plastics with the aqueous

media observed in ***Figure 4.4a***, there is clear separation evident between plastic particles at the bottom of the vial in ***Figure 4.4b***.

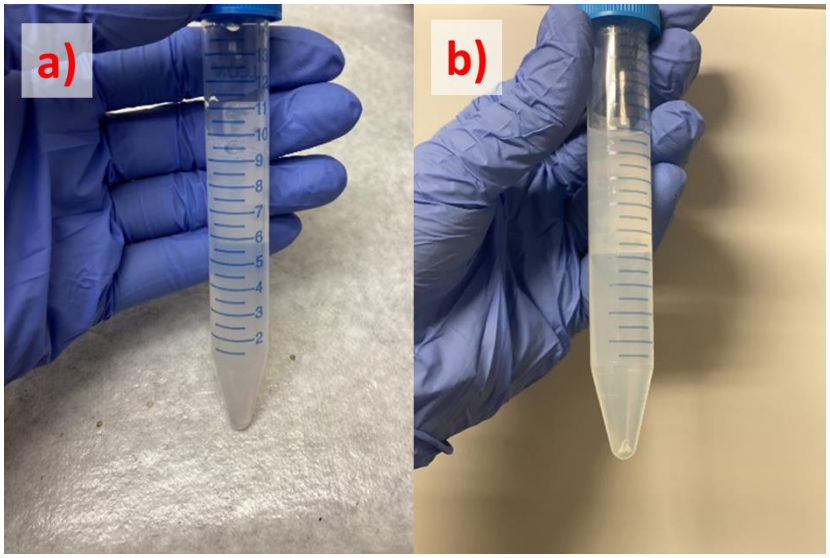

Figure 4.4. Visual of centrifuge tube before and after cloud point extraction. A) Before CPE temperature treatment and centrifugation; no separation is observed. B) After CPE centrifuge step; surfactant-rich phase with polystyrene microparticles is evident at bottom of the tube.

To ensure that the technique yields only plastic particles, the product of CPE was measured on FTIR. FTIR group frequencies observed in pure polystyrene before CPE (***Figure 4.5a***) show a C-H aromatic stretch at 3000 – 3100 cm^{-1} and a C-H aliphatic stretch at 2850 - 2970 cm^{-1}. A C=C aromatic bend is noted at 1450 - 1510 cm^{-1} and a vinyl C-H in-plane bend at 1410 - 1420 cm^{-1}. Several small peaks can be observed between 1500 – 2000 cm-1 which can be attributed to aromatic combination bands.[126] In the fingerprint region, two strong peaks are observed between 600-800 cm^{-1} which is indicative of monosubstituted C-H bonds in alkenes and in aromatics. Polystyrene microparticles before CPE was done clearly match the spectra for pure polystyrene; this spectra served as a basis for comparison for CPE separated particles (***Figure 4.5a***). After CPE was conducted, pure polystyrene particles continued to closely match the spectra for polystyrene with no other added materials present (***Figure 4.5b***). However,

qualitative results show that peak amplitude decreased slightly which indicate that less bonds in the fingerprint area exist. Loss of single bonded C-H bonds could be affected by factors manipulated in CPE isolation such as high temperatures and hydrolysis.

The observations reflected throughout the CPE process as well as the lack of impurity to the polystyrene particles in FTIR spectra give encouraging precent for further use of this technique in more complex sample mixtures. Efforts to separate plastic particles from environmental media is of particular interest due to the existence of plastic pollution in water habitats. In order to study the photochemical degradation of plastic in more complex environmental media, methods of separation and extraction techniques that leave minimal damage on a plastic polymer are critical. By using cloud point extraction, analytical monitoring may be conducted on photo-effected environmental samples with little external contamination from separation.

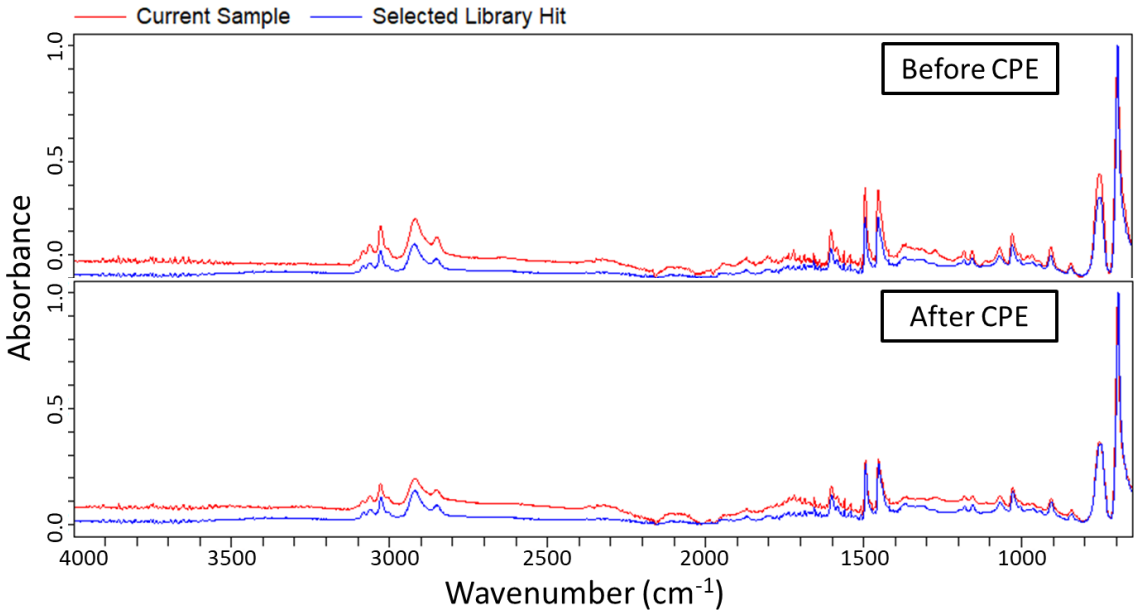

Figure 4.5. Pure polystyrene microparticles tested on ATR-FTIR (a) before CPE and (b) after CPE. The red line signifies the sample tested, while the blue line represents a material in the Agilent ATR library with peaks matching the given sample. The samples both matched library settings for common polystyrene peaks.

c. Surface Chemistry Changes on Plastic Films and Bags

To observe surface changes to commonly used and polluted plastic substances, both additive-free films and shopping bags were irradiated under UV light. Surface chemistry was analyzed by ATR-FTIR before and after irradiation of plastic bags and films.

Methods and Materials:

Materials:

Additive-free polyethylene and polystyrene films (both 0.05 mm thick) were purchased from Goodfellow and cut into 2 cm x 2 cm squares. Target, Walgreens and Lowes bags were obtained directly from respective stores and cut into 2 cm x 2 cm squares. Each bag had a different dye coloration with Target being the lightest color to Walgreens being the darkest. Swagelok steel tube fittings were obtained from Swagelok Louisiana (New Orleans, Louisiana, USA). All plastic films and bags were used as received.

Plastic Films and Grocery Bag Exposures:

Two types of plastic films (PE and PS) and three types of shopping bags (Target, Walgreens, Lowes) were irradiated. Each film and bag were secured in ¼ inch Swagelok fittings, respectively, to normalize irradiated surface area of each plastic (***Figure 4.6***). Each Swagelok fitting with a plastic bag and film was placed in a glass beaker and filled with nanopure water to completely cover each sample. The fittings were placed in a MGR photoreactor equipped with 300-nm lamps for up to 72 hours. An Agilent Cary 630 FTIR was used for all ATR-FTIR spectra collection. FTIR instrumentation parameters precisely follow those outlined in Chapter 4b.

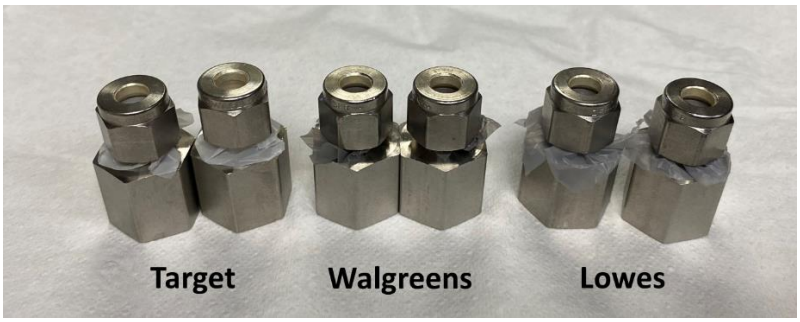

Figure 4.6. Target, Walgreens, Lowes bags secured in ¼ inch Swagelok fittings.

Results and Discussion:

Pure, additive-free PE and PS films were irradiated under 300-nm lamps in a MGR photoreactor for up to 72 hours. Both types of films were tested with ATR-FTIR to determine if any changes to the plastic film surface resulted after exposure to UV-radiation. PE films before and after irradiation have peaks that match characteristic PE peaks of Agilent's library for plastic samples in ***Figure 4.7a***. There is a CH_2 asymmetric C-H stretch at 2920 cm^{-1}, a CH_2 symmetric C-H stretch at 2850 cm^{-1}, a CH_2 bend at 1470 cm^{-1}, and a split CH_2 rock at 720-730 cm^{-1}. Peaks measured for PS samples before and after irradiation also directly match characteristic PS peaks in the software's library (***Figure 4.7b***). Little change is exhibited in the functional groups present in each sample type. Despite how thin the tested plastic films were, it is likely that 72-hours under direct UV-light is not enough time to observe noticeable changes to surface functional groups; studies have shown surface chemistry changes in polyethylene films for up to 60 days of constant UV-light.[127] The plastic samples used fall underneath the criteria of macro-sized particles (>1mm diameter); a larger diameter size significantly diminishes the affected surface area owing to the slow degradation seen here. It is also important to note that very little change to color and consistency was observed for these plastics.

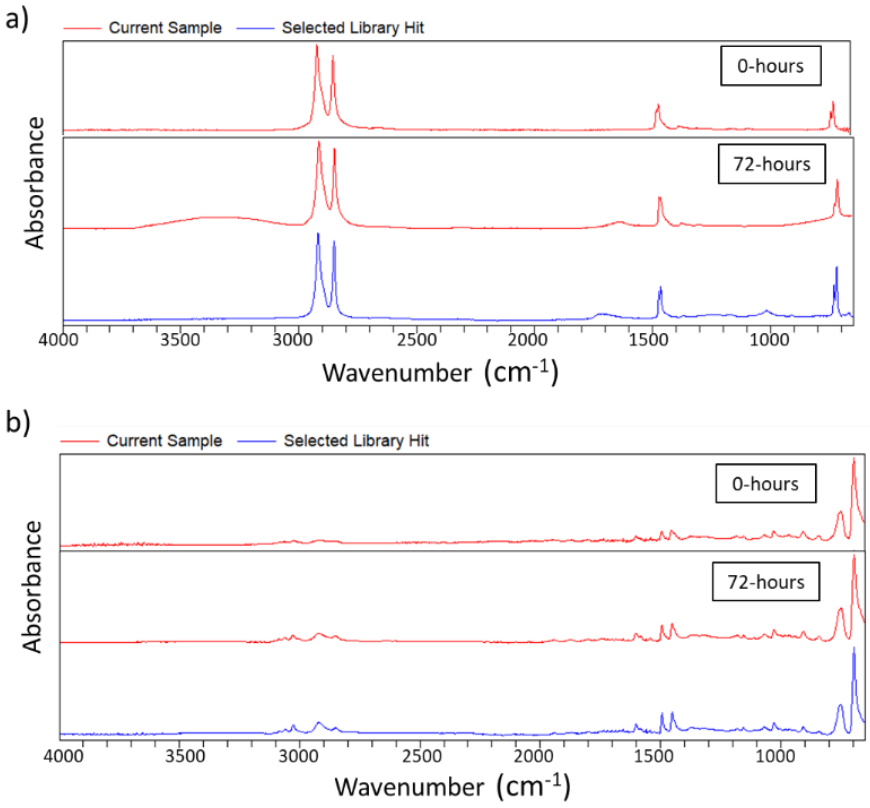

Figure 4.7. ATR-FTIR absorbance spectra of (a) pure polyethylene films (0.05 mm) at 0- and 72-hours irradiation, and (b) pure polystyrene films (0.05 mm) at 0- and 72-hours irradiation.

Using the same methods, commonly used shopping bags were tested under ATR-FTIR to determine if changes to functional groups are present after irradiation. It is well known that these plastic bags contain large amounts of polyethylene polymers.[121] ***Figures 4.8 – 4.10*** show characteristic peaks for polyethylene in each shopping bag with two large C-H stretching peaks at 2920 cm^{-1} and 2850 cm^{-1}, however other peaks are present: two sharp peaks at ~870 and 720 cm^{-1} which may signify TiO_2 and $CaCO_3$ additives, and a large evidently split peak ~1450 cm^{-1} could be due to C-H bending vibrations.[120] After 72 hours of irradiation time, there is evident decrease in absorbance of peaks at ~870 and 720 cm^{-1} in each plastic bag as well as the split peak around 1450 cm^{-1}, but very little in C-H stretching peaks at 2920 and 2850 cm^{-1} (***Figures 4.8-4.10***). Evidence of photodegradation of polyethylene includes hydrogen abstraction and oxygen

addition resulting in the formation of double bonds between carbon and oxygen (C=O) as well as between carbon and carbon (C=C) in the polymer backbone.[32] This effect is not evident in the FTIR spectra of irradiated plastic bags. This could possibly be due to the fact that conjugated double bonds are less stable to the effects of photodegradation and so the polymer breaks into smaller fragments. Less intense peaks at 1450 cm^{-1} (C-H bending vibrations) among all plastic bags could be the result of this process.

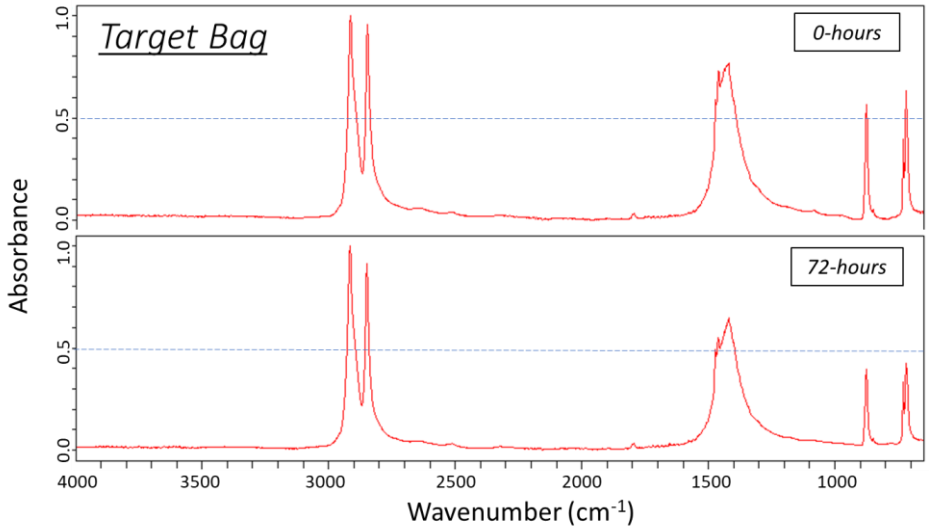

Figure 4.8. ATR-FTIR absorbance spectra of an irradiated Target bag at 0- and 72-hours under 300-nm lamps.

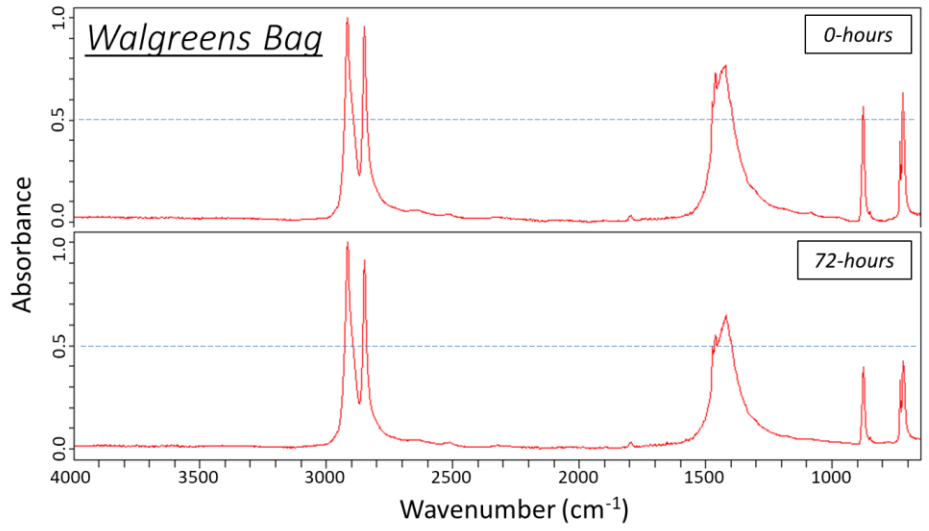

Figure 4.9. ATR-FTIR absorbance spectra of an irradiated Walgreens bag at 0- and 72-hours under 300-nm lamps.

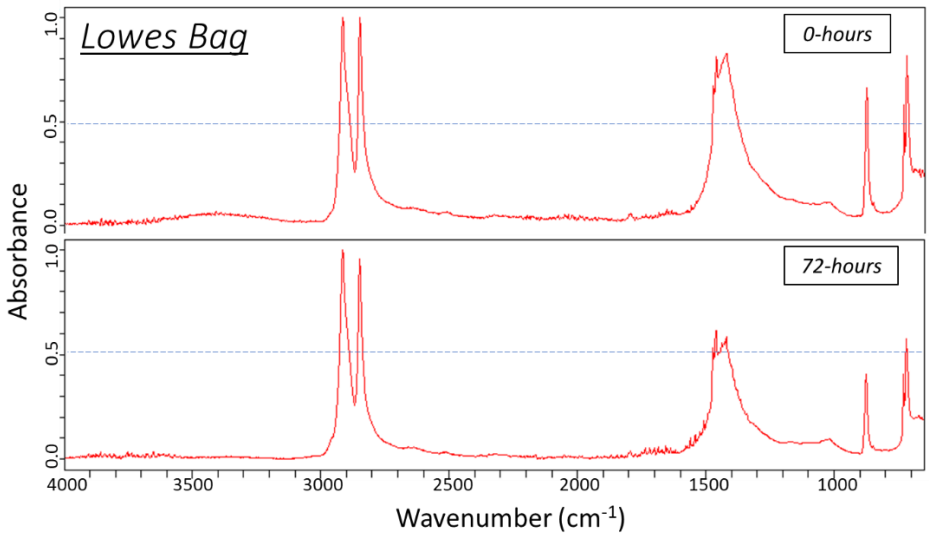

Figure 4.10. ATR-FTIR absorbance spectra of an irradiated Lowes bag at 0- and 72-hours under 300-nm lamps.

Plastic PS and PE films (***Figure 4.7a-b***) showed very little functional group change due to 72-hours of photodegradation, while plastic bags largely made of polyethylene showed noticeable changes of photodegradation after 72-hours. A possible reason for this is that the plastic PS and PE films were additive free, while it is possible that the plastic shopping bags used had an additive within its polymer structure. It has been found that plastic retail bags contain additives that may act as UV screeners, exited state deactivators, hydroperoxide decomposers, and radical scavengers. [27, 48, 121] One common additive detected in plastic bags is TiO_2 which is used as a white pigment in the bags.[27] Further examination into additive composition in commercially available shopping bags is imperative to understanding "real world" pollution photodegradation.

Conclusions:

Baseline experimentation on studying plastic in environmentally relevant media is established in this study: ROS production of plastic in nanopure and NOM water, the isolation of plastic from aqueous media, and the surface photochemistry changes of commonly used plastic

bags. This study also establishes that further research into plastic degradation mechanisms in natural waters is necessary.

By using chemical probes with known rate constants, total moles and steady state concentrations of ·OH and $^1O_2$ were able to be monitored indirectly. It has been established in this study that ·OH is readily produced from UV-degraded nano and micro-sized plastics, while multiple interferences with $^1O_2$ monitoring under UV-degradation still exist. As expected, nano-sized plastics produce more ·OH than micro-sized plastics due to increased surface area. Little to no differences to ·OH production were noticed between PS and PET plastic types likely due to immediate reaction with aromatic structures. Elongating exposure time is expected to uncover changes to ·OH production between PS and PET due to differences in chemical bonds of the two polymer backbones. Additionally, the present study shows that degradation of nanosized plastic in the presence of NOM water adds complexity to current methods of ROS monitoring due to natural water's ability to be a source and scavenger of reactive transients. There is yet room to establish if NOM inhibits or promotes the production and degradation of plastic by ROS.

The present study also exhibits initial steps to understand surface chemistry changes to shopping bags commonly polluting the environment. Small decays to absorbance spectra show that shopping bags are being affected by UV-light in water, but no additional functional groups are present at 72-hours exposure. To view further evidence and changes to the plastic material, it is suggested that exposure to UV-radiation should be elongated to observe possible changes to functional groups.

Further experimentation of ROS production and utilization in plastic degradation, and subsequent surface chemistry changes, is needed. The apparent production of ROS from plastic, namely ·OH, can have both helpful and harmful effects on environmentally relevant scenarios:

ROS production is helpful in that photo-oxidation can be deemed a tool to degrade large amounts of plastic in aquatic ecosystems, but is also harmful in that ROS can increase solubility of organic matter thereby increasing the likelihood of plastics entering the bloodstreams of organisms. Regardless, additional study into the behavior of ROS and subsequent functional group changes, especially of real-world plastic pollutants, is essential to understanding the behavior and toxicity of plastic pollution in aquatic ecosystems.

Chapter 5: Future Work

Optical Methods for Monitoring Oil Photoproducts in the Arctic

Future studies with ANS crude oil and refined fuels should include large scale experimentation using similar methods of photoproduct monitoring employed in this thesis. Large-scale oil and fuel spills have the potential of adding supplemental variables not included in laboratory settings, such as mechanical breakdown of wind, rain, and waves, as well as the addition of biotic degradation pathways. Using optical techniques such as fluorescence spectroscopy and molecular analytical techniques such as FT-ICR MS, photoproducts of large-scale and real-world degradation pathways can be determined.

Reactive Transients

Determination of ·OH from nano and micro plastics with hydrocarbon backbones, such as PE, should be tested in comparison to plastics with natural chromophores, such as PS and PET. Additionally, experiments should be lengthened for all degradation exposures for up to 60 days of UV-degradation, and more for solar simulation. Determination of $^1O_2$ steady state concentration under short-wavelength UV radiation using FFA as a chemical probe is not an effective method. However, experiments discussed in this thesis are preliminary and encourage further experimentation where singlet oxygen production from degraded plastics might be measurable and significantly different under solar simulation.

It has been shown that plastics have the ability to transport other persistent organic pollutants. In this way, persistent organic pollutants should be added to plastic degradation experiments to determine the effect of OH production when plastics adsorb to pollutants.

Persistent organic pollutants to be tested include polycyclic aromatic hydrocarbons, pharmaceuticals, and per and polyfluoroalkyl substances. Methods of OH production should use the methods utilized in this thesis.

Surface Chemistry and Real-World Plastic Pollution

FTIR has been used extensively to determine degradation mechanisms and observe changes to surface functional groups of plastic polymers. Similar methods should be used for plastic particles collected from the environment. Continuing laboratory-controlled studies of photo-degraded plastic bags should be continued under UV-radiation with longer irradiation times. Present exposures lasted for up to three days, while other studies have exposed plastic under UV-radiation for upwards of 60 days.[127] Additionally, it is well known that most manufactured and used plastic contains metal additives. ICP-MS should be used to test for Ti and Ca initially.

References

1. Iroegbu, A. O. C.; Ray, S. S.; Mbarane, V.; Bordado, J. C.; Sardinha, J. P., Plastic Pollution: A Perspective on Matters Arising: Challenges and Opportunities. *ACS Omega* **2021,** *6* (30), 19343-19355.
2. Coxon, J. M.; Halton, B., *Organic photochemistry*. 2nd ed.; Cambridge University Press: New York;Cambridge [Cambridgeshire];, 1987.
3. Kelen, T., *Polymer degradation*. Van Nostrand Reinhold Co: New York, 1983.
4. Prince, R., Crude Oil Releases to the Environment: Natural Fate and Remediation Options. 2014.
5. Steinberg, C. E. W.; Paul, A., Photolysis. In *Encyclopedia of Ecology*, Jørgensen, S. E.; Fath, B. D., Eds. Academic Press: Oxford, 2008; pp 2724-2732.
6. Zafiriou, O. C.; Joussot-Dubien, J.; Zepp, R. G.; Zika, R. G., Photochemistry of natural waters. *Environmental Science & Technology* **1984,** *18* (12), 358A-371A.
7. Kaplan, L. A.; Cory, R. M., Chapter 6 - Dissolved Organic Matter in Stream Ecosystems: Forms, Functions, and Fluxes of Watershed Tea. In *Stream Ecosystems in a Changing Environment*, Jones, J. B.; Stanley, E. H., Eds. Academic Press: Boston, 2016; pp 241-320.
8. Zhao, S.; Xue, S.; Zhang, J.; Zhang, Z.; Sun, J., Dissolved organic matter-mediated photodegradation of anthracene and pyrene in water. *Scientific Reports* **2020,** *10* (1), 3413.
9. Bekins, B. A.; Cozzarelli, I. M.; Erickson, M. L.; Steenson, R. A.; Thorn, K. A., Crude Oil Metabolites in Groundwater at Two Spill Sites. *Groundwater* **2016,** *54* (5), 681-691.
10. Hill, V. J.; Zimmerman, R. C., Characteristics of colored dissolved organic material in first year landfast sea ice and the underlying water column in the Canadian Arctic in the early spring. *Marine Chemistry* **2016,** *180*, 1-13.
11. Lee, Y. K.; Murphy, K. R.; Hur, J., Fluorescence Signatures of Dissolved Organic Matter Leached from Microplastics: Polymers and Additives. *Environmental Science & Technology* **2020,** *54* (19), 11905-11914.
12. Murphy, K. R.; Boehme, J. R.; Brown, C.; Noble, M.; Smith, G.; Sparks, D.; Ruiz, G. M., Exploring the limits of dissolved organic matter fluorescence for determining seawater sources and ballast water exchange on the US Pacific coast. *Journal of Marine Systems* **2013,** *111-112*, 157-166.
13. Murphy, K. R.; Stedmon, C. A.; Waite, T. D.; Ruiz, G. M., Distinguishing between terrestrial and autochthonous organic matter sources in marine environments using fluorescence spectroscopy. *Marine Chemistry* **2008,** *108* (1), 40-58.
14. Podgorski, D. C.; Zito, P.; Kellerman, A. M.; Bekins, B. A.; Cozzarelli, I. M.; Smith, D. F.; Cao, X.; Schmidt-Rohr, K.; Wagner, S.; Stubbins, A.; Spencer, R. G. M., Hydrocarbons to carboxyl-rich alicyclic molecules: A continuum model to describe biodegradation of petroleum-derived dissolved organic matter in contaminated groundwater plumes. *Journal of hazardous materials* **2021,** *402*, 123998-123998.
15. Podgorski, D. C.; Zito, P.; McGuire, J. T.; Martinovic-Weigelt, D.; Cozzarelli, I. M.; Bekins, B. A.; Spencer, R. G. M., Examining Natural Attenuation and Acute Toxicity of Petroleum-Derived Dissolved Organic Matter with Optical Spectroscopy. *Environmental Science & Technology* **2018,** *52* (11), 6157-6166.
16. Stedmon, C. A.; Markager, S.; Bro, R., Tracing dissolved organic matter in aquatic environments using a new approach to fluorescence spectroscopy. *Marine Chemistry* **2003,** *82* (3), 239-254.
17. Yamashita, Y.; Boyer, J. N.; Jaffé, R., Evaluating the distribution of terrestrial dissolved organic matter in a complex coastal ecosystem using fluorescence spectroscopy. *Continental Shelf Research* **2013,** *66*, 136-144.
18. Yamashita, Y.; Kloeppel, B. D.; Knoepp, J.; Zausen, G. L.; Jaffé, R., Effects of Watershed History on Dissolved Organic Matter Characteristics in Headwater Streams. *Ecosystems* **2011,** *14* (7), 1110-1122.
19. Zito, P.; Podgorski, D. C.; Johnson, J.; Chen, H.; Rodgers, R. P.; Guillemette, F.; Kellerman, A. M.; Spencer, R. G. M.; Tarr, M. A., Molecular-Level Composition and Acute Toxicity of Photosolubilized Petrogenic Carbon. *Environmental Science & Technology* **2019,** *53* (14), 8235-8243.

20. Haag, W. R.; Hoigné, J., Photo-sensitized oxidation in natural water via .OH radicals. *Chemosphere* **1985,** *14* (11), 1659-1671.
21. Ray, P. Z.; Chen, H.; Podgorski, D. C.; McKenna, A. M.; Tarr, M. A., Sunlight creates oxygenated species in water-soluble fractions of Deepwater horizon oil. *Journal of hazardous materials* **2014,** *280*, 636-643.
22. Ray, P. Z.; Tarr, M. A., Solar production of singlet oxygen from crude oil films on water. *Journal of photochemistry and photobiology. A, Chemistry.* **2014,** *286*, 22-28.
23. Ray, P. Z.; Tarr, M. A., Petroleum films exposed to sunlight produce hydroxyl radical. *Chemosphere (Oxford)* **2014,** *103*, 220-227.
24. Ray, P. Z.; Tarr, M. A., Formation of organic triplets from solar irradiation of petroleum. *Marine chemistry* **2015,** *168*, 135-139.
25. Zhou, X.; Mopper, K., Determination of photochemically produced hydroxyl radicals in seawater and freshwater. *Marine Chemistry* **1990,** *30*, 71-88.
26. Page, S. E.; Arnold, W. A.; McNeill, K., Assessing the Contribution of Free Hydroxyl Radical in Organic Matter-Sensitized Photohydroxylation Reactions. *Environmental Science & Technology* **2011,** *45* (7), 2818-2825.
27. Feldman, D., Polymer Weathering: Photo-Oxidation. *Journal of Polymers and the Environment* **2002,** *10* (4), 163-173.
28. Gangadoo, S.; Owen, S.; Rajapaksha, P.; Plaisted, K.; Cheeseman, S.; Haddara, H.; Truong, V. K.; Ngo, S. T.; Vu, V. V.; Cozzolino, D.; Elbourne, A.; Crawford, R.; Latham, K.; Chapman, J., Nano-plastics and their analytical characterisation and fate in the marine environment: From source to sea. *Science of The Total Environment* **2020,** *732*, 138792.
29. Yousif, E.; Haddad, R., Photodegradation and photostabilization of polymers, especially polystyrene: review. *SpringerPlus* **2013,** *2* (1), 398.
30. Duan, J.; Li, Y.; Gao, J.; Cao, R.; Shang, E.; Zhang, W., ROS-mediated photoaging pathways of nano- and micro-plastic particles under UV irradiation. *Water Research* **2022,** *216*, 118320.
31. Gewert, B.; Plassmann, M. M.; MacLeod, M., Pathways for degradation of plastic polymers floating in the marine environment. *Environmental Science: Processes & Impacts* **2015,** *17* (9), 1513-1521.
32. Shi, X.; Chen, Z.; Liu, X.; Wei, W.; Ni, B. J., The photochemical behaviors of microplastics through the lens of reactive oxygen species: Photolysis mechanisms and enhancing photo-transformation of pollutants. *Sci Total Environ* **2022,** *846*, 157498.
33. Dissing, D.; Wendler, G., Solar Radiation Climatology of Alaska. *Theoretical and Applied Climatology* **1998,** *61* (3), 161-175.
34. Murphy, K. R.; Stedmon, C. A.; Graeber, D.; Bro, R., Fluorescence spectroscopy and multi-way techniques. PARAFAC. *Analytical Methods* **2013,** *5* (23), 6557-6566.
35. Yang, R.; Zhao, N.; Xiao, X.; Yin, G.; Yu, S.; Liu, J.; Liu, W., Quantifying PAHs in water by three-way fluorescence spectra and second-order calibration methods. *Optics express* **2016,** *24* (14), A1148-A1157.
36. Hendrickson, C. L.; Quinn, J. P.; Kaiser, N. K.; Smith, D. F.; Blakney, G. T.; Chen, T.; Marshall, A. G.; Weisbrod, C. R.; Beu, S. C., 21 Tesla Fourier Transform Ion Cyclotron Resonance Mass Spectrometer: A National Resource for Ultrahigh Resolution Mass Analysis. *Journal of The American Society for Mass Spectrometry* **2015,** *26* (9), 1626-1632.
37. Smith, D. F.; Podgorski, D. C.; Rodgers, R. P.; Blakney, G. T.; Hendrickson, C. L., 21 Tesla FT-ICR Mass Spectrometer for Ultrahigh-Resolution Analysis of Complex Organic Mixtures. *Analytical Chemistry* **2018,** *90* (3), 2041-2047.
38. Skoog, D. A.; Holler, F. J.; Nieman, T. A., *Principles of instrumental analysis*. 5th ed.; Saunders College Pub: Philadelphia, Pa;Orlando, Fla;, 1998.
39. Jelle, B. P.; Nilsen, T.-N.; Hovde, P. J.; Gustavsen, A., Accelerated climate aging of building materials and their characterization by Fourier transform infrared radiation analysis. *Journal of building physics* **2012,** *36* (1), 99-112.

40. PPR Spills Database Search. https://dec.alaska.gov/Applications/SPAR/PublicMVC/PERP/SpillSearch (accessed December 13).
41. Wagner, A. M.; Barker, A. J., Distribution of polycyclic aromatic hydrocarbons (PAHs) from legacy spills at an Alaskan Arctic site underlain by permafrost. *Cold regions science and technology* **2019,** *158*, 154-165.
42. Amos, R. T.; Bekins, B. A.; Cozzarelli, I. M.; Voytek, M. A.; Kirshtein, J. D.; Jones, E. J.; Blowes, D. W., Evidence for iron-mediated anaerobic methane oxidation in a crude oil-contaminated aquifer. *Geobiology* **2012,** *10* (6), 506-17.
43. Fingas, M. *Analysis of oil biodegradation products*; Prince William Sound Regional Citizens' Advisory Council, 2014.
44. Hazen, T. C.; Prince, R. C.; Mahmoudi, N., Marine Oil Biodegradation. *Environmental Science & Technology* **2016,** *50* (5), 2121-2129.
45. Townsend, G. T.; Prince, R. C.; Suflita, J. M., Anaerobic Oxidation of Crude Oil Hydrocarbons by the Resident Microorganisms of a Contaminated Anoxic Aquifer. *Environmental Science & Technology* **2003,** *37* (22), 5213-5218.
46. Essaid, H. I.; Bekins, B. A.; Herkelrath, W. N.; Delin, G. N., Crude Oil at the Bemidji Site: 25 Years of Monitoring, Modeling, and Understanding. *Groundwater* **2011,** *49* (5), 706-726.
47. Barker, C. H.; Kourafalou, V. H.; Beegle-Krause, C. J.; Boufadel, M.; Bourassa, M. A.; Buschang, S. G.; Androulidakis, Y.; Chassignet, E. P.; Dagestad, K.-F.; Danmeier, D. G.; Dissanayake, A. L.; Galt, J. A.; Jacobs, G.; Marcotte, G.; Özgökmen, T.; Pinardi, N.; Schiller, R. V.; Socolofsky, S. A.; Thrift-Viveros, D.; Zelenke, B.; Zhang, A.; Zheng, Y., Progress in Operational Modeling in Support of Oil Spill Response. *Journal of marine science and engineering* **2020,** *8* (9), 668.
48. Ward, C. P.; Sharpless, C. M.; Valentine, D. L.; French-McCay, D. P.; Aeppli, C.; White, H. K.; Rodgers, R. P.; Gosselin, K. M.; Nelson, R. K.; Reddy, C. M., Partial Photochemical Oxidation Was a Dominant Fate of Deepwater Horizon Surface Oil. *Environmental Science & Technology* **2018,** *52* (4), 1797-1805.
49. Bianchi, T. S.; Osburn, C.; Shields, M. R.; Yvon-Lewis, S.; Young, J.; Guo, L.; Zhou, Z., Deepwater Horizon Oil in Gulf of Mexico Waters after 2 Years: Transformation into the Dissolved Organic Matter Pool. *Environmental Science & Technology* **2014,** *48* (16), 9288-9297.
50. Dvorski, S. E. M.; Gonsior, M.; Hertkorn, N.; Uhl, J.; Müller, H.; Griebler, C.; Schmitt-Kopplin, P., Geochemistry of Dissolved Organic Matter in a Spatially Highly Resolved Groundwater Petroleum Hydrocarbon Plume Cross-Section. *Environmental Science & Technology* **2016,** *50* (11), 5536-5546.
51. Mirnaghi, F. S.; Pinchin, N. P.; Yang, Z.; Hollebone, B. P.; Lambert, P.; Brown, C. E., Monitoring of polycyclic aromatic hydrocarbon contamination at four oil spill sites using fluorescence spectroscopy coupled with parallel factor-principal component analysis. *Environ Sci Process Impacts* **2019,** *21* (3), 413-426.
52. Zhou, Z.; Guo, L.; Shiller, A. M.; Lohrenz, S. E.; Asper, V. L.; Osburn, C. L., Characterization of oil components from the Deepwater Horizon oil spill in the Gulf of Mexico using fluorescence EEM and PARAFAC techniques. *Marine Chemistry* **2013,** *148*, 10-21.
53. Brown, C. E.; Fingas, M. F., Review of the development of laser fluorosensors for oil spill application. *Marine Pollution Bulletin* **2003,** *47* (9), 477-484.
54. Bugden, J. B. C.; Yeung, C. W.; Kepkay, P. E.; Lee, K., Application of ultraviolet fluorometry and excitation–emission matrix spectroscopy (EEMS) to fingerprint oil and chemically dispersed oil in seawater. *Marine Pollution Bulletin* **2008,** *56* (4), 677-685.
55. Conmy, R. N.; Coble, P. G.; Farr, J.; Wood, A. M.; Lee, K.; Pegau, W. S.; Walsh, I. D.; Koch, C. R.; Abercrombie, M. I.; Miles, M. S.; Lewis, M. R.; Ryan, S. A.; Robinson, B. J.; King, T. L.; Kelble, C. R.; Lacoste, J., Submersible Optical Sensors Exposed to Chemically Dispersed Crude Oil: Wave Tank Simulations for Improved Oil Spill Monitoring. *Environmental Science & Technology* **2014,** *48* (3), 1803-1810.

56. Driskill, A. K.; Alvey, J.; Dotson, A. D.; Tomco, P. L., Monitoring polycyclic aromatic hydrocarbon (PAH) attenuation in Arctic waters using fluorescence spectroscopy. *Cold Regions Science and Technology* **2018,** *145*, 76-85.
57. Fingas, M.; Brown, C., Review of oil spill remote sensing. *Marine Pollution Bulletin* **2014,** *83* (1), 9-23.
58. Keizer, P. D.; Gordon, D. C., Detection of Trace Amounts of Oil in Sea Water by Fluorescence Spectroscopy. *Journal of the Fisheries Research Board of Canada* **1973,** *30* (8), 1039-1046.
59. Chen, M.; Nam, S. I.; Kim, J. H.; Kwon, Y. J.; Hong, S.; Jung, J.; Shin, K. H.; Hur, J., High abundance of protein-like fluorescence in the Amerasian Basin of Arctic Ocean: Potential implication of a fall phytoplankton bloom. *Sci Total Environ* **2017,** *599-600*, 355-363.
60. Jaggi, A.; Radović, J. R.; Snowdon, L. R.; Larter, S. R.; Oldenburg, T. B. P., Composition of the dissolved organic matter produced during in situ burning of spilled oil. *Organic Geochemistry* **2019,** *138*, 103926.
61. Tomco, P. L.; Duddleston, K. N.; Driskill, A.; Hatton, J. J.; Grond, K.; Wrenn, T.; Tarr, M. A.; Podgorski, D. C.; Zito, P., Dissolved organic matter production from herder application and in-situ burning of crude oil at high latitudes: Bioavailable molecular composition patterns and microbial community diversity effects. *Journal of Hazardous Materials* **2022,** *424*, 127598.
62. Koch, B. P.; Dittmar, T., From mass to structure: an aromaticity index for high-resolution mass data of natural organic matter. *Rapid Communications in Mass Spectrometry* **2006,** *20* (5), 926-932.
63. Šantl-Temkiv, T.; Finster, K.; Dittmar, T.; Hansen, B. M.; Thyrhaug, R.; Nielsen, N. W.; Karlson, U. G., Hailstones: a window into the microbial and chemical inventory of a storm cloud. *PLoS One* **2013,** *8* (1), e53550.
64. Aggarwal, S.; Schnabel, W.; Buist, I.; Garron, J.; Bullock, R.; Perkins, R.; Potter, S.; Cooper, D., Aerial application of herding agents to advance in-situ burning for oil spill response in the Arctic: A pilot study. *Cold Regions Science and Technology* **2017,** *135*, 97-104.
65. Buist, I.; Cooper, D.; Trudel, K.; Fritt-Rasmussen, J.; Wegeberg, S.; Gustavson, K.; Lassen, P.; Jomaas, G.; Zabilansky, L.; Rojas-Alva, U., *Research Investigations into Herder Fate, Effects and Windows-of-Opportunity*. 2017.
66. Buist, I.; Potter, S.; Nedwed, T.; Mullin, J., Herding surfactants to contract and thicken oil spills in pack ice for in situ burning. *Cold Regions Science and Technology* **2011,** *67* (1), 3-23.
67. Bullock, R. J.; Perkins, R. A.; Aggarwal, S., In-situ burning with chemical herders for Arctic oil spill response: Meta-analysis and review. *Science of The Total Environment* **2019,** *675*, 705-716.
68. Dittmar, T.; Koch, B.; Hertkorn, N.; Kattner, G., A simple and efficient method for the solid-phase extraction of dissolved organic matter (SPE-DOM) from seawater. *Limnology and Oceanography: Methods* **2008,** *6* (6), 230-235.
69. Corilo, Y. E., PetroOrg Software. University, F. S., Ed. Omics LLC: Tallahassee, Florida, 2014.
70. Hawkes, J. A.; D'Andrilli, J.; Agar, J. N.; Barrow, M. P.; Berg, S. M.; Catalán, N.; Chen, H.; Chu, R. K.; Cole, R. B.; Dittmar, T.; Gavard, R.; Gleixner, G.; Hatcher, P. G.; He, C.; Hess, N. J.; Hutchins, R. H. S.; Ijaz, A.; Jones, H. E.; Kew, W.; Khaksari, M.; Palacio Lozano, D. C.; Lv, J.; Mazzoleni, L. R.; Noriega-Ortega, B. E.; Osterholz, H.; Radoman, N.; Remucal, C. K.; Schmitt, N. D.; Schum, S. K.; Shi, Q.; Simon, C.; Singer, G.; Sleighter, R. L.; Stubbins, A.; Thomas, M. J.; Tolic, N.; Zhang, S.; Zito, P.; Podgorski, D. C., An international laboratory comparison of dissolved organic matter composition by high resolution mass spectrometry: Are we getting the same answer? *Limnology and Oceanography: Methods* **2020,** *18* (6), 235-258.
71. O'Donnell, J. A.; Aiken, G. R.; Butler, K. D.; Guillemette, F.; Podgorski, D. C.; Spencer, R. G. M., DOM composition and transformation in boreal forest soils: The effects of temperature and organic-horizon decomposition state. *Journal of Geophysical Research: Biogeosciences* **2016,** *121* (10), 2727-2744.
72. Zito, P.; Podgorski, D. C.; Bartges, T.; Guillemette, F.; Roebuck, J. A.; Spencer, R. G. M.; Rodgers, R. P.; Tarr, M. A., Sunlight-Induced Molecular Progression of Oil into Oxidized Oil Soluble Species, Interfacial Material, and Dissolved Organic Matter. *Energy & Fuels* **2020,** *34* (4), 4721-4726.

73. Aitani, A., Crude Oil Refining: Chemical Conversion. 2014.
74. Painter, S. C.; Lapworth, D. J.; Woodward, E. M. S.; Kroeger, S.; Evans, C. D.; Mayor, D. J.; Sanders, R. J., Terrestrial dissolved organic matter distribution in the North Sea. *Science of The Total Environment* **2018,** *630*, 630-647.
75. Retelletti Brogi, S.; Ha, S. Y.; Kim, K.; Derrien, M.; Lee, Y. K.; Hur, J., Optical and molecular characterization of dissolved organic matter (DOM) in the Arctic ice core and the underlying seawater (Cambridge Bay, Canada): Implication for increased autochthonous DOM during ice melting. *Sci Total Environ* **2018,** *627*, 802-811.
76. D'Andrilli, J.; McConnell, J. R., Polar ice core organic matter signatures reveal past atmospheric carbon composition and spatial trends across ancient and modern timescales. *Journal of Glaciology* **2021,** *67* (266), 1028-1042.
77. Ohno, T.; Chorover, J.; Omoike, A.; Hunt, J., Molecular weight and humification index as predictors of adsorption for plant- and manure-derived dissolved organic matter to goethite. *European Journal of Soil Science* **2007,** *58* (1), 125-132.
78. McKenna, A. M.; Nelson, R. K.; Reddy, C. M.; Savory, J. J.; Kaiser, N. K.; Fitzsimmons, J. E.; Marshall, A. G.; Rodgers, R. P., Expansion of the Analytical Window for Oil Spill Characterization by Ultrahigh Resolution Mass Spectrometry: Beyond Gas Chromatography. *Environmental Science & Technology* **2013,** *47* (13), 7530-7539.
79. Harriman, B. H.; Zito, P.; Podgorski, D. C.; Tarr, M. A.; Suflita, J. M., Impact of Photooxidation and Biodegradation on the Fate of Oil Spilled During the Deepwater Horizon Incident: Advanced Stages of Weathering. *Environmental Science & Technology* **2017,** *51* (13), 7412-7421.
80. Roebuck, J. A.; Podgorski, D. C.; Wagner, S.; Jaffé, R., Photodissolution of charcoal and fire-impacted soil as a potential source of dissolved black carbon in aquatic environments. *Organic Geochemistry* **2017,** *112*, 16-21.
81. Wagner, S.; Ding, Y.; Jaffé, R., A New Perspective on the Apparent Solubility of Dissolved Black Carbon. *Frontiers in earth science (Lausanne)* **2017,** *5*.
82. Wagner, S.; Jaffé, R., Effect of photodegradation on molecular size distribution and quality of dissolved black carbon. *Organic Geochemistry* **2015,** *86*, 1-4.
83. Wagner, S.; Jaffé, R.; Stubbins, A., Dissolved black carbon in aquatic ecosystems. *Limnology and Oceanography Letters* **2018,** *3* (3), 168-185.
84. Aeppli, C.; Carmichael, C. A.; Nelson, R. K.; Lemkau, K. L.; Graham, W. M.; Redmond, M. C.; Valentine, D. L.; Reddy, C. M., Oil Weathering after the Deepwater Horizon Disaster Led to the Formation of Oxygenated Residues. *Environmental Science & Technology* **2012,** *46* (16), 8799-8807.
85. Kim, M.; Yim, U. H.; Hong, S. H.; Jung, J.-H.; Choi, H.-W.; An, J.; Won, J.; Shim, W. J., Hebei Spirit oil spill monitored on site by fluorometric detection of residual oil in coastal waters off Taean, Korea. *Marine Pollution Bulletin* **2010,** *60* (3), 383-389.
86. Lundstedt, S.; White, P. A.; Lemieux, C. L.; Lynes, K. D.; Lambert, I. B.; Oberg, L.; Haglund, P.; Tysklind, M., Sources, fate, and toxic hazards of oxygenated polycyclic aromatic hydrocarbons (PAHs) at PAH-contaminated sites. *Ambio* **2007,** *36* (6), 475-85.
87. Murphy, K. R.; Stedmon, C. A.; Wenig, P.; Bro, R., OpenFluor– an online spectral library of auto-fluorescence by organic compounds in the environment. *Analytical Methods* **2014,** *6* (3), 658-661.
88. Spencer, R. G. M.; Bolton, L.; Baker, A., Freeze/thaw and pH effects on freshwater dissolved organic matter fluorescence and absorbance properties from a number of UK locations. *Water Research* **2007,** *41* (13), 2941-2950.
89. Stedmon, C. A.; Bro, R., Characterizing dissolved organic matter fluorescence with parallel factor analysis: a tutorial. *Limnology and Oceanography: Methods* **2008,** *6* (11), 572-579.
90. Weishaar, J. L.; Aiken, G. R.; Bergamaschi, B. A.; Fram, M. S.; Fujii, R.; Mopper, K., Evaluation of Specific Ultraviolet Absorbance as an Indicator of the Chemical Composition and Reactivity of Dissolved Organic Carbon. *Environmental Science & Technology* **2003,** *37* (20), 4702-4708.

91. Borrelle, S. B.; Ringma, J.; Law, K. L.; Monnahan, C. C.; Lebreton, L.; McGivern, A.; Murphy, E.; Jambeck, J.; Leonard, G. H.; Hilleary, M. A.; Eriksen, M.; Possingham, H. P.; De Frond, H.; Gerber, L. R.; Polidoro, B.; Tahir, A.; Bernard, M.; Mallos, N.; Barnes, M.; Rochman, C. M., Predicted growth in plastic waste exceeds efforts to mitigate plastic pollution. *Science* **2020,** *369* (6510), 1515-1518.
92. Geyer, R.; Jambeck, J. R.; Law, K. L., Production, use, and fate of all plastics ever made. *Science Advances* **2017,** *3* (7), e1700782.
93. Hoornweg, D.; Bhada-Tata, P., What a waste: a global review of solid waste management. *Urban Dev Ser Knowl Pap* **2012,** *15*, 87-88.
94. Kaza, S.; Yao, L.; Bhada-Tata, P.; VanWoerden, F., What a Waste 2.0: A global snapshot of solid waste management to 2050. *Urban Dev Ser Knowl Pap* **2018**, 87-100.
95. Lebreton, L.; Slat, B.; Ferrari, F.; Sainte-Rose, B.; Aitken, J.; Marthouse, R.; Hajbane, S.; Cunsolo, S.; Schwarz, A.; Levivier, A.; Noble, K.; Debeljak, P.; Maral, H.; Schoeneich-Argent, R.; Brambini, R.; Reisser, J., Evidence that the Great Pacific Garbage Patch is rapidly accumulating plastic. *Scientific Reports* **2018,** *8* (1), 4666.
96. Pattiaratchi, C.; van der Mheen, M.; Schlundt, C.; Narayanaswamy, B. E.; Sura, A.; Hajbane, S.; White, R.; Kumar, N.; Fernandes, M.; Wijeratne, S., Plastics in the Indian Ocean – sources, transport, distribution, and impacts. *Ocean Sci.* **2022,** *18* (1), 1-28.
97. Derraik, J. G. B., The pollution of the marine environment by plastic debris: a review. Elsevier Ltd: Oxford, 2002; Vol. 44, pp 842-852.
98. Barnes, D. K. A.; Galgani, F.; Thompson, R. C.; Barlaz, M., Accumulation and fragmentation of plastic debris in global environments. *Philosophical Transactions of the Royal Society B: Biological Sciences* **2009,** *364* (1526), 1985-1998.
99. Gigault, J.; Halle, A. t.; Baudrimont, M.; Pascal, P.-Y.; Gauffre, F.; Phi, T.-L.; El Hadri, H.; Grassl, B.; Reynaud, S., Current opinion: What is a nanoplastic? *Environmental pollution (1987)* **2018,** *235*, 1030-1034.
100. Jiang, B.; Kauffman, A. E.; Li, L.; McFee, W.; Cai, B.; Weinstein, J.; Lead, J. R.; Chatterjee, S.; Scott, G. I.; Xiao, S., Health impacts of environmental contamination of micro- and nanoplastics: a review. *Environmental health and preventive medicine* **2020,** *25* (1), 1-29.
101. Gijsman, P.; Meijers, G.; Vitarelli, G., Comparison of the UV-degradation chemistry of polypropylene, polyethylene, polyamide 6 and polybutylene terephthalate. *Polymer Degradation and Stability* **1999,** *65* (3), 433-441.
102. Carlsson, D. J.; Garton, A.; Wiles, D. M., Initiation of Polypropylene Photooxidation. 2. Potential Processes and Their Relevance to Stability. *Macromolecules* **1976,** *9* (5), 695-701.
103. Lucki, J.; Rånby, B., Photo-oxidation of polystyrene—Part 2: Formation of carbonyl groups in photo-oxidised polystyrene. *Polymer Degradation and Stability* **1979,** *1* (3), 165-179.
104. McKellar, J. F.; Allen, N. S., *Photochemistry of man-made polymers*. Applied Science Publishers: London, 1979.
105. Rabek, J. F., Degradation of polymers initiated by radicals formed from photolysis of different compounds. In *Polymer Photodegradation: Mechanisms and experimental methods*, Rabek, J. F., Ed. Springer Netherlands: Dordrecht, 1995; pp 377-398.
106. Rabek, J. F., Photodegradation of polymers in extreme conditions. In *Polymer Photodegradation: Mechanisms and experimental methods*, Rabek, J. F., Ed. Springer Netherlands: Dordrecht, 1995; pp 420-432.
107. Rabek, J. F., Photodegradation and photo-oxidative degradation of homochain polymers. In *Polymer Photodegradation: Mechanisms and experimental methods*, Rabek, J. F., Ed. Springer Netherlands: Dordrecht, 1995; pp 67-254.
108. Rabek, J. F.; Rånby, B., Studies on the photooxidation mechanism of polymers. I. Photolysis and photooxidation of polystyrene. *Journal of Polymer Science: Polymer Chemistry Edition* **1974,** *12* (2), 273-294.

109. Ranby, B.; Lucki, J., New aspects of photodegradation and photooxidation of polystyrene. *Pure and Applied Chemistry* **1980,** *52* (2), 295-303.
110. Rånby, B. G.; Rabek, J. F., *Photodegradation, photo-oxidation, and photostabilization of polymers: principles and applications*. Wiley: London;New York;, 1975.
111. Trozzolo, A. M.; Winslow, F. H., A Mechanism for the Oxidative Photodegradation of Polyethylene. *Macromolecules* **1968,** *1* (1), 98-100.
112. Gardette, M.; Perthue, A.; Gardette, J.-L.; Janecska, T.; Földes, E.; Pukánszky, B.; Therias, S., Photo- and thermal-oxidation of polyethylene: Comparison of mechanisms and influence of unsaturation content. *Polymer Degradation and Stability* **2013,** *98* (11), 2383-2390.
113. Liu, L.; Xu, M.; Ye, Y.; Zhang, B., On the degradation of (micro)plastics: Degradation methods, influencing factors, environmental impacts. *Science of The Total Environment* **2022,** *806*, 151312.
114. Zhu, K.; Jia, H.; Zhao, S.; Xia, T.; Guo, X.; Wang, T.; Zhu, L., Formation of Environmentally Persistent Free Radicals on Microplastics under Light Irradiation. *Environmental Science & Technology* **2019,** *53* (14), 8177-8186.
115. Zepp, R. G.; Schlotzhauer, P. F.; Sink, R. M., Photosensitized transformations involving electronic energy transfer in natural waters: role of humic substances. *Environmental Science & Technology* **1985,** *19* (1), 74-81.
116. Zepp, R. G.; Wolfe, N. L.; Baughman, G. L.; Hollis, R. C., Singlet oxygen in natural waters. *Nature* **1977,** *267* (5610), 421-423.
117. Haag, W. R.; Hoigne´, J. r.; Gassman, E.; Braun, A. M., Singlet oxygen in surface waters — Part I: Furfuryl alcohol as a trapping agent. *Chemosphere* **1984,** *13* (5), 631-640.
118. Zvekic, M.; Richards, L. C.; Tong, C. C.; Krogh, E. T., Characterizing photochemical ageing processes of microplastic materials using multivariate analysis of infrared spectra. *Environmental Science: Processes & Impacts* **2022,** *24* (1), 52-61.
119. Hamzah, M.; Khenfouch, M.; Rjeb, A.; Sayouri, S.; Houssaini, D. S.; Darhouri, M.; Srinivasu, V. V., Surface chemistry changes and microstructure evaluation of low density nanocluster polyethylene under natural weathering: A spectroscopic investigation. *Journal of Physics: Conference Series* **2018,** *984*, 012010.
120. Markowicz, F.; Szymańska-Pulikowska, A., Assessment of the Decomposition of Oxo- and Biodegradable Packaging Using FTIR Spectroscopy. *Materials (Basel)* **2021,** *14* (21).
121. Walsh, A. N.; Reddy, C. M.; Niles, S. F.; McKenna, A. M.; Hansel, C. M.; Ward, C. P., Plastic Formulation is an Emerging Control of Its Photochemical Fate in the Ocean. *Environmental Science & Technology* **2021,** *55* (18), 12383-12392.
122. Buxton, G. V.; Greenstock, C. L.; Helman, W. P.; Ross, A., Critical Review of rate constants for reactions of hydrated electrons, hydrogen atoms and hydroxyl radicals (·OH/·O− in Aqueous Solution. *Journal of Physical and Chemical Reference Data* **1988,** *17*, 513-886.
123. NIST, Solution Kinetics Database Resources.
124. Li, Q.-c.; Lai, Y.-j.; Yu, S.-j.; Li, P.; Zhou, X.-x.; Dong, L.-j.; Liu, X.; Yao, Z.-w.; Liu, J.-f., Sequential Isolation of Microplastics and Nanoplastics in Environmental Waters by Membrane Filtration, Followed by Cloud-Point Extraction. *Analytical Chemistry* **2021,** *93* (10), 4559-4566.
125. Zhou, X. X.; Hao, L. T.; Wang, H. Y.; Li, Y. J.; Liu, J. F., Cloud-Point Extraction Combined with Thermal Degradation for Nanoplastic Analysis Using Pyrolysis Gas Chromatography-Mass Spectrometry. *Anal Chem* **2019,** *91* (3), 1785-1790.
126. Nandiyanto, A.; Oktiani, R.; Ragadhita, R., How to Read and Interpret FTIR Spectroscope of Organic Material. *Indonesian Journal of Science and Technology* **2019,** *4*, 97-118.
127. Martínez-Romo, A.; Mota, R.; Soto-Bernal, J.; Reyes, C.; Candelas, I., Effect of ultraviolet radiation in the photo-oxidation of High Density Polyethylene and Biodegradable Polyethylene films. *Journal of Physics: Conference Series* **2015,** *582*, 012026.

Appendix A: Chapter 3 Copyright Permission

7/11/22, 11:19 AM Rightslink® by Copyright Clearance Center

CCC RightsLink

Home | Help | Live Chat | Sign in | Create Account

ACS Publications
Most Trusted. Most Cited. Most Read.

Unique Molecular Features of Water-Soluble Photo-Oxidation Products among Refined Fuels, Crude Oil, and Herded Burnt Residue under High Latitude Conditions

Author: Elizabeth A. Whisenhant, Phoebe Zito, David C. Podgorski, et al
Publication: ACS ES&T Water
Publisher: American Chemical Society
Date: Jun 1, 2022

Copyright © 2022, American Chemical Society

PERMISSION/LICENSE IS GRANTED FOR YOUR ORDER AT NO CHARGE

This type of permission/license, instead of the standard Terms and Conditions, is sent to you because no fee is being charged for your order. Please note the following:

- Permission is granted for your request in both print and electronic formats, and translations.
- If figures and/or tables were requested, they may be adapted or used in part.
- Please print this page for your records and send a copy of it to your publisher/graduate school.
- Appropriate credit for the requested material should be given as follows: "Reprinted (adapted) with permission from {COMPLETE REFERENCE CITATION}. Copyright {YEAR} American Chemical Society." Insert appropriate information in place of the capitalized words.
- One-time permission is granted only for the use specified in your RightsLink request. No additional uses are granted (such as derivative works or other editions). For any uses, please submit a new request.

If credit is given to another source for the material you requested from RightsLink, permission must be obtained from that source.

BACK CLOSE WINDOW

Appendix B: Chapter 3 Supporting Information

Experimental Design:

Samples were thermostatically controlled at 5.5°C to match the annual water temperature in the Gulf of Alaska.

Measurement Parameters:

The dissolved organic carbon concentration of samples was determined using a calibration curve of five standards between 1 and 50 ppm of potassium hydrogen phthalate (KHP) solutions. Checks were put into place to ensure that the TOC instrument was measuring correctly by washing sample lines with nanopure water after each sample measurement and adding KHP standards after 12 samples were measured.

Samples were measured in a 10 mm quartz cuvette in an excitation range of 240 to 800 nm at 5 nm increments, and in an emission range of 247.40 nm to 829.36 nm at 2nm increments. Prior to EEM measurements, all samples were dilution corrected to $A_{254} = 0.09$ to reduce inner filter effects. The collected EEMs were corrected for Rayleigh and Raman Scattering, blank nanopure water acquisition detracted, and further inner filter effect modified.

Processed excitation and emission matrix DAT files were exported and entered into the drEEM toolbox for MATLAB (Mathworks, Natick, MA, U.S.A.). A four component PARAFAC model was validated after inspection of spectral loadings and split-half validation, where each component peak characterizes a common chemical feature bound by fluorescent similarities.[34] The Fmax values from drEEM were calculated in relative percent contributions of each sample. Maximum excitation and emission wavelengths were uploaded onto OpenFluor database for

comparison and characterization of each fluorescent component where components are compared with a 95% similarity criteria.[87]

Relative contributions of the fluorescence components are visually analyzed using principal component analysis (PCA) for specific sample and time point visualization. The humification index (HIX)[77] was exported from drEEM, and the specific ultraviolet absorption (SUVA) at a wavelength of 254 nm was obtained by dividing the measured absorption coefficient at 254 nm by the DOC concentration.[90]

Analytical examination for phenylalanine:

According to component matching, a similarity exists between C4 Ex/Em and the fluorophore wavelengths of phenylalanine. To test if phenylalanine is present in the samples, samples were analyzed (1000 µgC/mL) on a Vanquish UHPLC system coupled to an Exploris 120 orbitrap mass spectrometer (Thermo Scientific) at 10 day irradiation, where fluorescence data predicts phenylalanine would be in greatest abundance. Samples were injected (20 µL) onto a Kinetix C18 column (150 x 2.1mm; 1.7µ) with a UHPLC C18 2.1 mm Security Guard Column (Phenomenex) and eluted using a gradient of water (A) and acetonitrile (B) each containing 0.1% formic acid (v/v). The column was maintained at 60 °C while the mobile phase composition was ramped from 5 to 99% B over 15 min and held for 10 min before resetting to initial conditions; total run time was 32 min. Eluted compounds were ionized via negative mode electrospray ionization (3200V). The nitrogen sheath gas, auxiliary gas, and sweep gas flows were 50, 5, and 5 arbitrary units, respectively. The vaporizer and ion transfer tube temperatures were 350 and 300 °C. Ionization parameters were optimized by infusing the calibration solution (FlexMix,

Thermo Scientific) into 0.4 mL/min 50% A post column at 5 µL/min. Full scans were collected over the range 150-1500 m/z with a resolution of 120,000 and RF lens set to 70%. Automatic gain control was used to accumulate 1e6 ions in the trap using 1 microscan and a maximum injection time of 200 ms. Orbitrap mass accuracy was externally calibrated prior to analysis via infusion of the calibration solution while a mass lock was established during each scan using the fluoranthene (M-, 202.0788 m/z) internal calibrant discharge source (Easy-IC, Thermo Scientific). A 5 µL injection containing 10 µg/mL phenylalanine yielded a signal in ESI(-) m/z = 164.0717 ($[M-H]^-$, $C_9H_{10}NO_2^-$) with retention time = 1.46 minutes. Phenylalanine was not detected in the 10 day irradiated samples. From these tests, it is evident that phenylalanine is absent from our dataset and the compound is not a major product of hydrocarbon metabolism.

Table S1. Experiment design. Triplicates of each treatment group were prepared with both seawater and freshwater. 10ppm of each treatment were tested with both freshwater and seawater under UV exposure and no UV exposure, thermostatically controlled at 5.5°C. Each beaker represented a single point; these being 0-, 24-, 96-, and 240-hour. Total samples, N=384.

Treatment	Water Medium	Light Treatment	Temperature Control	Test Duration
No Fuel	Freshwater + Seawater	Sunlight Simulation + Complete Darkness	5.5 °C	240 h
Heating Oil				
Jet A-50 Fuel				
Unleaded Gasoline				
Diesel Fuel				
Kerosene				
ANS Crude Oil				
ANS Crude Oil + Burning				

Table S2. Crude Oil in-situ burn experiment design. Triplicates were taken from HDPE jars at 0-, 24-, 96-, and 240-hour. Total samples, N=48.

Treatment	Water Medium	Light Treatment	Temperature Control	Test Duration
Oil + ISB	Seawater	Sunlight Simulation + Complete Darkness	15°C	240 hr
Oil + ISB + OP40				

Table S3a. DOC, SUVA254, and Spectral Index data for treatments containing no fuel and heating oil.

Treatment	Water Type	Light Type	Irradiation Period (day)	DOC (mg/L)	SUVA254 (L mg-1 cm-1)	C	A	T	B	M	FI	HIX	FRESH	BIX
No Fuel	FW	Light	0	1.81	0.013	0.51	1.09	0.25	0.11	0.61	1.68	6.85	0.74	0.74
			1	5.51	0.005	0.29	0.81	0.29	0.18	0.39	1.55	3.55	0.77	0.76
			4	4.26	0.006	0.18	0.61	0.23	0.29	0.26	1.56	2.17	0.74	0.73
			10	2.28	0.015	0.17	0.84	0.50	0.77	0.27	1.47	0.84	0.73	0.74
		Dark	0	1.28	0.026	0.52	1.11	0.22	0.07	0.62	1.66	8.41	0.73	0.72
			1	2.82	0.011	0.58	1.30	0.36	0.15	0.69	1.68	5.45	0.75	0.75
			4	3.04	0.008	0.64	1.41	0.28	0.13	0.77	1.71	8.55	0.74	0.73
			10	3.33	0.007	0.57	1.35	0.25	0.17	0.71	1.71	6.63	0.72	0.72
	SW	Light	0	0.80	0.011	0.07	0.19	0.19	0.18	0.10	1.71	1.17	1.17	1.14
			1	3.57	0.003	0.05	0.18	0.14	0.17	0.08	1.69	1.04	1.08	1.05
			4	2.97	0.005	0.08	0.33	0.13	0.14	0.11	1.42	2.02	0.84	0.84
			10	1.65	0.014	0.11	0.52	0.51	0.66	0.16	1.52	1.25	0.88	0.86
		Dark	0	0.79	0.013	0.07	0.19	0.21	0.19	0.10	1.73	1.19	1.13	1.12
			1	1.71	0.005	0.07	0.17	0.08	0.11	0.09	1.81	1.97	1.06	1.06
			4	1.79	0.002	0.07	0.18	0.09	0.11	0.09	1.72	1.97	1.08	1.05
			10	2.90	0.004	0.07	0.18	0.12	0.12	0.09	1.80	2.00	1.10	1.09
Heating Oil	FW	Light	0	1.46	0.028	0.71	1.54	0.43	3.59	0.86	1.65	1.63	0.74	0.73
			1	39.94	0.012	4.00	30.08	117.05	72.38	9.07	8.65	1.89	9.59	9.24
			4	89.63	0.015	6.69	37.51	127.69	212.33	16.09	21.19	2.80	17.07	16.29
			10	132.94	0.011	4.02	30.27	95.59	178.84	11.11	23.50	2.79	18.24	17.63
		Dark	0	2.45	0.017	0.69	1.48	0.42	3.57	0.84	1.64	1.56	0.74	0.73
			1	2.27	0.015	0.60	1.57	1.46	15.51	0.79	1.69	0.35	0.84	0.81
			4	2.45	0.012	0.86	2.35	1.96	23.42	1.18	1.74	0.35	0.86	0.85
			10	5.34	0.005	0.96	3.82	2.05	18.61	1.17	1.98	0.51	0.81	0.79
	SW	Light	0	1.03	0.009	0.07	0.18	0.24	3.11	0.11	1.77	0.24	1.35	1.33
			1	78.72	0.007	3.40	23.62	97.37	64.65	7.71	7.46	1.62	8.90	8.49
			4	83.49	0.014	9.40	47.10	116.27	233.14	17.11	19.85	3.59	14.11	13.54
			10	94.57	0.014	3.67	26.36	92.31	199.40	10.01	22.14	2.39	17.86	16.79
		Dark	0	1.66	0.006	0.07	0.18	0.20	3.42	0.12	1.64	0.24	1.28	1.24
			1	1.61	0.011	0.14	0.51	1.14	17.01	0.22	1.61	0.10	1.42	1.31
			4	1.71	0.006	0.18	0.87	1.44	20.21	0.29	2.05	0.12	1.39	1.31
			10	2.87	0.006	0.16	0.83	1.38	18.09	0.25	1.88	0.12	1.39	1.40

Table S3b. DOC, SUVA254, and Spectral Index data for treatments containing Jet A-50 Fuel and unleaded gasoline.

Treatment	Water Type	Light Type	Irradiation Period (day)	DOC (mg/L)	SUVA254 (L mg-1 cm-1)	C	A	T	B	M	FI	HIX	FRESH	BIX
Jet Fuel	FW	Light	0	1.79	0.024	0.71	1.53	0.43	4.39	0.86	1.65	1.39	0.74	0.73
			1	41.00	0.013	3.54	25.69	119.40	83.76	9.15	9.12	1.64	11.21	10.73
			4	96.91	0.008	5.10	47.80	176.90	159.07	14.22	13.96	2.47	15.52	14.84
			10	98.79	0.011	4.12	32.72	106.42	216.34	11.07	19.29	2.03	15.33	14.71
		Dark	0	1.53	0.028	0.74	1.61	0.49	5.29	0.91	1.66	1.25	0.75	0.74
			1	2.23	0.014	0.55	1.40	1.41	17.09	0.74	1.66	0.29	0.91	0.88
			4	1.82	0.018	0.77	2.22	1.95	22.97	1.09	1.73	0.31	0.85	0.85
			10	9.40	0.005	0.91	3.44	2.14	19.09	1.13	1.90	0.47	0.86	0.84
	SW	Light	0	2.50	0.005	0.07	0.21	0.29	4.67	0.12	1.66	0.18	1.43	1.31
			1	24.02	0.025	2.83	20.27	79.24	47.95	5.88	5.52	1.27	6.26	6.08
			4	91.97	0.008	4.75	41.33	149.04	155.47	12.14	14.13	2.66	15.95	15.21
			10	176.26	0.012	4.25	30.89	120.75	297.08	11.45	32.51	2.65	28.02	26.31
		Dark	0	3.34	0.005	0.08	0.21	0.31	4.50	0.13	1.75	0.18	1.41	1.30
			1	2.08	0.015	0.33	1.29	1.62	18.93	0.66	1.50	0.22	1.24	1.17
			4	1.74	0.008	0.14	0.66	1.43	18.16	0.26	1.88	0.11	1.31	1.24
			10	4.91	0.003	0.21	1.14	1.47	18.03	0.30	1.99	0.15	1.37	1.33
Gasoline	FW	Light	0	1.79	0.025	0.66	1.44	0.28	0.99	0.79	1.64	1.93	0.71	0.70
			1	2.39	0.022	0.47	2.18	1.95	6.84	0.66	1.53	0.52	0.91	0.89
			4	4.72	0.019	0.57	3.89	5.64	13.14	1.02	1.58	0.30	1.17	1.14
			10	3.98	0.014	0.28	1.83	1.85	4.94	0.56	1.52	0.31	1.07	1.02
		Dark	0	2.33	0.018	0.75	1.64	0.29	0.61	0.90	1.67	3.52	0.71	0.71
			1	1.64	0.014	0.53	1.14	0.34	2.70	0.63	1.79	0.66	0.78	0.76
			4	2.31	0.014	0.73	1.79	0.49	0.75	0.92	1.69	2.30	0.75	0.74
			10	5.27	0.006	0.65	1.58	0.45	0.52	0.80	1.67	2.48	0.73	0.72
	SW	Light	0	1.36	0.007	0.07	0.19	0.10	0.41	0.10	1.70	0.67	1.14	1.11
			1	3.28	0.016	0.37	2.70	4.31	9.02	0.52	1.67	0.30	1.45	1.44
			4	2.47	0.009	0.15	0.98	0.85	1.67	0.27	1.72	0.49	1.10	1.07
			10	3.05	0.010	0.14	0.79	1.00	1.65	0.27	1.53	0.37	1.41	1.32
		Dark	0	1.90	0.006	0.07	0.18	0.09	0.40	0.10	1.77	0.69	1.10	1.08
			1	0.93	0.008	0.08	0.19	0.14	1.67	0.11	1.73	0.20	0.99	0.97
			4	2.88	0.003	0.09	0.28	0.23	0.72	0.13	1.73	0.52	1.06	1.04
			10	7.53	0.001	0.08	0.25	0.49	0.70	0.11	1.81	0.21	1.30	1.24

Table S3c. Experiment 1; DOC, SUVA254, and Spectral Index results for treatments containing diesel fuel and kerosene.

Treatment	Water Type	Light Type	Irradiation Period (day)	DOC (mg/L)	SUVA254 (L mg-1 cm-1)	C	A	T	B	M	FI	HIX	FRESH	BIX
Diesel	FW	Light	0	1.87	0.022	0.54	1.24	0.18	0.18	0.67	1.69	8.36	0.72	0.71
			1	26.06	0.011	3.00	16.65	51.38	102.82	4.64	4.79	0.94	3.59	3.57
			4	59.23	0.008	2.15	10.26	21.93	117.59	3.36	6.92	0.94	4.07	3.93
			10	323.67	0.012	4.71	40.22	65.90	657.97	9.58	57.08	2.99	32.46	31.24
		Dark	0	2.39	0.017	0.51	1.15	0.20	0.21	0.62	1.70	6.28	0.72	0.72
			1	1.59	0.013	0.51	1.13	0.32	0.98	0.63	1.76	2.24	0.76	0.75
			4	2.78	0.017	0.62	1.54	0.45	1.48	0.78	1.67	1.82	0.73	0.72
			10	3.31	0.007	0.59	1.36	0.45	1.64	0.72	1.70	1.55	0.75	0.74
	SW	Light	0	1.17	0.008	0.07	0.19	0.12	0.23	0.09	1.77	1.36	1.11	1.09
			1	22.32	0.011	2.30	12.35	33.63	70.56	2.75	4.58	0.99	3.27	3.30
			4	37.34	0.012	2.47	9.91	11.21	133.18	2.82	8.31	1.04	3.00	3.02
			10	228.11	0.012	2.93	13.79	36.06	325.28	5.13	44.95	2.07	20.64	19.56
		Dark	0	1.78	0.005	0.07	0.17	0.13	0.22	0.09	1.75	1.30	1.11	1.09
			1	0.85	0.007	0.07	0.19	0.08	0.54	0.09	1.69	0.80	1.03	1.02
			4	1.61	0.006	0.14	0.47	0.31	0.95	0.20	1.65	0.86	0.93	0.91
			10	10.58	0.002	0.10	0.28	0.21	0.99	0.13	1.34	0.45	1.06	1.02
Kerosene	FW	Light	0	1.65	0.024	0.61	1.39	0.28	0.37	0.75	1.67	5.17	0.72	0.72
			1	7.23	0.014	1.18	9.24	22.54	14.49	1.62	2.25	0.85	1.51	1.51
			4	41.17	0.015	2.42	18.88	81.20	131.56	5.56	10.64	1.14	10.42	10.04
			10	123.20	0.012	2.49	16.10	67.82	300.79	5.35	23.34	1.05	16.87	16.11
		Dark	0	1.60	0.025	0.69	1.58	0.35	0.43	0.85	1.68	4.85	0.73	0.72
			1	1.88	0.016	0.60	1.40	0.58	1.92	0.76	1.68	1.12	0.75	0.74
			4	10.13	0.003	0.65	1.58	0.61	2.02	0.81	1.65	1.25	0.74	0.74
			10	4.47	0.009	0.70	1.66	0.91	2.15	0.88	1.70	1.06	0.78	0.76
	SW	Light	0	0.95	0.009	0.08	0.20	0.21	0.35	0.09	1.78	0.96	1.16	1.14
			1	4.91	0.012	0.63	5.06	13.04	8.39	0.76	1.91	0.75	1.26	1.30
			4	33.05	0.014	1.99	13.62	40.69	77.10	3.26	8.35	1.13	6.29	6.12
			10	80.02	0.011	1.50	8.69	31.35	178.62	2.91	13.88	0.65	8.62	8.27
		Dark	0	0.80	0.010	0.07	0.20	0.20	0.29	0.09	1.76	1.04	1.23	1.19
			1	1.92	0.005	0.09	0.24	0.21	1.03	0.12	1.77	0.45	1.24	1.17
			4	8.80	0.002	0.09	0.23	0.28	1.36	0.13	1.80	0.33	1.21	1.16
			10	3.01	0.005	0.12	0.32	0.68	1.91	0.19	1.55	0.26	1.42	1.32

Table S3d. Experiment 1; DOC, SUVA254, and Spectral Index results for treatments containing crude oil and crude oil under ISB.

Treatment	Water Type	Light Type	Irradiation Period (day)	DOC (mg/L)	SUVA254 (L mg-1 cm-1)	C	A	T	B	M	FI	HIX	FRESH	BIX
Crude Oil	FW	Light	0	1.72	0.026	0.64	1.55	0.77	1.20	0.83	1.70	1.94	0.90	0.89
			1	6.37	0.011	1.22	6.98	9.63	11.46	2.44	1.64	0.72	1.75	1.69
			4	27.17	0.010	3.48	21.35	22.49	23.30	7.04	4.43	2.66	3.68	3.57
			10	43.50	0.013	6.71	45.02	48.07	43.43	12.43	9.30	5.57	8.43	8.21
		Dark	0	1.50	0.030	0.63	1.52	0.67	1.16	0.81	1.68	1.92	0.86	0.85
			1	2.37	0.016	0.76	2.60	7.40	14.39	1.52	1.72	0.30	2.07	1.97
			4	3.02	0.018	0.88	3.19	8.79	18.28	1.81	1.69	0.30	2.13	2.03
			10	7.34	0.007	0.87	3.50	10.74	19.53	1.96	1.66	0.28	2.16	2.06
	SW	Light	0	2.04	0.007	0.07	0.23	0.35	0.85	0.12	1.69	0.50	1.71	1.64
			1	6.47	0.009	0.87	5.77	7.49	10.55	1.88	1.63	0.75	2.02	1.92
			4	18.34	0.012	2.90	17.27	20.38	19.44	5.47	3.66	2.17	3.49	3.39
			10	38.93	0.015	6.51	43.64	39.31	33.68	12.06	8.96	6.18	6.98	6.78
		Dark	0	1.36	0.010	0.08	0.25	0.39	0.96	0.14	1.70	0.50	1.72	1.65
			1	2.11	0.008	0.21	1.15	4.29	12.23	0.70	1.86	0.19	3.26	2.97
			4	2.69	0.007	0.18	1.28	5.72	16.44	0.81	1.75	0.15	3.97	3.61
			10	3.42	0.005	0.22	1.49	6.23	15.83	0.90	1.57	0.17	3.69	3.35
Crude and Burning	FW	Light	0	1.83	0.019	0.87	2.75	5.75	12.06	1.50	1.74	0.36	1.66	1.61
			1	10.63	0.012	2.22	12.32	17.16	16.88	4.51	2.21	0.95	2.20	2.11
			4	22.21	0.016	5.41	33.33	34.67	31.37	10.98	6.32	4.05	5.89	5.67
			10	67.39	0.014	12.67	86.05	77.17	53.82	24.54	15.53	12.16	13.19	12.80
		Dark	0	1.44	0.020	0.78	2.52	5.53	11.67	1.42	1.73	0.35	1.79	1.71
			1	2.86	0.012	0.80	3.08	8.95	15.29	1.71	1.74	0.28	2.19	2.08
			4	3.52	0.014	0.96	3.98	10.91	20.92	2.08	1.71	0.29	2.24	2.13
			10	3.65	0.013	0.94	4.24	12.92	21.10	2.16	1.69	0.26	2.37	2.24
	SW	Light	0	1.56	0.009	0.20	1.01	3.38	10.34	0.53	1.86	0.17	3.20	2.95
			1	7.15	0.012	1.74	10.59	10.39	14.11	3.44	1.62	0.67	1.85	1.78
			4	21.29	0.013	4.54	28.19	29.22	25.34	8.74	4.89	3.29	4.68	4.52
			10	52.80	0.013	12.00	79.88	76.06	50.87	22.87	12.40	9.25	10.82	10.51
		Dark	0	1.55	0.009	0.19	1.05	3.43	10.54	0.55	1.89	0.18	3.20	2.95
			1	2.45	0.010	0.32	1.96	6.01	13.35	0.99	1.74	0.22	2.75	2.56
			4	3.37	0.007	0.29	2.02	7.00	17.49	1.03	1.77	0.19	3.25	2.98
			10	2.72	0.008	0.36	2.39	8.18	15.61	1.15	1.63	0.22	2.99	2.80

Table S4a. Fluorescence component contributions (%) of no fuel, gasoline, kerosene, and jet fuel

Fluorescence Component Contributions:			C1 (%)		C2 (%)		C3 (%)		C4 (%)	
Treatment	Light Type	Irradiation Period (day)	Average	Std. Dev.	Average	Std. Dev.	Average	Std. Dev.	Average	Std. Dev.
No Fuel	Light	0	50.98	27.35	24.85	11.96	23.34	16.27	0.83	1.30
		1	39.31	18.43	36.06	8.62	17.71	8.34	6.92	5.49
		4	38.88	5.92	34.79	8.03	17.27	5.04	9.06	6.12
		10	20.21	12.42	38.49	9.23	20.91	4.39	20.38	5.18
	Dark	0	54.16	31.15	22.79	14.21	22.52	17.38	0.54	1.18
		1	53.48	17.40	24.74	7.13	14.12	6.92	7.66	5.57
		4	59.66	23.85	20.26	10.81	14.41	7.62	5.67	6.41
		10	56.68	23.46	22.42	15.98	15.92	6.57	4.98	6.19
Gasoline	Light	0	21.98	10.68	6.48	5.97	2.89	7.07	68.66	14.72
		1	6.58	5.81	24.83	9.57	19.38	9.96	49.21	20.58
		4	7.85	3.59	40.70	6.03	32.49	5.27	18.96	10.14
		10	7.04	2.18	41.45	5.45	27.73	7.44	23.78	7.00
	Dark	0	30.62	21.47	6.17	5.66	3.54	6.33	59.68	24.07
		1	8.51	5.29	3.49	0.91	2.32	3.53	85.69	7.24
		4	30.60	19.77	20.47	6.40	20.21	5.65	28.72	17.57
		10	30.97	26.50	32.59	12.08	31.52	12.39	4.93	2.86
Kerosene	Light	0	43.92	26.26	18.79	8.05	31.16	17.90	6.13	3.50
		1	5.82	4.88	55.43	4.50	33.72	2.17	5.03	1.38
		4	0.46	0.74	45.00	4.13	27.19	3.09	27.35	6.19
		10	0.06	0.15	26.73	2.45	23.38	0.89	49.83	2.74
	Dark	0	43.35	24.19	20.71	9.83	28.25	15.28	7.69	1.72
		1	18.31	8.76	13.98	1.53	36.31	7.26	31.41	1.69
		4	18.04	11.83	14.19	2.38	34.98	5.67	32.79	5.79
		10	15.31	11.62	25.23	6.72	32.29	3.55	27.16	8.19
Jet Fuel	Light	0	16.39	13.13	2.44	4.22	77.49	10.98	3.68	1.52
		1	0.29	0.39	69.12	2.96	20.10	3.59	10.49	4.19
		4	1.10	1.49	62.71	3.94	17.58	4.21	18.61	3.99
		10	0.18	0.43	41.76	3.26	20.98	1.42	37.08	3.36
	Dark	0	15.42	11.74	2.14	3.75	78.64	9.59	3.80	1.44
		1	6.13	3.17	5.98	5.78	86.13	8.44	1.76	0.97
		4	5.26	2.78	4.75	1.50	87.24	5.42	2.75	2.55
		10	7.33	5.14	7.92	3.64	84.05	8.18	0.70	0.94

Table S4b. Fluorescence component contributions (%) of diesel, heating oil, crude oil and crude oil/burning.

Fluorescence Component Contribution:			C1 (%)		C2 (%)		C3 (%)		C4 (%)	
Treatment	Light Type	Irradiation Period (day)	Average	Std. Dev.	Average	Std. Dev.	Average	Std. Dev.	Average	Std. Dev.
Diesel	Light	0	55.21	30.02	13.98	10.98	23.24	14.07	7.57	6.59
		1	2.04	0.63	33.99	6.86	39.92	2.17	24.05	7.65
		4	2.48	1.20	15.73	7.79	34.00	2.01	47.79	9.84
		10	0.00	0.00	16.93	1.15	24.58	0.69	58.49	0.63
	Dark	0	50.57	27.15	18.53	11.19	23.94	13.04	6.96	3.76
		1	28.26	12.41	8.62	4.56	25.94	7.28	37.18	7.41
		4	24.93	10.25	19.10	7.65	23.23	3.38	32.75	4.65
		10	21.22	10.99	13.10	3.33	30.26	5.73	35.42	5.80
Heating Oil	Light	0	19.06	14.56	4.46	3.42	73.45	11.45	3.03	1.69
		1	0.55	0.48	69.73	1.71	19.08	2.49	10.65	3.41
		4	1.21	1.04	47.10	12.86	19.85	5.29	31.84	7.94
		10	1.98	3.49	42.23	7.40	20.01	2.05	35.78	5.20
	Dark	0	18.82	13.94	2.02	0.88	76.34	13.05	2.82	1.61
		1	5.59	3.20	4.46	1.66	89.09	5.38	0.86	0.84
		4	5.90	3.07	4.43	0.88	89.30	3.26	0.37	0.64
		10	7.52	4.98	7.45	2.39	84.74	6.99	0.30	0.73
Crude Oil	Light	0	22.02	14.18	30.74	1.78	23.41	4.77	23.83	10.88
		1	10.58	0.32	54.97	2.91	24.23	1.67	10.22	3.97
		4	13.35	1.82	59.08	5.03	17.72	4.88	9.85	2.14
		10	13.19	2.50	61.25	6.44	12.04	6.80	13.53	2.14
	Dark	0	21.35	13.54	28.19	3.99	21.11	6.60	29.35	3.63
		1	3.70	1.41	43.84	4.03	42.22	5.65	10.24	1.90
		4	3.22	1.77	44.08	4.12	43.15	6.38	9.56	5.29
		10	3.04	1.27	48.52	4.85	42.86	5.14	5.58	4.96
Crude and Burning	Light	0	4.73	2.63	42.67	3.76	44.31	4.69	8.28	1.89
		1	11.08	0.75	61.64	1.53	20.94	1.88	6.34	1.61
		4	14.42	2.59	61.80	6.93	15.35	7.51	8.43	2.11
		10	15.74	1.56	68.11	1.82	7.76	1.43	8.38	2.65
	Dark	0	4.59	2.32	43.18	3.87	44.43	4.69	7.80	1.53
		1	3.79	0.96	49.80	3.65	37.80	3.52	8.61	0.89
		4	3.39	1.21	48.84	3.13	41.68	3.31	6.08	1.05
		10	3.03	0.82	54.20	2.57	38.47	1.98	4.31	1.64

Table S5. Fluorescent component matches to studies on the OpenFluor database. Tucker congruence coefficient (TCC) is indicated for excitation (Ex) and emission (Em) wavelengths. Each comparison is given by model name and link to publications.

Model Name	DOI Link:	Component (this study)	Component comparisons	TCC_{Em}	TCC_{Ex}	TCC_{Ex} x TCC_{Em}
Graeber_2012 (ID : 7)	https://doi.org/10.1016/j.scitotenv.2012.08.087	1	4	0.97	0.95	0.92
Graeber_2012 (ID : 7)	https://doi.org/10.1016/j.scitotenv.2012.08.087	3	7	0.99	0.96	0.95
IPY-C3O (ID : 9)	https://doi.org/10.1002/2013JC009173	1	1	0.97	0.99	0.96
Omdrev (ID : 10)	https://doi.org/10.1111/gcb.12488	1	4	0.96	0.96	0.92
AMT20 (ID : 12)	https://doi.org/10.1016/j.marchem.2013.10.004	3	4	0.98	0.99	0.97
Lena2013 (ID : 15)	https://doi.org/10.3389/fmars.2015.00108	1	1	0.97	0.97	0.94
dtEEM (ID : 18)	https://doi.org/10.1039/C3AY41160E	1	1	0.97	0.98	0.95
Horsens (ID : 19)	ISBN: 9780521152594	2	5	0.96	0.99	0.95
Kauai (ID : 20)	https://doi.org/10.1016/j.marchem.2007.10.003	2	7	0.99	0.99	0.98
RecycleBY (ID : 21)	https://doi.org/10.1021/es103015e	2	5	0.97	0.98	0.95
RecycleG7 (ID : 22)	https://doi.org/10.1021/es103015e	3	7	0.99	0.99	0.98
RecycleRH (ID : 24)	https://doi.org/10.1021/es103015e	2	4	0.95	0.95	0.91
RecycleWRAMS (ID : 26)	https://doi.org/10.1021/es103015e	3	3	0.95	0.98	0.93
RecycleWRAMS (ID : 26)	https://doi.org/10.1021/es103015e	4	7	0.95	0.95	0.91
SalmoDOM (ID : 35)	https://doi.org/10.1016/j.scitotenv.2015.07.160	1	4	0.96	0.98	0.94
Shutova_F (ID : 42)	https://doi.org/10.1016/j.watres.2014.01.053	1	1	0.98	0.97	0.96
Shutova_G (ID : 43)	https://doi.org/10.1016/j.watres.2014.01.053	1	2	0.96	0.97	0.93
Drink (ID : 49)	https://doi.org/10.1016/j.watres.2011.08.066	1	1	0.98	0.97	0.95
Galathea (ID : 51)	https://doi.org/10.1016/j.marchem.2011.05.002	1	1	0.98	0.99	0.97
Galathea (ID : 51)	https://doi.org/10.1016/j.marchem.2011.05.002	2	6	0.97	0.98	0.94
Horsens2005 (ID : 53)	https://doi.org/10.4319/lo.2005.50.2.0686	2	7	0.98	0.97	0.95
Horsens2005 (ID : 53)	https://doi.org/10.4319/lo.2005.50.2.0686	3	8	0.96	0.98	0.94
Kattegat (ID : 54)	https://doi.org/10.1016/j.marchem.2011.06.007	2	5	0.96	0.96	0.92
vale3C (ID : 56)	https://doi.org/10.1002/lno.10258	1	1	0.97	0.99	0.95
Beringia (ID : 58)	https://doi.org/10.1029/2009JG000990	1	1	0.98	0.99	0.96
Partners (ID : 59)	https://doi.org/10.1002/2013JG002320	2	5	0.96	0.97	0.93
ONstreams (ID : 61)	https://doi.org/10.4319/lo.2010.55.3.1159	1	3	0.97	0.97	0.95
OrganicCompounds1 (ID : 62)	https://doi.org/10.3389/fmars.2015.00098	3	6	0.98	0.99	0.97
OrganicCompounds2 (ID : 63)	https://doi.org/10.3389/fmars.2015.00098	3	3	0.97	0.98	0.95
CWT (ID : 64)	https://doi.org/10.1007/s10021-011-9469-z	1	1	0.98	0.97	0.96
CWT (ID : 64)	https://doi.org/10.1007/s10021-011-9469-z	2	5	0.98	0.99	0.97
CWT (ID : 64)	https://doi.org/10.1007/s10021-011-9469-z	3	4	0.97	0.98	0.95
FCE (ID : 66)	https://doi.org/10.1007/s10021-010-9370-1	1	3	0.96	0.97	0.93
FloridaKeys (ID : 67)	https://doi.org/10.1016/j.csr.2013.06.010	3	3	0.98	0.99	0.98
TropicalRivers (ID : 70)	https://doi.org/10.1029/2009JG000987	1	1	0.99	0.96	0.95
WAIS_LD_2 (ID : 171)	https://doi.org/10.5194/cp-13-533-2017	3	2	0.98	0.99	0.97
WAIS_LGM_2 (ID : 172)	https://doi.org/10.5194/cp-13-533-2017	3	2	0.98	0.99	0.97
Meuse River (ID : 198)	https://doi.org/10.1007/s10533-017-0387-9	1	1	0.97	0.96	0.93
Congo River (ID : 199)	https://doi.org/10.5194/bg-13-5405-2016	2	6	1.00	0.99	0.99
SoyangWatershed (ID : 222)	https://doi.org/10.1016/j.scitotenv.2017.11.067	1	1	0.98	0.99	0.97
Sea Ice (ID : 243)	https://doi.org/10.1016/j.scitotenv.2018.01.251	1	2	0.99	0.99	0.98
LeafLeachate (ID : 269)	https://doi.org/10.1002/2016JG003677	2	2	0.95	0.97	0.93
Painter_NorthSea (ID : 281)	https://doi.org/10.1016/j.scitotenv.2018.02.237	1	2	0.98	0.99	0.98
Painter_NorthSea (ID : 281)	https://doi.org/10.1016/j.scitotenv.2018.02.237	3	3	0.99	0.99	0.97
Rainwater (ID : 289)	https://doi.org/10.1016/j.ecss.2018.11.002	1	3	0.99	0.97	0.96
Skio_dock (ID : 377)	https://doi.org/10.1016/j.ecss.2016.08.046	1	1	1.00	0.96	0.96
Skio_dock (ID : 377)	https://doi.org/10.1016/j.ecss.2016.08.046	2	3	0.96	0.98	0.94
osPARAFAC_Lillsjoen (ID : 380)	https://doi.org/10.1021/acs.est.7b03260	1	1	0.96	0.96	0.92
osPARAFAC_RioNegro (ID : 381)	https://doi.org/10.1021/acs.est.7b03260	1	1	0.96	0.98	0.94
osPARAFAC_PonyLake (ID : 386)	https://doi.org/10.1021/acs.est.7b03260	2	1	1.00	1.00	0.99
Minjiang Estuary (ID : 534)	https://doi.org/10.1007/s11356-019-05700-2	1	1	0.96	0.99	0.95
Minjiang Estuary (ID : 534)	https://doi.org/10.1007/s11356-019-05700-2	3	5	0.96	0.97	0.93

Model Name	DOI Link:	Component (this study)	Component comparisons	TCC_{Em}	TCC_{Ex}	TCC_{Ex} x TCC_{Em}
ArcticFjords_org (ID : 660)	https://doi.org/10.1016/j.marchem.2018.08.010	2	6	0.96	0.96	0.92
ArcticFjords_PPL (ID : 661)	https://doi.org/10.1016/j.marchem.2018.08.010	2	4	0.98	0.99	0.97
ArcticFjords_PPL (ID : 661)	https://doi.org/10.1016/j.marchem.2018.08.010	3	5	0.97	0.99	0.97
Antarctic DOM (ID : 663)	https://doi.org/10.1016/j.watres.2019.114901	3	1	0.95	0.96	0.91
LaSelvaDOM (ID : 680)	https://doi.org/10.1002/2017JG003960	2	6	0.96	0.95	0.92
DW_Sweden_Gavle (ID : 691)	https://doi.org/10.1016/j.watres.2017.08.020	2	4	0.98	0.96	0.94
ES&T_MKE_River (ID : 748)	https://doi.org/10.1021/acs.est.9b07123	1	1	0.95	0.99	0.94
Landscape_DOM (ID : 880)	https://doi.org/10.1016/j.scitotenv.2019.05.396	2	3	0.99	0.96	0.96
Qilian (ID : 929)	https://doi.org/10.1029/2020JG006222	1	3	0.98	0.96	0.94
Qilian (ID : 929)	https://doi.org/10.1029/2020JG006222	3	2	0.98	0.99	0.97
GrassLeafPine_Stream (ID : 959)	https://doi.org/10.1007/s10533-018-00534-5	1	1	0.99	1.00	0.99
GrassLeafPine_Stream (ID : 959)	https://doi.org/10.1007/s10533-018-00534-5	3	2	0.99	1.00	0.99
NICE_4C (ID : 1015)	https://doi.org/10.1016/j.scitotenv.2019.133740	1	2	0.99	0.98	0.97
EndMembersMixing (ID : 1109)	https://doi.org/10.1016/j.scitotenv.2019.02.258	1	1	0.98	0.99	0.98
POM_subtropical_estuary (ID : 1119)	https://doi.org/10.1016/j.jmarsys.2019.103264	1	1	0.96	0.97	0.93
BeaufortPW (ID : 1150)	https://doi.org/10.1016/j.marchem.2019.03.009	1	1	0.98	0.96	0.94
BeaufortPW (ID : 1150)	https://doi.org/10.1016/j.marchem.2019.03.009	3	4	0.95	0.96	0.91
Korean porewaters and bottom waters (ID : 1158)	https://doi.org/10.1016/j.watres.2017.05.022	1	1	0.99	1.00	0.99
Korean porewaters and bottom waters (ID : 1158)	https://doi.org/10.1016/j.watres.2017.05.022	3	3	0.99	0.99	0.98
mud_volcanoes_water (ID : 1164)	https://doi.org/10.1038/s41598-021-82632-3	1	1	0.97	0.98	0.95
Borisover_Kishon river (ID : 1206)	https://doi.org/10.1007/s11270-011-0821-x	1	1	0.98	0.97	0.95
Borisover_Kishon river (ID : 1206)	https://doi.org/10.1007/s11270-011-0821-x	2	2	0.96	0.97	0.93
RaskaDOM (ID : 1434)	https://doi.org/10.1016/j.jaridenv.2019.04.013	1	1	0.97	0.98	0.95
ES&T_VeteransLagoon (ID : 1609)	https://doi.org/10.1021/acs.est.9b07123	1	2	0.98	0.96	0.95
Porewater_Degradation (ID : 1633)	https://doi.org/10.1016/j.scitotenv.2019.133714	3	3	0.95	0.99	0.95
Shakil_Peel2015t2017_5comp (ID : 1778)	https://doi.org/10.1088/1748-9326/abac36	1	3	0.97	0.97	0.94
Shakil_Peel2015t2017_5comp (ID : 1778)	https://doi.org/10.1088/1748-9326/abac36	3	5	0.97	0.95	0.93
Anammox_EPS (ID : 1896)	https://doi.org/10.1021/acs.est.6b05761	1	3	0.99	0.99	0.97
ORCA_flume (ID : 2094)	https://doi.org/10.3390/w12113246	2	2	0.97	0.95	0.93
Vines_LakeT (ID : 2301)	https://doi.org/10.1002/aws2.1201	1	1	0.99	0.99	0.98
Vines_BWR (ID : 2302)	https://doi.org/10.1002/aws2.1201	1	1	0.98	0.98	0.95
Biodegradation_ArtificialSediment (ID : 2332)	https://doi.org/10.1016/j.watres.2020.115588	1	1	0.96	0.95	0.91
BacTank (ID : 2472)	https://doi.org/10.1007/s11356-021-13148-6	1	1	0.95	0.96	0.91
Dimer (ID : 2495)	https://doi.org/10.1002/lol2.10154	3	1	0.97	0.99	0.95
MEX-DOC-GOLD (ID : 2601)	https://doi.org/10.1016/j.watres.2019.115460	1	1	1.00	0.95	0.95
CavialnueNaturalSamples (ID : 2619)	https://doi.org/10.1016/j.saa.2020.118278	1	1	0.96	0.99	0.96
FREEDOMproject (ID : 2694)	doi.org/10.1002/lno.11606	1	2	0.95	0.98	0.93
FREEDOMproject (ID : 2694)	doi.org/10.1002/lno.11606	2	4	0.96	0.96	0.91
SPE_augmentation (ID : 2877)	https://doi.org/10.1016/j.watres.2020.116730	1	5	0.97	0.96	0.93
ES&T_GreenBay (ID : 3169)	https://doi.org/10.1021/acs.est.9b07123	1	1	0.99	1.00	0.99
y2015_WS_KS_LS_NZ (ID : 3855)	https://doi.org/10.1016/j.chemolab.2020.104176	1	1	0.96	0.97	0.94
Gueguen_JOIS (ID : 4431)	https://doi.org/10.1029/2020JC016578	3	6	0.97	0.99	0.97
Dainard_Bering2013 (ID : 4440)	https://doi.org/10.1016/j.marchem.2013.10.007	2	3	0.96	0.96	0.92
Dainard_BeaufortBering2013 (ID : 4442)	https://doi.org/10.1016/j.marchem.2013.10.007	2	4	0.97	0.97	0.94
Combinations-R (ID : 5496)	https://doi.org/10.1016/j.saa.2021.119800	2	3	0.99	0.97	0.96
Combinations-L (ID : 5497)	https://doi.org/10.1016/j.saa.2021.119800	1	2	0.96	0.96	0.92
Combinations-O/R/S (ID : 5498)	https://doi.org/10.1016/j.saa.2021.119800	2	3	0.99	0.97	0.96
Combinations-O/L (ID : 5499)	https://doi.org/10.1016/j.saa.2021.119800	1	1	0.96	0.95	0.92
Combinations-R/S/L (ID : 5500)	https://doi.org/10.1016/j.saa.2021.119800	1	1	0.98	0.99	0.98
Combinations-O/R/S/L (ID : 5502)	https://doi.org/10.1016/j.saa.2021.119800	1	1	0.95	0.99	0.94
Urban_Coastal_Drainage (ID : 5519)	https://doi.org/10.1029/2020JG006146	1	1	0.97	0.99	0.96
Kungalv_5 (ID : 5631)	https://doi.org/10.1021/acsestwater.0c00105.	2	5	0.96	0.98	0.94
PYL_5rivers&lakes (ID : 5754)	https://doi.org/10.1016/j.chemosphere.2021.131604	1	1	0.99	0.97	0.97
Arctic_Circle_Traverse_IceCore_3 (ID : 6385)	https://doi.org/10.1017/jog.2021.51	4	3	0.97	0.95	0.92

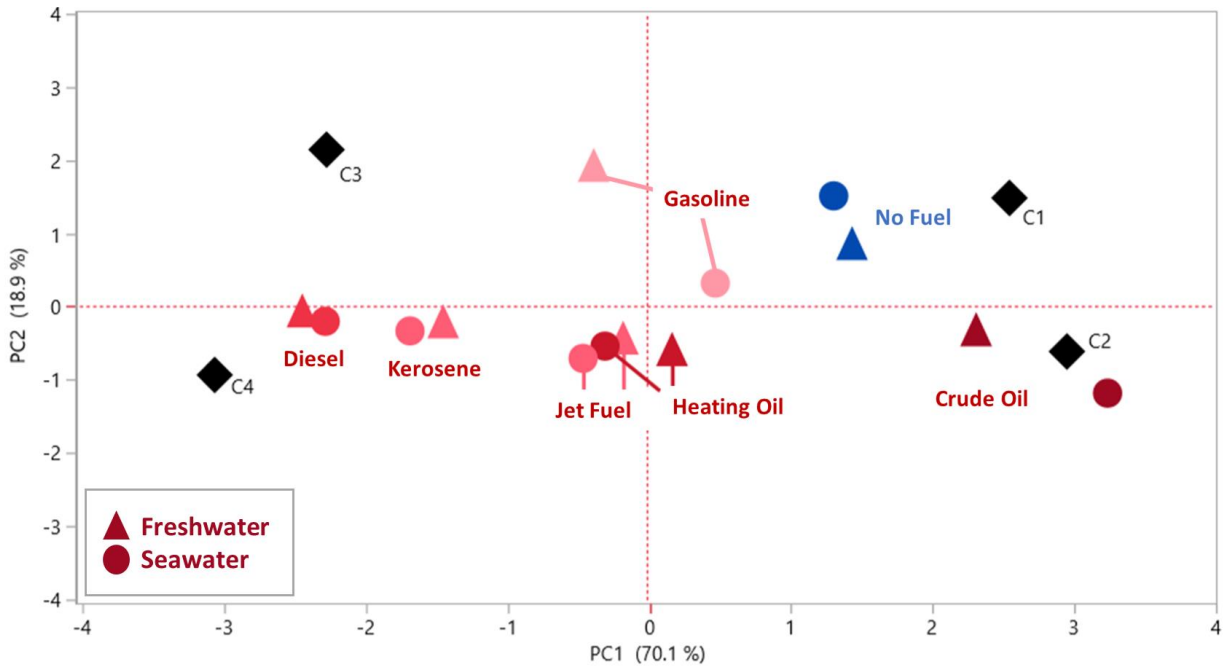

Figure S1. Optical differences between freshwater and seawater at 10 days light exposure. Shaded by boiling points (i.e. dark color to light color; highest boiling point to lowest boiling point).[48] Triangle shapes represent freshwater samples while circle shapes represent seawater samples.

Table S6a. FT-ICR MS molecular classifications and average masses for no fuel, gasoline, kerosene, and jet fuel. Averages represent N=2.

Molecular Classification:			UHO		ULO		Aliphatic		CA		Aromatic		Average Mass %RA	
Treatment	Light Type	Irradiation Period (days)	Average	Std. Dev.	Average	Std. Dev.	Average	Std. Dev.	Average	Std. Dev.	Average	Std. Dev.	Average	Std. Dev.
No Fuel	Light	0	45.39	2.30	40.63	5.21	2.59	0.84	1.72	1.03	9.56	2.89	532.34	20.90
		10	31.50	3.95	46.10	4.70	12.89	3.62	1.19	0.52	8.26	2.46	509.56	21.89
	Dark	0	44.46	0.30	41.39	3.16	2.77	0.56	1.64	1.00	9.45	2.83	530.45	17.68
		10	34.04	9.20	44.41	6.30	11.27	5.62	2.18	2.10	8.04	2.50	515.01	18.35
Gasoline	Light	0	43.87	1.04	39.18	5.91	6.07	2.27	1.81	1.19	8.98	3.01	480.29	39.91
		1	40.93	3.26	40.92	2.33	4.86	0.65	2.23	1.15	10.95	2.72	477.97	29.25
		4	40.59	4.23	41.29	2.66	4.37	0.53	2.20	0.74	11.46	3.61	491.09	26.61
		10	37.39	2.42	41.10	2.12	8.45	2.68	2.36	0.72	10.63	2.61	485.94	28.56
	Dark	0	44.72	1.90	40.39	4.28	5.18	1.76	1.64	1.39	8.00	4.80	493.21	38.11
		1	40.16	1.50	42.50	3.70	5.67	2.05	1.98	1.42	9.60	3.75	488.34	40.11
		4	40.77	3.30	42.72	2.97	6.73	1.99	1.60	1.06	8.12	3.50	490.24	48.36
		10	40.95	2.58	41.23	2.11	6.09	2.27	2.09	1.45	9.53	3.54	486.76	41.84
Kerosene	Light	0	45.21	0.92	41.92	3.98	3.11	0.85	1.62	1.35	8.04	3.87	489.65	44.51
		1	26.83	6.27	47.28	2.25	5.82	0.43	2.95	1.07	17.09	4.20	460.11	53.80
		4	18.69	7.82	49.80	3.03	5.84	1.20	4.00	0.89	21.63	4.02	455.79	56.83
		10	16.67	3.47	55.84	4.96	6.83	0.60	2.90	0.82	17.69	1.47	453.31	35.69
	Dark	0	45.30	1.68	42.52	4.59	3.41	0.82	1.33	1.09	7.41	3.99	490.12	45.40
		1	43.14	1.60	43.46	5.54	3.09	0.86	1.57	1.28	8.69	3.85	489.84	49.78
		4	42.73	3.88	42.41	4.74	5.97	2.80	1.28	1.15	7.56	3.69	480.39	51.19
		10	40.81	1.79	41.47	4.28	5.08	0.87	2.14	1.06	10.40	2.19	498.43	36.86
Jet Fuel	Light	0	41.30	4.75	42.39	4.87	5.80	1.62	1.68	1.26	8.75	3.87	507.40	24.04
		1	7.74	2.10	30.59	2.43	54.97	1.83	0.45	0.14	6.23	1.16	360.16	2.56
		4	10.08	1.35	45.10	0.88	27.38	2.33	2.26	0.73	15.15	0.70	409.08	10.72
		10	15.32	0.99	46.71	5.68	20.01	5.73	2.44	0.52	15.44	1.28	438.49	17.03
	Dark	0	43.06	2.99	41.36	4.14	4.31	1.52	1.87	1.38	9.30	3.84	505.98	23.46
		1	41.48	1.80	42.76	3.75	3.90	0.83	1.91	1.46	9.86	3.84	521.24	18.11
		4	39.96	2.00	42.49	4.06	5.70	3.18	1.97	1.43	9.81	3.70	512.22	10.79
		10	41.24	2.95	43.02	3.92	3.20	0.77	2.08	1.50	10.34	4.03	513.37	22.77

Table S6b. FT-ICR MS molecular classifications and average masses for diesel, heating oil, and crude oil. Averages represent N=2.

Molecular Classification:			UHO		ULO		Aliphatic		CA		Aromatic		Average Mass %RA	
Treatment	Light Type	Irradiation Period (days)	Average	Std. Dev.	Average	Std. Dev.	Average	Std. Dev.	Average	Std. Dev.	Average	Std. Dev.	Average	Std. Dev.
Diesel	Light	0	44.06	2.00	42.12	4.72	3.41	0.72	1.69	1.45	8.65	3.92	483.40	49.68
		1	20.26	5.62	52.93	2.24	5.98	1.32	2.41	0.35	18.38	1.95	453.25	49.35
		4	18.96	7.24	57.54	9.29	5.42	0.86	2.22	0.54	15.83	1.30	453.31	47.73
		10	22.64	1.73	54.76	1.69	6.69	0.78	1.72	0.25	14.08	0.93	468.55	27.39
	Dark	0	44.99	3.65	41.89	4.48	3.86	0.66	1.60	1.44	7.61	5.02	477.84	51.83
		1	41.45	5.34	43.33	5.42	3.88	0.75	1.75	1.07	9.53	2.45	488.40	50.96
		4	40.99	4.37	41.85	5.48	5.93	2.38	1.80	1.16	9.38	3.33	480.59	44.31
		10	43.43	4.14	40.22	4.23	8.42	6.03	1.31	1.23	6.57	5.08	483.87	57.63
Heating Oil	Light	0	40.96	4.01	43.30	5.63	4.62	1.31	1.59	1.16	9.37	3.13	523.07	18.20
		1	7.17	1.38	34.37	3.59	47.47	10.52	2.68	4.55	8.31	3.52	363.06	11.35
		4	8.42	2.03	45.23	5.71	32.33	8.76	2.38	3.25	11.61	4.43	403.70	22.99
		10	16.13	3.43	46.92	4.55	17.13	7.52	2.96	2.37	16.77	4.67	438.85	8.23
	Dark	0	43.16	4.55	42.83	7.12	3.49	1.50	1.56	1.28	8.83	3.83	526.65	23.26
		1	40.40	5.51	43.22	6.31	4.81	3.56	1.64	1.16	9.74	3.30	514.69	30.54
		4	39.92	4.52	42.78	5.06	5.55	3.02	1.73	1.18	9.83	3.55	510.80	15.33
		10	39.43	5.58	43.40	4.51	6.20	4.20	1.78	1.82	8.97	5.68	516.36	6.36
Crude Oil	Light	0	42.09	3.85	41.67	3.89	6.47	1.76	1.61	1.24	8.11	3.93	464.57	46.35
		1	13.93	4.89	28.45	4.73	52.33	11.55	0.63	0.43	4.65	1.84	381.37	29.93
		4	8.35	4.15	34.73	6.42	48.76	14.07	0.99	0.64	7.16	3.18	384.98	40.27
		10	7.07	1.51	40.95	3.74	43.04	7.96	1.14	0.66	7.80	2.76	388.43	37.32
	Dark	0	45.93	2.79	40.43	4.82	4.12	1.18	1.37	1.05	8.07	3.72	494.64	42.79
		1	40.20	4.06	41.18	4.33	9.17	3.94	1.52	1.19	7.92	4.00	475.24	37.41
		4	43.47	3.23	41.78	4.39	6.50	3.22	1.22	1.27	6.99	4.67	481.11	56.37
		10	41.41	1.13	40.34	3.90	7.54	5.76	1.93	1.61	8.72	5.01	475.05	42.37

Table S7. FT-ICR MS molecular classifications and average masses for diesel, heating oil, and crude oil. Averages represent N=2.

Molecular Classification:			UHO		ULO		Aliphatic		CA		Aromatic		Average Mass %RA	
Treatment	Light Type	Irradiation Period (days)	Average	Std. Dev.	Average	Std. Dev.	Average	Std. Dev.	Average	Std. Dev.	Average	Std. Dev.	Average	Std. Dev.
Oil + ISB	Light	0	38.52	0.84	43.41	2.44	12.23	4.66	0.49	0.17	5.33	1.18	458.30	56.16
		1	10.05	2.89	24.94	3.71	61.54	7.27	0.39	0.02	3.08	0.64	360.98	28.16
		10	3.21	1.08	33.57	2.86	57.43	4.82	0.50	0.08	5.29	0.79	365.00	24.00
	Dark	0	38.72	0.36	41.88	1.94	14.54	3.28	0.39	0.13	4.45	1.56	459.19	45.84
		1	38.40	1.02	42.92	1.84	13.84	4.63	0.35	0.13	4.47	1.62	463.12	48.24
		4	37.66	0.74	42.69	1.44	14.00	2.51	0.44	0.05	5.19	0.30	455.12	43.93
		10	36.89	1.71	42.19	2.03	15.48	5.62	0.47	0.12	4.92	1.72	450.45	56.27
Oil + ISB + OP40	Light	0	36.27	--	40.05	--	22.73	--	0.10	--	0.84	--	408.38	--
		4	10.62	2.81	36.53	4.16	44.92	8.73	1.15	0.43	6.77	1.33	390.63	33.50
		10	10.17	0.62	38.69	3.24	41.10	3.45	1.73	0.08	8.31	0.75	392.95	30.60
	Dark	0	32.33	1.04	51.09	8.21	12.84	9.45	0.23	0.04	3.48	0.24	474.50	33.23
		1	37.05	3.76	47.73	6.78	12.73	4.85	0.17	0.08	2.30	1.74	460.14	57.53
		4	33.28	1.64	51.52	2.64	11.00	0.71	0.28	0.10	3.90	0.18	466.06	19.46
		10	29.77	1.23	50.94	1.02	12.36	0.24	1.99	0.15	4.89	0.61	473.96	25.37

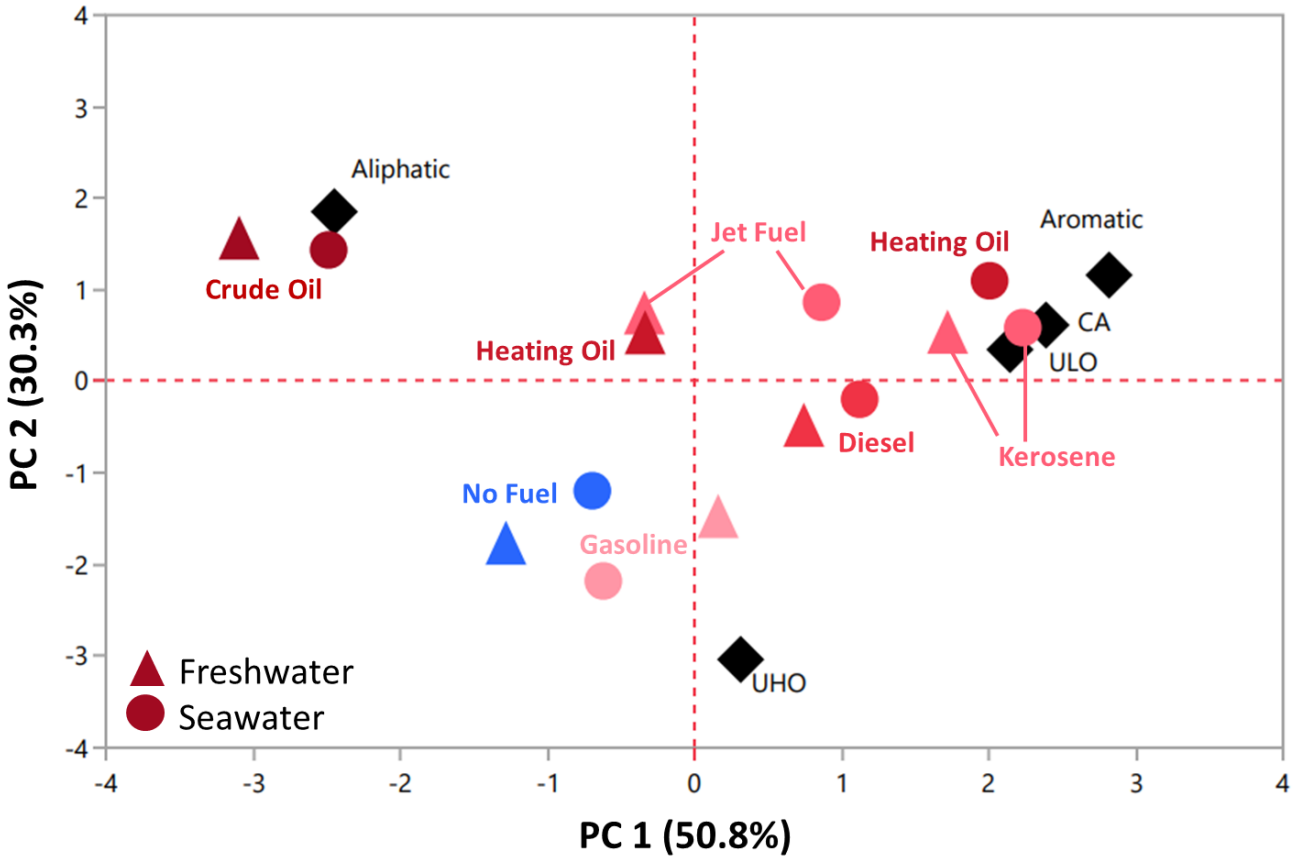

Figure S2. PCA plot. Molecular differences between freshwater and seawater at 10 days light exposure as expressed by FT-ICR MS van Krevelen space. Data are shaded by boiling points (i.e. dark color to light color; highest boiling point to lowest boiling point).[48] Triangle shapes represent freshwater samples while circle shapes represent seawater samples.

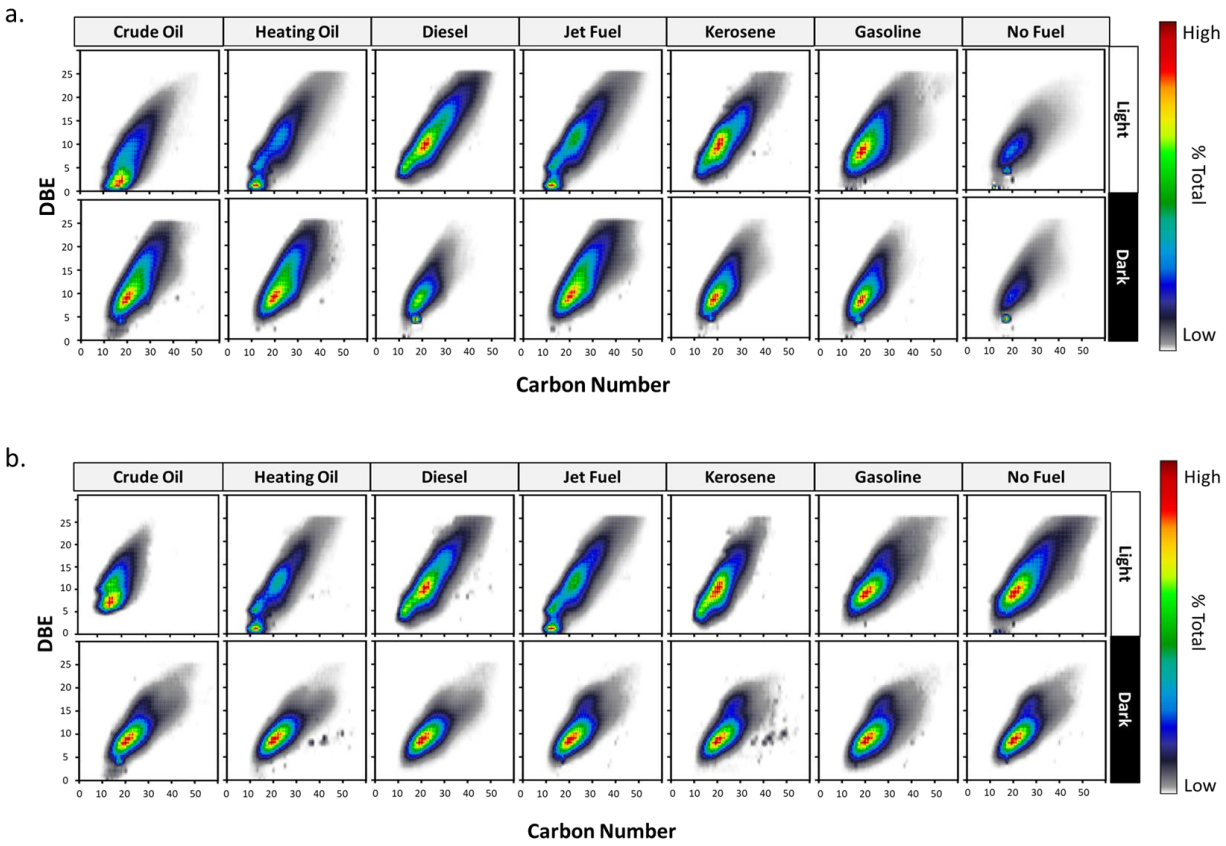

Figure S3. a) Double-bond equivalent (DBE) versus carbon number plots for freshwater(a) and seawater(b) samples at 10-days of light exposure and dark controls.

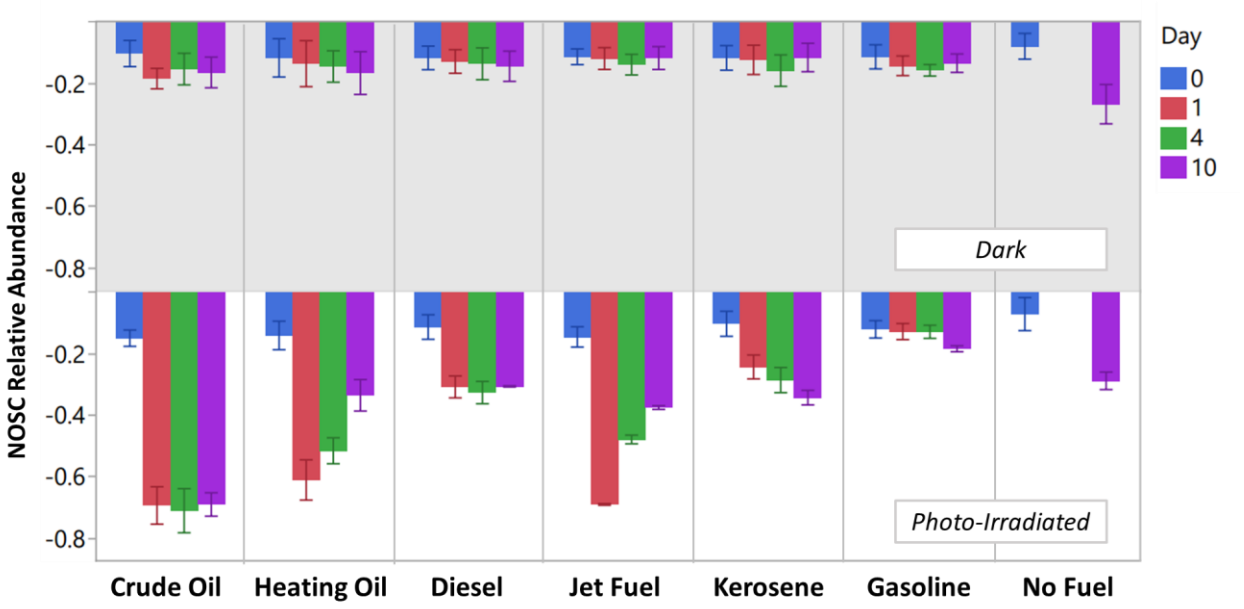

Figure S4. Nominal carbon oxidation states (NOSC) of fuel types in light-exposed and dark controlled treatments for 0-10 days (N= +/- 1 SE).

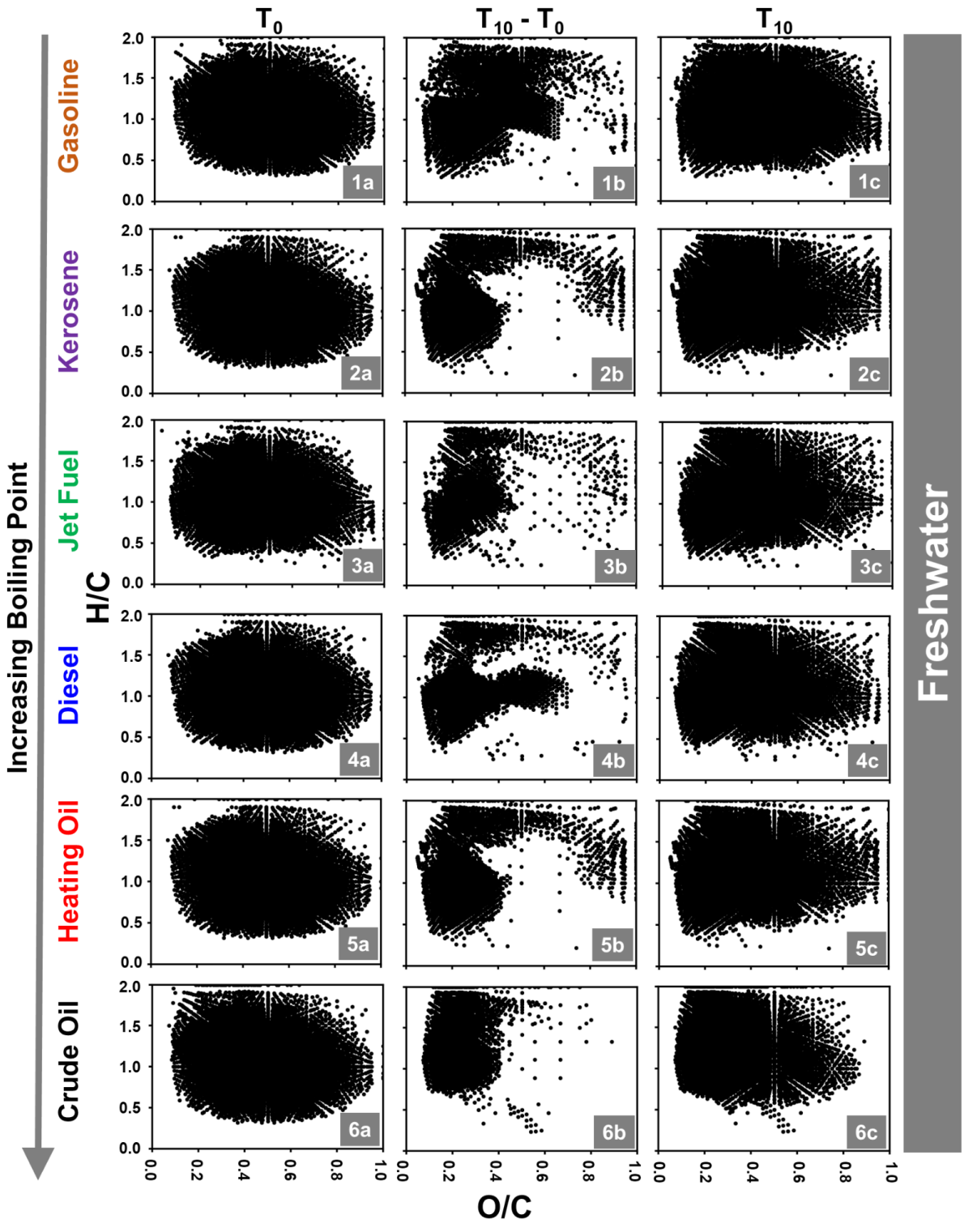

Figure S5. Van Krevelen plots of refined fuel and crude oil samples in freshwater. Subtraction plots (T_F - T_0) show oxidative molecular differences between samples undergoing 10-days of light exposure (T_F) and samples without light exposure (T_0).

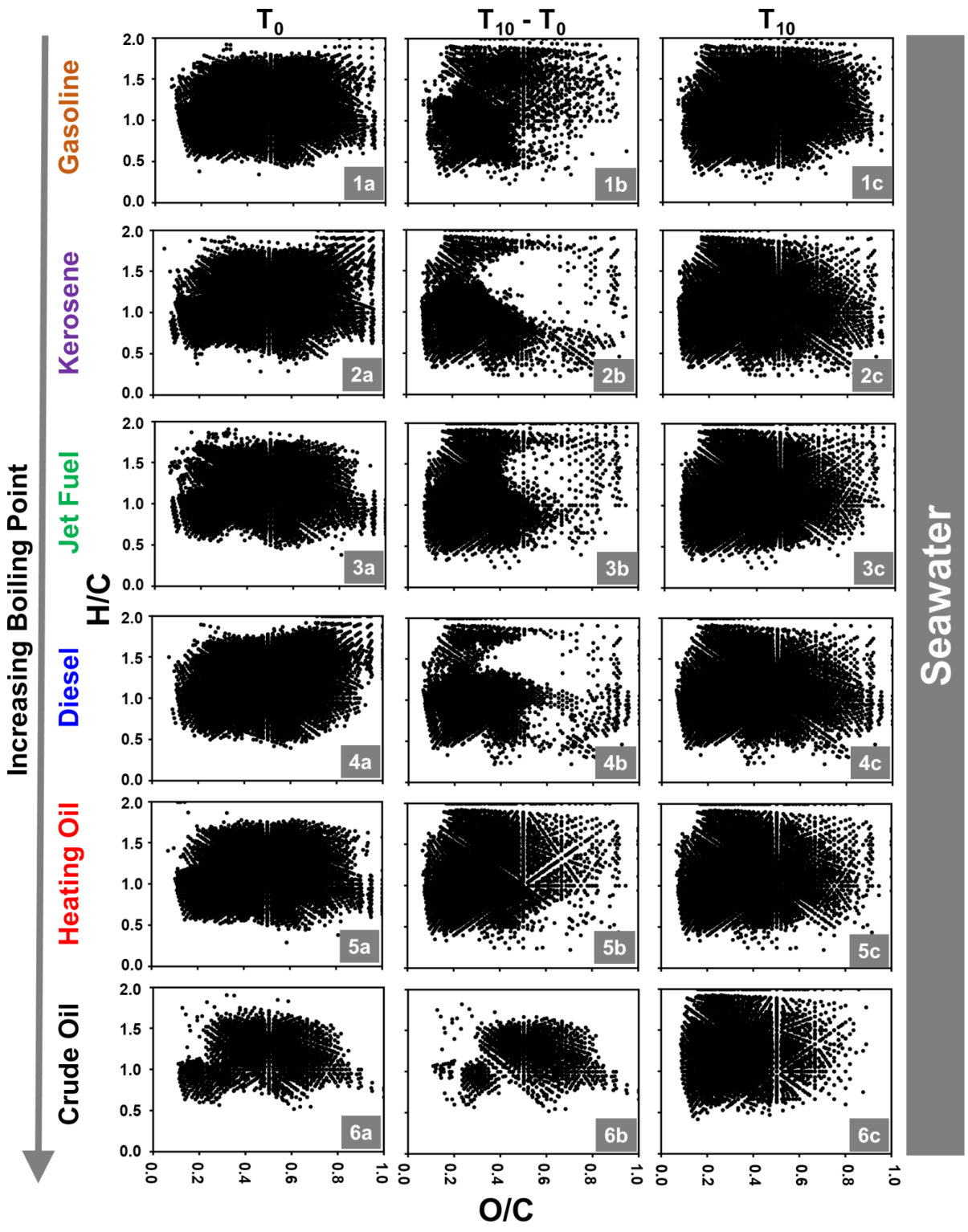

Figure S6. Van Krevelen plots of refined fuel and crude oil samples in seawater. Subtraction plots (T_F - T_0) show oxidative molecular differences between samples undergoing 10-days of light exposure (T_F) and samples without light exposure (T_0).

Table S8. DOC, SUVA254, and Spectral Index results of Experiment 2, testing differences of ISB versus ISB with a chemical herder (Siltech OP-40).

Treatment	Water Type	Light Type	Irradiation Period (day)	DOC (mg/L)	SUVA254 (L mg-1 cm-1)	C	A	T	B	M	FI	HIX	FRESH	BIX
Oil + ISB	SW	Light	0	1.61	0.034	0.25	1.98	4.93	11.54	0.87	1.77	0.20	2.22	2.11
			1	5.43	0.012	0.97	6.90	13.69	15.86	2.83	1.65	0.36	2.75	2.55
			4	11.73	0.013	2.90	18.38	28.76	19.38	6.80	2.80	1.09	3.63	3.42
			10	21.37	0.016	8.22	48.72	62.83	30.00	17.77	6.49	3.80	6.56	6.27
		Dark	0	1.77	0.012	0.19	1.49	4.55	11.49	0.72	1.78	0.17	2.79	2.59
			1	2.01	0.011	0.22	1.65	5.24	14.17	0.81	1.66	0.17	2.92	2.74
			4	2.20	0.011	0.25	1.89	6.61	14.59	0.99	1.66	0.17	2.95	2.75
			10	2.98	0.009	0.33	2.22	6.57	11.61	1.14	1.60	0.25	2.67	2.48
Oil+ ISB + OP40	SW	Light	0	8.11	0.003	0.30	2.01	4.87	9.73	0.89	1.79	0.26	2.30	2.18
			1	9.05	0.006	0.74	4.62	7.99	11.32	1.39	1.56	0.39	1.98	1.92
			4	16.84	0.008	1.73	11.02	11.29	12.20	2.81	2.22	1.07	1.76	1.75
			10	28.51	0.010	3.27	22.41	15.30	18.63	5.49	5.14	3.73	3.43	3.40
		Dark	0	7.40	0.003	0.30	1.98	4.93	9.63	0.87	1.77	0.26	2.32	2.21
			1	5.60	0.004	0.32	2.30	5.21	9.82	0.94	1.72	0.28	2.33	2.23
			4	5.83	0.005	0.38	2.64	7.05	11.49	1.20	1.63	0.25	2.47	2.36
			10	6.21	0.005	0.54	3.36	8.76	8.93	1.53	1.67	0.34	2.43	2.26

Table S9. Fluorescence component contributions (%) of Oil + ISB and Oil+ISB+OP40.

Fluorescence Component Contributions:			C1 (%)		C2 (%)		C3 (%)		C4 (%)	
Treatment	Light Type	Irradiation Period (day)	Average	Std. Dev.	Average	Std. Dev.	Average	Std. Dev.	Average	Std. Dev.
Oil + ISB	Light	0	3.18	0.05	46.10	1.79	36.61	1.73	14.11	0.06
		1	5.96	0.28	63.09	0.60	22.70	0.55	8.25	0.34
		4	10.35	0.08	72.61	0.11	12.79	0.15	4.25	0.05
		10	14.51	0.02	75.34	0.01	7.75	0.06	2.40	0.04
	Dark	0	2.15	0.01	43.01	0.82	39.44	0.45	15.39	0.52
		1	2.25	0.06	43.67	0.21	42.06	0.15	12.02	0.18
		4	2.09	0.06	48.14	0.11	38.99	0.18	10.78	0.13
		10	3.65	0.25	54.98	0.85	34.39	0.65	6.97	0.44
Oil + ISB + OP40	Light	0	4.14	0.07	50.46	0.15	34.35	0.05	11.06	0.18
		1	5.84	0.18	54.25	3.26	30.04	2.06	9.86	1.02
		4	11.94	0.09	54.34	0.16	23.56	0.04	10.15	0.09
		10	16.07	0.04	50.89	0.18	16.25	0.18	16.79	0.09
	Dark	0	4.00	0.17	51.06	0.14	34.41	0.34	10.53	0.31
		1	4.28	0.07	51.93	0.06	33.22	0.17	10.57	0.14
		4	3.61	0.06	55.63	0.24	30.74	0.16	10.03	0.36
		10	4.78	0.21	67.75	0.23	22.10	0.22	5.38	0.18

Vita

The author was born in Fairbanks, Alaska. Elizabeth A. Whisenhant worked as a laboratory technician in an analytical chemistry lab for one year in Anchorage, Alaska. She received her bachelor's degree in chemistry at the University of Alaska Anchorage in 2019. She joined the University of New Orleans chemistry graduate program in analytical chemistry and became a member of Dr. Matthew Tarr's and Dr. Phoebe Zito's groups in 2021.